Universidad de Sevilla
Escuela Técnica Superior de Ingeniería

Doctoral Thesis

Aircraft Trajectory Optimization Using Singular Optimal Control Theory

Thesis submitted to Dpto. de Ingeniería Mecánica y de los Materiales,
for the doctoral degree at
Universidad de Sevilla

Author: Antonio Franco Espín
Supervisor: Prof. Damián Rivas Rivas, Dr.
Dpto. Ingeniería Aeroespacial y Mecánica de Fluidos
Tutor: Miguel Pérez-Saborid Sánchez-Pastor, Dr.
Dpto. Ingeniería Aeroespacial y Mecánica de Fluidos

Sevilla, February, 2014

Contents

List of Figures

List of Tables

This page intentionally left blank

Abstract

The optimization of aircraft trajectories using the theory of singular optimal control is studied in this thesis. To describe the aircraft motion, a general nonlinear 3-degree-of-freedom point-mass model is adopted, along with realistic aerodynamic and propulsion models. The controlled motion of an aircraft is modeled as a control system whose performance can be optimized according to some performance index. This control system exhibits different dynamics, constraints and performance indices depending on the flight phase considered, which leads to a multiphase control system formulation.

An indirect optimization method is applied, in which necessary conditions for optimality are explicitly involved into the problem resolution. The method proposed in this thesis exploits the singular character of the problem in order to provide analytical state-feedback control laws. With this approach, assuming a prescribed solution structure in terms of phase sequence and sequence of singular and bang arcs within each phase, the problem of finding the optimal control is transformed into the problem of finding the values of some unknowns such that the necessary conditions for optimality as well as the initial and final conditions are satisfied, that is, the problem of solving a nonlinear system of equations.

Optimizing global trajectories implies not only addressing each flight phase, but also taking into account the interactions among them as well as looking for a global objective. Therefore, an optimal global trajectory cannot be obtained by simply piecing individually optimized phases together, not even when each phase is optimized with a performance index suitable for a global objective. However, by choosing appropriate performance indices, conclusions regarding the optimal control and optimal path structure for a single-phase optimal trajectory also apply at each phase of an optimal multiphase trajectory. As a consequence, prior to applying this approach to the problem of multiphase trajectories of commercial transport aircraft providing minimum fuel consumption, this approach is applied to three auxiliary single-phase problems.

First, the problem of fuel-optimal fixed-rating aircraft climb in the presence of altitude-dependent winds is analyzed. The climb is optimized to give minimum contribution to the global-trajectory fuel consumption. The optimal control is of the bang-singular-bang type, and the optimal trajectories are formed by a singular arc and two minimum-path-angle arcs joining the singular arc with the given initial and final points. This analysis is used to assess the optimality of a standard climb procedure defined by segments with constant calibrated air speed and Mach number. Linear wind profiles defined by two parameters, the average wind and the wind shear, are considered. The effects of the wind profile and of the initial aircraft weight on the results are studied. Comparison with the optimal results shows that the performance of the optimized standard climb, in terms of global variables such as fuel

consumption, flight time and horizontal distance travelled, is very close to optimal.

Second, minimum-fuel cruise at constant altitude with the constraint of a fixed arrival time is analyzed, including the effects of average horizontal winds. Again, the optimal control is of the bang-singular-bang type, and the optimal trajectories are formed by a singular arc and two minimum/maximum-thrust arcs joining the singular arc with the given initial and final points. The effects of average horizontal winds on the optimal results are analyzed, both qualitatively and quantitatively. The influence of the initial aircraft weight and the given cruise altitude is analyzed as well. Two applications are studied: first, the cost of meeting the given arrival time under mismodeled winds, and second, the cost of flight delays imposed on a nominal optimal path. The optimal results are used to assess the optimality of cruising at constant speed; the results show that the standard constant-Mach cruise is very close to optimal.

Third, unpowered descents of commercial transport aircraft are optimized in the presence of altitude-dependent winds, with the objective of maximizing range. The optimal problem and an optimized constant-calibrated-airspeed procedure are analyzed. The optimal control is of the bang-singular-bang type, and the optimal trajectories are formed by a singular arc and two maximum-path-angle arcs joining the singular arc with the given initial and final points. Linear wind profiles defined by two parameters, the average wind and the wind shear, are considered. The effects of both the average wind and the wind shear on the optimal results, as well as the effects of the aircraft weight, are analyzed. The wind shear is shown to have a clear effect on the maximum range. The comparison between the two sets of results shows that the optimized constant-calibrated-airspeed descent is very close to optimal.

Once the auxiliary single-phase problems are solved, the problem of global trajectories of commercial transport aircraft providing minimum fuel consumption is analyzed. The global trajectories are considered to be composed of three types of phases: climb, cruise, and unpowered descent. The optimal control in every phase is of the bang-singular-bang type, and the optimal climb, cruise and descent trajectories are formed by a singular arc and two minimum/maximum-control arcs joining the singular arc with the given initial and final points. The optimal trajectories and controls, the minimum fuel consumption and some interesting global results are computed for an aircraft performing a climb-cruise-climb-cruise-descent trajectory. Linear wind profiles defined by two parameters, the average wind and the wind shear, are considered. The influence of the aircraft weight and the wind profile on the results is analyzed.

Foreword

This PhD thesis has been conducted under the supervision of Professor Damián Rivas, from the Technical School of Engineering at the University of Seville.

The work presented in this document is the result of original research carried out by myself, in collaboration with others, while enrolled in the Department of Aerospace Engineering and Fluid Mechanics as a Lecturer and candidate for the degree of Doctor of Philosophy. This work has not been submitted for any other degree or award in any other university or educational establishment.

On one hand, some of this work has been previously published or accepted for publication in the following papers:

- Franco, A., Rivas, D., and Valenzuela, A., "Minimum-Fuel Cruise at Constant Altitude with Fixed Arrival Time", *Journal of Guidance, Control, and Dynamics*, Vol. 33, No. 1, 2010, pp. 280-285. doi: 10.2514/1.46465.

- Franco, A., Rivas, D., and Valenzuela, A., "Optimization of unpowered descents of commercial aircraft in altitude-dependent winds", *Journal of Aircraft*, Vol. 49, No. 5, 2012, pp. 1460-1470. doi: 10.2514/1.C031737.

- Franco, A., and Rivas, D., "Analysis of optimal aircraft cruise with fixed arrival time including wind effects", accepted for publication in *Aerospace Science and Technology*, 2013. doi: 10.1016/j.ast.2013.10.005.

On the other hand, some of this work either has been already submitted for publication or belongs to the following papers in progress:

- Franco, A., Rivas, D., and Valenzuela, A., "Analysis of fuel-optimal fixed-rating aircraft climbs in altitude-dependent winds", submitted for publication to *Journal of Aircraft*, 2013.

- Franco, A., and Rivas, D., "Analysis of fuel-optimal, global trajectories in the presence of altitude-dependent winds", in progress, 2013.

This page intentionally left blank

Acknowledgements

I wish to express my deepest gratitude to my mentor and supervisor, Professor Damián Rivas, for his extraordinary help, advices, corrections, guidance and endless support without which this work would not have been possible. I appreciate all these years of close collaboration; they have left their mark on me.

A special thanks goes to Dr. Alfonso Valenzuela, for his useful insights and discussions in our shared office, his assistance in editing this thesis, and his willingness to help. I would also like to thank the rest of the Aerospace Engineering Group: Carlos Antúnez, Antonio Corrales, Sergio Esteban, Francisco Gavilán and Rafael Vázquez, for their friendship, and for creating an excellent working atmosphere full of passion for research and education. I also wanted to thank Dr. Miguel Pérez-Saborid for accepting being the tutor of this thesis.

Thanks to all of my friends, for being always there and for their understanding and support.

I would also like to thank my family, with a special thought for those who left us. Thanks to my parents, for instilling an insatiable thirst for knowledge into me, for being the best examples to follow, and for their unconditional love. Thanks to my wonderful brothers, my best friends, for showing me that my happiness is theirs. Finally, thanks to my best behalf and my whole life, Diana, for her genuine love, encouragement, support and infinite patience. This thesis is dedicated to them.

Antonio Franco Espín

This page intentionally left blank

If I have seen further it is by standing on the shoulders of giants.

Isaac Newton

This page intentionally left blank

1 Introduction

1.1 Motivation

Aviation industry plays a key role in the social and economic development of Nations, apart from being itself an indicator of the level of that development. A snapshot of air transport sector in 2010 reveals that it supports 56.6 million jobs worldwide and 3.5% of global gross domestic product (GDP) [1]. Both figures take into account direct, indirect, induced and tourism-catalytic impacts, but do not include other economic benefits like the existence of companies or industries because air travel makes them possible.

Despite the global economic crisis, air transport industry has not stopped growing. In 2011, more than 2800 million passenger flew, which compared to 1800 million passengers in 2003 implies an average, sustained rate of increase of 5.7% per year [2]. Also in 2011, airlines all over the world spent $176000 million in fuel, four times what they spent in 2003 ($44000 million)[3]. Moreover, fuel relative impact on airlines operating costs has also experienced a dramatic increase, raising from 14% in 2003 to 28% in 2011. Hence, it is increasingly important for airlines to implement measures to improve efficiency in fuel consumption, not only for the positive impact on companies' income statements but also to reduce the environmental impact. In fact, air transport industry is committed to reduce the environmental impact, even though airline operations only accounts for the 2% of the total human CO_2 emissions.

The aviation industry agreed in 2008 upon a set of aggressive targets with the aforementioned two incentives: Reducing charbon dioxide emissions, and reducing operating costs associated to the largest budget line in relative terms[4]. Thus, in this industry it is broadly accepted that the following targets have to be sequentially satisfied:

1. To improve fleet fuel efficiency by 1.5% per year between 2009 and 2020.

2. To stabilize net CO_2 emissions from aviation from 2020 through carbon-neutral growth.

3. To reduce net CO_2 emissions from aviation by half by 2050, as compared with 2005.

[1] Source: Air Transport Action Group (ATAG),
`http://www.aviationbenefitsbeyondborders.org`

[2] Source: International Air Transport Association (IATA),
`http://www.iata.org/whatwedo/Documents/economics/Industry-Outlook-Presentation-Dec2012.pdf`

[3] Source: International Air Transport Association (IATA),
`http://www.iata.org/pressroom/facts_figures/fact_sheets/Documents/fuel-fact-sheet.pdf`

[4] Source: Air Transport Action Group (ATAG),
`http://www.atag.org/component/downloads/downloads/201.html`

In order to achieve these targets, companies across the sector make use of a four-pillar strategy: new technology, efficient operations, improved infrastructure and economic measures to fill the remaining emissions gap. In this context, aircraft trajectory optimization as well as optimality assessment of standard flight procedures are important tools to improve the efficiency of operations.

The participation of Spain in the modernization of the air navigation systems is mainly carried out by its participation in SESAR, but also national projects are promoted as, for example, the projects CENIT ATLANTIDA (*Application of Leading Technologies to Unmanned Aerial Vehicles for Research and Development in ATM*) and CENIT SINTONIA (*SIstemas No Tripulados Orientados al Nulo Impacto Ambiental*). The first develops innovative concepts for the automation in air-traffic management, testing them in high-fidelity simulations and experiments based on the use of UAVs (*Unmanned Air Vehicles*); whereas the second tries to increase the efficiency and to reduce the environmental impact of UAVs through the introduction of improvements in the whole life cycle, including the generation of optimal trajectories.

Since 2005, the Department of Aerospace Engineering and Fluid Mechanics has conducted several studies in the fields of trajectory prediction and optimization. In this context, the Aerospace Engineering Group has participated in the following projects: IMPACT (*Advanced Multi-Purpose Infrastructure for Trajectory Computation*), funded by Boeing Research and Technology Europe, for the development of trajectory calculators; CENIT ATLANTIDA, for the development of conflict resolution algorithms in arrival air traffic in the terminal maneuvering area; CENIT SINTONIA, for the development of an automatic optimal-trajectory generator for UAVs; and, nowadays, the group is the scientific leader of the ComplexWorld network established within the framework of SESAR, for the understanding and modeling of the behavior and evolution of the air-traffic management system.

The thesis presented in this document is the result of research in aircraft trajectory optimization. In the next section, the main objective of the thesis is described.

1.2 Objective

The main goal of this thesis is to study the optimization of global multiphase aircraft trajectories composed of climb, cruise and descent phases, by using the singular optimal control theory (see Bell and Jacobson [4]). With this approach, control variables do not take a constant value (as in parametric optimization) but vary along time. To solve the singular control problem, an indirect method is proposed, in which necessary conditions for optimality (adjoint dynamic equations, transversality conditions and Hamiltonian minimization condition) are explicitly used to obtain the optimal trajectory, i.e., the optimal control time function (or the optimal control feedback law) and the associate evolution of the states that optimize some property derived from the trajectory (e.g., fuel consumption, flight time, range, etc.).

Optimizing global multiphase aircraft trajectories implies not only addressing each flight phase, but also taking into account the interactions among them as well as looking for a global objective. Nevertheless, it is convenient to previously solve some related single-phase problems (optimal climb, optimal cruise and optimal descent), not only because they are interesting *per se*, but also because their resolution provides some valuable insight into the

optimization of global multiphase aircraft trajectories (they act as auxiliary problems). In fact, as it will be seen latter, the optimal control and optimal path structure for an optimal single-phase aircraft trajectory also apply at each phase of an optimal multiphase aircraft trajectory.

Therefore, some intermediate goals of this thesis can be pointed out:

- General formulation of multiphase aircraft trajectory optimization problem as a singular optimal control problem.
- Optimization of the fixed-rating aircraft climb in the presence of altitude-dependent winds.
- Optimization of the cruise at constant altitude with the constraint of a fixed arrival time and in the presence of an average uniform wind.
- Optimization of the unpowered descent in the presence of altitude-dependent winds.
- Optimality assessment of standard flight procedures commonly used in practice, such as CAS/Mach climbs, constant-Mach cruises and Mach/CAS descents.
- Study of the effects of some factors, such as wind speed distribution or the initial aircraft weight, on the optimal trajectories.

After having solved the three aforementioned auxiliary problems, the optimization approach is applied to the study of minimum-fuel global trajectories in the presence of altitude-dependent winds, where the effects of the wind profile and of the initial aircraft weight on the results are analyzed as well.

The employed optimization approach features the following advantages:

1. It provides analytical state-feedback control laws, allowing for an easy implementation.
2. It leads to more accurate results than those obtained by direct trajectory optimization methods.
3. It allows for generating trajectories with the best performance which, although these may not be flyable according to present-day air-traffic-control procedures and regulations, they can be used either as references to the design of improved flight procedures, or to assess the optimality of standard flight procedures commonly used in practice, such as CAS/Mach climbs, constant-Mach cruises and Mach/CAS descents.

To describe the aircraft motion, a general nonlinear 3-degree-of-freedom point-mass model, along with realistic aerodynamic and propulsion models, is adopted. This model is commonly used for trajectory prediction. Plane Earth, rigid and symmetric aircraft, symmetric flight (there is no slip), and thrust parallel to the aircraft aerodynamic velocity are considered as hypothesis. These assumptions are appropriate for subsonic, transport aircraft.

1.3 Outline

This thesis is organized as follows.

In Chapter 2, after a brief overview of references in optimal control theory (including the special cases of singular optimal control problems and switched dynamical systems), a review of the state of the art in numerical methods for trajectory optimization as well as in aircraft trajectory optimization is presented.

In Chapter 3 the formulation of an optimal control problem is first presented, including the necessary conditions for optimality and analyzing the special cases of singular optimal control problems and control problems of switched control systems; second, the equations governing the motion of an aircraft under appropriate assumptions are included; and third, the procedure to compute optimal aircraft trajectories developed in this thesis is explained.

In Chapter 4 the optimal control formulation is applied to the optimization of a fixed-rating climb in the presence of altitude-dependent winds, with the objective to give minimum contribution to the global-trajectory fuel consumption.

In Chapter 5 the formulation is used to analyze the minimum-fuel cruise at constant altitude with the constraint of a fixed arrival time, including the effects of average horizontal winds.

In Chapter 6 the formulation is applied to the analysis of the maximum-range unpowered descent in the presence of altitude-dependent winds.

In Chapter 7 the problem of minimum-fuel global trajectories in the presence of altitude-dependent winds is analyzed by means of the previously developed formulation.

Finally, some conclusions are presented in Chapter 8, and the future lines of research are drawn in Chapter 9.

The nomenclature and the supplementary models used throughout this document are included in Appendices A and B, respectively. The functions which describe the optimal singular control during climb are defined in Appendix C. The optimized standard climb and descent procedures are included in Appendix D.

2 Literature Review

Different classifications of optimization problems can be considered. Biegler and Grossmann [8] propose a possible classification attending to the nature of the *decision variables*. In this sense, there are *parametric optimization problems*, commonly referred to as programming problems (in which each variable can only have a single value from a given set), *optimal control problems*, commonly referred to as trajectory optimization problems (which usually correspond to dynamic systems in which the decision variables are functions of the independent variable, for instance, time), and *stochastic optimization problems* (in which the variables are defined by probability functions). Aircraft trajectory optimization can be considered as an optimal control problem in which the control variables are time varying. As a consequence, the present thesis is not addressing parametric nor stochastic optimization problems.

In this chapter, an overview of references in optimal control theory is first addressed, including works related to singular optimal control problems and optimal control for switched control systems. Then, a review of the state of the art in numerical methods for trajectory optimization is included. Finally, a review in aircraft trajectory optimization is presented.

2.1 Optimal Control

Many authors agree on considering the optimal control as an extension of the calculus of variations, among which Sussman and Willems [72] and Bryson [16], both citing the work of Goldstine [35], regarding the history of the calculus of variations from its beginnings to the Chicago school in the early 20th century.

Sussman and Willems [72] address the historical evolution of the optimal control from what they consider its origin: the publication of the solution to the Brachistochrone problem in 1697 by Johann Bernoulli. They defend that the early contributions of Leibniz, Jacob Bernoulli, Tschirnhaus, L'Hôpital and Newton paved the way for the optimal control to be born. They also remark, first, the key role performed by Euler, Lagrange and Legendre in setting up the classical theory of the calculus of variations; second, the advantages behind the reformulation proposed by Hamilton; third, the important advances made by Wierstrass; and finally, the formal appearance of the optimal control, thanks to the statement of the Maximum Principle by Pontryagin and his group.

Bryson [16] addresses optimal control developments from 1950 to 1985. He points out that optimal control has also roots in some other scientific fields (not only calculus of variations), such as classical control theory, random processes theory and parametric optimization theory

(linear and nonlinear programming).

There exist plenty of books addressing optimal control theory, from which one can stand out those from Athans and Falb [2], Bryson and Ho [15], Leitmann [41], Ben-Asher [6], Speyer and Jacobson [71], and Clarke [24].

2.1.1 Singular Optimal Control

Following the definition from Ben-Asher [6], *singular optimal control problems* are a subclass of optimal control problems in which the Hamiltonian minimization condition (see Chapter 3) does not yield a definite value for the control. This type of problems arises, in particular, when the Hamiltonian is linear on the control variable. Bell and Jacobson [4] give insight into the theory of singular optimal control, addressing necessary conditions for optimality of this type of problems.

Singular optimal control theory has been used, among other works, to analyze maximum-range cruise at constant altitude (Pargett and Ardema [51] and Rivas and Valenzuela [55]), minimum fuel cruise at constant altitude with fixed arrival time (Franco et al. [30] and Franco et al. [33], the latter in the presence of a constant wind), minimum-cost cruise including both the DOC and the arrival-error cost associated to not meeting the scheduled time of arrival (Franco and Rivas [31]), maximum-range unpowered descents in the presence of altitude dependent winds (Franco et al. [32]) and fuel-optimal fixed-rating climbs in the presence of altitude dependent winds (Franco et al. [34]).

2.1.2 Optimal Control for Switched Dynamical Systems

In this work the theory of optimal control for *switched dynamical systems* is applied. Optimal control problems of switched dynamical systems are contained into a broader class of problems called hybrid optimal control problems. Branicky et al. [12] propose a very general framework that systematizes the notion of a hybrid system. They introduce a mathematical model of hybrid systems as interacting collections of dynamical systems, evolving on continuous-variable state spaces and subject to continuous controls and discrete transitions. Hybrid systems can be seen as a generalization of the concept of multiprocesses, previously stated by Clarke and Vinter [23].

Numerous authors (among which Sussmann [73], Riedinger et al. [54], Caines et al. [19], and Shaikh and Caines [62]), have developed necessary conditions for optimality, in the form of a maximum principle for hybrid optimal control problems. They address different cases such as fixed and variable time interval problems ([73, 54]), and with and without pathwise state constraints ([19]). Shaikh and Caines [62] also present algorithms for hybrid systems optimization. Dimitruk and Kaganovich [27] state that results in Sussmann [73] (and, by extension, the maximum principle for hybrid optimal control) cannot be recognized as a new independent result, but as a direct application of the original Pontryagin maximum principle to an appropriately transformed problem.

As Xu and Antsaklis [83] pointed out, the feature distinguishing a switched system from a general hybrid system is that its continuous state does not exhibit jumps at the switching instants. Such a feature makes the computation of continuous inputs amenable via the

usage of conventional optimal control methods, such as those methods developed for singular optimal control problems.

2.2 Numerical Methods for Trajectory Optimization

There exist several techniques for numerically solving trajectory optimization problems. According to numerous authors (Von Stryk and Bulirsch [80], Betts [7] and Rao [53], among many others) the methods most widely used today can be classified into two broad categories, *indirect methods* and *direct methods* depending on whether or not they explicitly consider the necessary conditions for optimality. Direct and indirect methods can also be classified into *shooting methods* and *transcription methods* (also called *collocation methods*). On one hand, shooting methods are characterized by performing an initial value problem (IVP) at each iteration step and by defining, as decision variables, those needed to perform that IVP. On the other hand, transcription or collocation methods define, as decision variables, the values of continuous variables (state, control and, eventually, adjoints) at some time instants called nodes, approximate these continuous variables by a piecewise continuous interpolant polynomial and enforce the satisfaction of the differential equations at some points between each pair of contiguous nodes.

Some other methods such as those based on dynamic programming and direct search have been also developed, although these are generally not computationally competitive with direct and indirect methods. Betts [7] provides an excellent survey of numerical methods for trajectory optimization, focusing on direct and indirect methods, and including practical examples and main issues of them. Some remarkable aspects of the research therein are highlighted in the sections below.

2.2.1 Direct Methods

Direct methods do not require an analytical expression for the necessary conditions for optimality and, hence, do not involve definitions of adjoint variables as well as initial guesses for them. Instead, the dynamic variables (state and control) are adjusted to directly optimize the objective function. All direct methods introduce some parametric representation for the control variables (and, possibly, for the sate variables). Hence, the original optimal control problem, which can be seen as an infinite dimensional optimization problem, is transformed into a finite dimensional optimization problem, which in general is a nonlinear programming (NLP) problem.

For simple shooting, the control variables are defined by a relatively small number of NLP variables. For direct multiple shooting and direct transcription methods the number of NLP variables used to describe the control increases, ultimately including values at each mesh point of the integration interval.

Advantages and disadvantages of direct methods are the disadvantages and advantages, respectively, of the indirect methods explained in the following section.

2.2.2 Indirect Methods

Indirect methods are characterized by explicitly considering the necessary conditions for optimality, which are stated in terms of the adjoint differential equations, the Maximum Principle, and the transversality conditions. Hence, the dynamic variables (state and control) are adjusted to satisfy optimality conditions instead of to directly optimize the objective function. In general, and depending on the optimal control problem, the indirect approach can lead to stating a nonlinear two-point or multipoint boundary value problem, which can be solved by a simple shooting, a multiple shooting or a transcription method. Hence, to solve the original optimal control problem it is necessary to solve a system of nonlinear equations.

On one hand, there are three main disadvantages of using indirect methods.

First, in order to implement an indirect method it is necessary to previously derive analytic expressions for the necessary conditions of optimality. This can be difficult to perform and automatize, specially when nonlinear systems with complicated dynamics or constraints are considered.

Second, when indirect methods are applied to problems with path inequalities or to singular optimal control problems one has to impose the sequence of constrained and unconstrained subarcs or the sequence of bang and singular arcs. Special intuition regarding the particular problem being solved (for instance, based on previous pieces of research or on the results form applying a direct method) is necessary, because the solution structure is a priori unknown, in general.

Third, the resolution of optimal control problem by means of an indirect method implies, as previously mentioned, solving a system of nonlinear equations with, in most cases, poor convergence properties. The region of convergence is very small, specially when it is necessary to guess values for the adjoints variables, which may not have an obvious physical interpretation and whose dynamics exhibits an unstable behavior.

On the other hand, there is an important advantage of using indirect methods: the accuracy of the solution is higher than with direct methods. In fact, since the solution structure is directly involved in the method, discontinuities in the control function at junction points (when entering or leaving a path constraint or a singular arc) can be easily taken into account.

2.2.3 Other Methods

Methods based on dynamic programming, also called extremal field methods, rely on a necessary condition for optimality consisting of a system of first-order partial differential equations known as the Hamilton-Jacobi-Bellman equation (see Bellman [5]). Dynamic programming has been successfully applied to discrete optimal control problems, as well as to special classes of continuous optimal control problems for which there is an analytical solution of the HJB equation (linear systems with quadratic costs). However, for solving nonlinear continuous optimal control problems, dynamic programming can hardly be used as the basis for a viable numerical method due to the curse of dimensionality. This term means that, as the time, state and control have to be sampled, the computational complexity increases exponentially with the dimensions of the state and control.

Methods based on direct search can be considered as a special class of direct methods in which the original optimal control problem is transformed into a nonlinear programming problem (as in the rest of direct methods) but the resolution proposed do not make use of derivatives. Instead, the basic notion of evolutionary algorithms (such as genetic algorithm and particle swarm method), simulated annealing, tabu search and Monte Carlo method is to randomly select values for the unknown variables. When a sufficiently high number of random samples have been taken, the best one is considered the solution. These methods are very attractive because they are very easy to apply. Nevertheless, since less information about the function being minimized is used (as they do not compute gradients), methods based on direct search are not computationally competitive with respect to direct and indirect methods.

2.3 Aircraft Trajectory Optimization

Aircraft trajectory optimization is, from the operational point of view, a subject of great importance in air traffic management (ATM), that aims at defining optimal flight procedures for the given aircraft mission that lead to energy-efficient flights and enable for optimality assessment of standard flight procedures.

In order to optimize an aircraft trajectory one must take into account that it is composed of different flight phases (see Torenbeek [75]): take off, climb, cruise, descent, loiter, approach and landing. In each one, equations of motion can be different from one another. In a sufficiently simple but fairly general model, a global trajectory is formed by a climb phase, a cruise phase and a descent phase. The next step in complexity could be to split the cruise phase into two different ones by adding an intermediate climb phase. In that case the global trajectory would be formed by an initial climb phase, a first cruise phase, a climb between the two cruise levels, a second cruise phase and a descent. For any given solution structure (i.e., sequence of flight phases), optimizing global trajectories implies not only addressing each flight phase (as many authors have already done), but also taking into account the interactions among them as well as looking for a global objective.

In practice, the airlines consider a cost index (CI) and define the direct operating cost (DOC) as the combined cost of fuel consumed and flight time weighted by the CI. Their goal is to minimize the DOC of the global trajectory.

2.3.1 Global Trajectory Optimization

Before the seventies, there are not many works about global-trajectory optimization. As pointed out by Schultz and Zagalsky [60], previous works focus on optimizing one trajectory phase, with the exception of Bryson et al. [14], who studied climb-descent trajectories by using the *energy-state approximation*. This approach is characterized by considering, on one hand, the specific energy as a state variable and the speed as the control variable, and, on the other hand, that kinetic and potential energy interchanges are instantaneous (leading to discontinuities in speed and altitude laws).

From then on, different authors have addressed minimum-DOC problem for global trajectories. Barman and Erzberger [3] and Erzberger and Lee [28] analyze minimum-DOC problem for global trajectories (climb-cruise-descent), considering steady cruise and taking

the aircraft mass as constant. In particular, Erzberger and Lee [28] consider an altitude-dependent horizontal wind, although they do not take into account the acceleration term in the dynamic equation, so that equations of motion are the same as with a constant wind. Burrows [17] also analyzes minimum-DOC problem for global-trajectories, without the assumption of constant mass, but with the assumption that the cruise phase takes place in the stratosphere.

Some other authors have studied minimum-fuel-consumption global trajectories, which can be thought of as a particular case of minimum-DOC global trajectories with CI equals zero. For example, Schultz and Zagalsky [60] address minimum-fuel-consumption problem for global trajectories considering steady cruise and constant mass. Zagalsky et al. [84] analyze minimum-fuel-consumption problem for global trajectories considering the energy-state approximation and constant mass. They find the velocity set to be nonconvex, which implies first that optimal control solutions only contain full-powered climbs and unpowered descents, and second, that certain suboptimal solutions containing a minimum-fuel cruise segment attain fuel economies superior to any optimal control solution. Newman and Kreindler [49] study minimum-fuel, three-dimensional flight paths; non-turning paths (in a vertical plane) are considered as a particular case. Control variables are the thrust, the path angle and the bank angle. They show that for the most part of the trajectory the flight path angle is a singular control. The main simplifications are constant aircraft mass and constant thrust for each power setting. Only short (up to 50 nmi), low-altitude (below 10000 ft) flights are considered. Final values of altitude and speed are given, whereas the final time and the final horizontal distance travelled are unspecified. A comparison with non-optimal standard climbs is also performed.

Sorensen and Waters [68], Burrows [18], Chakravarty [21] and Williams [81] analyze minimum-fuel-consumption trajectories with fixed arrival time as minimum-DOC trajectories with free final time (the problem is to find the time cost for which the corresponding free final time DOC-optimal trajectory arrives at the assigned time); the two last authors address the problem by considering a minimum-DOC steady cruise as the outer solution of a singular perturbation solution for the global trajectory. Burrows [18] considers a general point-mass model and a constant wind throughout the entire trajectory and, although a variable-mass model is considered, only presents results for the constant-mass case. Chakravarty [21] considers a simpler model (by using the *energy-state approximation*), obtains as a result a quasi-steady cruise with altitude and speed varying as mass diminishes, and analyzes the effects of an altitude-dependent horizontal wind on cruise-descent trajectories (although, as in Ref. [28], the acceleration term in the dynamic equation is neglected). Williams [81] also addresses that problem, analyzing the effects of mismodeled constant winds in a scenario formed by the final cruise and the descent phases, although wind effects on the whole cruise phase are not considered.

Chakravarty [22] and Liden [42] analyze minimum-cost global trajectories (climb-cruise-descent), considering not only the DOC but also the arrival-error cost which takes into account some other factors such as crew overtime cost, passenger dissatisfaction cost and losses due to missed connections. They also describe procedures to select the best CI based on what they call optimal flight schedule, and consider different wind conditions.

Recently, Soler et al. [67] address minimum-fuel-consumption trajectories composed of seven flight phases (takeoff, initial climb, climb, cruise, descent, approach and landing) by using a hybrid optimal control approach in which the phase sequence is predefined but the switching times are included as unknown variables. The resolution method employed is a direct collocation method or direct transcription method, which transforms the original trajectory optimization problem into a non-linear programming problem (that is, into a parametric optimization problem).

Nevertheless, some authors have exclusively addressed a single flight phase in the sense that they have optimized one phase, not only without taking into account the interactions among the different phases, but also considering different performance indices.

2.3.2 Climb Phase Optimization

In the optimization of the climb flight of commercial aircraft, the objective is to minimize the economical and environmental impacts, by defining the best flight procedure for the given aircraft mission. Depending on the mission, different performance indices can be considered (such as minimum time, minimum fuel consumption or minimum emissions).

Minimum-time climb deserved great attention in the early works on trajectory optimization, especially for supersonic aircraft, see for example the works of Bryson and Denham [13] and Vincent et al. [77, 78], in which thrust is given and the angle of attack (or the lift coefficient) is taken as control variable, and the work of Bryson et al. [14]. In this work, the energy-state approximation is used, with the speed as control variable; the solution is formed by a central path and, depending on the initial and final conditions, by zoom climbs or zoom dives with constant energy (performed instantaneously). These works also review the early work (made in the 1950's) on trajectory optimization.

Minimum-fuel climb in a vertical plane between two given points (given speed and altitude, V_i, h_i and V_f, h_f) has been analyzed by Miele [47] using a method based on Green's theorem, in the case of given thrust (depending both on speed and altitude), using the limiting constraint $h_i \leq h \leq h_f$, and with the simplification of constant aircraft mass. The solution is formed by a central climbing path and two accelerations at constant altitude (at h_i and h_f). This problem is also analyzed by Bryson et al. [14] in the case of supersonic aircraft, using the energy-state approximation, with the speed as control variable; the solution structure is the same (zoom-central-zoom) as for the minimum-time problem, although the central path is different.

Some authors optimize the climb as part of a global climb-cruise-descent trajectory in a vertical plane (see for example the works of Schultz and Zagalsky [60], Barman and Erzberger [3], Erzberger and Lee [28] and Burrows [17, 18]), considering different performance indices, such as minimum direct operating cost and minimum fuel consumption with fixed arrival time. In all these cases the final range is fixed, and thrust is used as a control variable. In some of these works the formulation is simplified by taking the aircraft mass as constant, or by taking the lift equal to the constant weight in the calculation of the aerodynamic drag. More recently, climb (and descent) optimization to reduce noise at small altitudes has been given special attention (see the works of Visser and Wijnen [79], Ho and Clarke [37], Torres et al. [76]), with the goal of defining noise abatement procedures.

In the previous works, wind effects are not taken into account. Wu and Zhao [82] optimize climb trajectories considering different performance indices and wind effects; although the nominal wind is zero, sensitivities with respect to wind uncertainties are analyzed. In this analysis, lift coefficient and thrust are taken as control variables, and the formulation is simplified by considering constant specific fuel consumption. The optimization is formulated as a parameter optimal control problem, in which a predefined trajectory profile (formed by a series of pre-ordered flight phases) is considered.

2.3.3 Cruise Phase Optimization

Some authors have exclusively addressed optimal aircraft cruise independently considered.

Minimum-DOC cruise has been studied by different authors. Bilimoria et al. [9] analyze the minimum-DOC steady cruise as the outer solution when applying a singular perturbation approach. They point out that non-convexity in the fuel-flow vs airspeed graph has the important consequence of defining a velocity segment that is nonoptimal, which leads to the sometime occurrence of time-shared operation between two altitude-airspeed combinations for optimal steady cruise. Franco and Rivas [31] analyze minimum-cost cruise including both the DOC and the arrival-error cost associated to not meeting the scheduled time of arrival. They obtain that, for some values of the parameters present in the problem, the solution is obtained by fixing the final time to be the scheduled time of arrival, whereas for some other values of the parameters, the solution is obtained by solving a minimum-DOC problem with free final time and a cost index different from the original one. The related problem of finding the minimum-fuel cruise at constant altitude with fixed arrival time is analyzed, among others, by Franco et al. [30] and Franco et al. [33] (the latter in the presence of a constant wind).

The particular case of minimum-fuel cruise (CI equal to zero) has been considered by others. For example, Speyer [69], Schultz [61], and Speyer [70] analyze the optimality of the steady-state cruise, taking the aircraft mass as constant. For an aircraft model where the control variables are thrust and flight path angle, Speyer [69] shows that cruise condition is a doubly singular arc which is non-minimizing because it fails to satisfy a necessary condition for optimality. For an aircraft model where the control variables are the thrust and the lift coefficient, Schultz [61] considers that the cruise solution is a thrust-singular arc and shows that, unlike with the energy state equations or with the intermediate model considered in Ref. [69], the cruise is now a minimizing-arc. In response to Ref. [61], Speyer [70] applies a frequency domain version of the Jacobi test to the Goh's transformation of a point-mass-model, and shows that the steady-state cruise is nonoptimal over long ranges because of the appearance of conjugate points. He also points out that a small-amplitude oscillatory cruise can provide slight improvements in fuel consumption with respect to steady-sate cruise. The equivalent problem of finding the maximum-range cruise at constant altitude for a fixed amount of fuel is analyzed, among others, by Pargett and Ardema [51], Rivas and Valenzuela [55], and Rivas et al. [56].

Some authors have explored nonconventional cruise, such as chattering cruise, and optimal cyclic cruise with the objective of minimizing fuel consumption per range travelled or per flight time. Houlihan et al. [38] study the minimum-fuel chattering cruise as the outer solution of

a singular perturbation solution, considering the energy-state approximation and a constant-mass model. They obtain that, when the velocity set is not convex, a chattering cruise only shows a substantial improvement with respect to steady cruise at low energy levels; therefore, from a practical point of view, chattering cruise implies at best only a small advantage over conventional cruise. Sachs and Christodoulou [59] analyze the problem of finding periodic flight paths that maximize either the ratio of the horizontal cycle range to the fuel consumed in a cycle, or the ratio of the cycle time to the fuel consumed in a cycle. They consider a constant-mass model with the throttle parameter and the lift coefficient as controls and a maximum altitude constraint. Optimal cyclic paths are obtained, which are bang-bang in the thrust and can be decomposed into two flight segments, a maximum thrust segment and a minimum thrust segment. For range maximization per fuel consumed, important improvements with respect to steady-state cruise can be achieved for low maximum altitudes and without considering compressibility effects, whereas negligible improvements are obtained if the admissible altitude is high enough and compressible effects are taken into account. Finally, Menon [46] performs an interesting survey of aircraft cruise optimization and provides further insight into minimum-fuel oscillatory cruise.

2.3.4 Descent Phase Optimization

In the optimization of the descent flight of commercial aircraft, the objective is to descend and decelerate continuously, so that the economical and environmental impacts are minimized, keeping thrust as low as possible for as long as possible. An example is the continuous descent approach (CDA) procedure (see for instance Clarke et al. [25] where the design and flight test of a CDA as a noise abatement procedure is presented).

Maximum-range glide between two given points (given speed and altitude, V_i, h_i and V_f, h_f) has been analyzed by different authors using different procedures. For instance, Miele [47] analyzes the problem using a method based on Green's theorem, using the limiting constraint $h_f \leq h \leq h_i$; the solution is formed by a central pattern and two decelerations at constant altitude (h_i and h_f). Bryson et al. [14] present an analysis using the energy-state approximation, with speed as control variable; the solution structure is the same (zoom-central-zoom) as for the climb problems. More recently, Shapira and Ben-Asher [64, 65] use singular perturbation theory, considering two and three timescales, and obtain the inner and outer solutions using optimal control theory; the inner (boundary layer) solution is characterized by an increase in altitude, a decrease in speed, and large values of flight-path angle; the outer (slow) solution is a steady-state glide; these analyses are made for the simple incompressible case of a parabolic drag polar of constant coefficients. In all these works wind effects are not taken into account; however, some other authors have taken into account wind effects when addressing descent trajectories within the context of global trajectory optimization (see Refs. [28, 18, 21]).

This page intentionally left blank

3 Formulation of the Optimal Control Problem

In this chapter, the singular optimal approach is applied to optimize aircraft trajectories. For that purpose, the formulation of an optimal control problem is first presented, including the necessary conditions for optimality and analyzing the special cases of singular optimal control problems and optimal control problems of switched systems. The explicit statement of the necessary conditions for optimality is needed because an indirect numerical method is considered. Then, the equations governing the motion of an aircraft under appropriate assumptions are included. Finally, the procedure to compute optimal aircraft trajectories developed in this thesis is explained.

3.1 Optimal Control Theory

The outline of this section is as follows. First, a general formulation of an optimal control problem is presented, preceded by the definition of some standard terminology based on the works of Bryson and Ho [15] and Clarke [24]. Second, necessary conditions for a solution candidate to be optimal are included, with a formulation based on the works of Ross [58] and Clarke [24]. Third, particular considerations regarding singular optimal control problems are addressed, including additional necessary conditions for such a type of problems. Finally, an extension of the formulation of an optimal control problem to switched dynamical systems is performed including, as well, additional necessary conditions for such a type of problems.

3.1.1 Optimal Control Problem

Let consider a time interval $[t_0, t_f]$, the *dynamics function* $\mathbf{f} : [t_0, t_f] \times \mathbb{R}^n \times \mathbb{R}^m \mapsto \mathbb{R}^n$, and the *control set* $U \subset \mathbb{R}^m$. A *control* is an m-vector function on $[t_0, t_f]$ with values in U, whereas the *state*, or *state trajectory*, corresponding to the control $\mathbf{u}$ refers to a solution $\mathbf{y}$ of the initial-value problem (IVP) given by

$$\begin{aligned} &\dot{\mathbf{y}} = \mathbf{f}\left[t, \mathbf{y}\left(t\right), \mathbf{u}\left(t\right)\right], \qquad \forall t \in [t_0, t_f] \\ &\mathbf{y}(t_0) = \mathbf{y}_0 \end{aligned} \tag{3.1}$$

where $\mathbf{y}_0 \in \mathbb{R}^n$ is a prescribed initial condition, t is the time, and the dot denotes derivation with respect to t (i.e., $\dot{\mathbf{y}} = \dfrac{\mathrm{d}\mathbf{y}}{\mathrm{d}t}$). Hence, $\mathbf{y} : [t_0, t_f] \mapsto \mathbb{R}^n$ is an n-vector function with continuous components. The ordinary differential equation (ODE) system (3.1) linking the

control $\mathbf{u}$ and the state $\mathbf{y}$ is referred to as the *state equation*. The couple $(\mathbf{f}, U)$ is referred to as the *control system*. A *process* of the control system $(\mathbf{f}, U)$ is the couple $(\mathbf{y}, \mathbf{u})$ consisting of an n-vector function with continuous components $\mathbf{y}$ and an m-vector function $\mathbf{u}$ which satisfy the state equation (3.1). The cost functional $J(\mathbf{y}, \mathbf{u})$ is defined by

$$J(\mathbf{y}, \mathbf{u}) = \phi\left[t_f, \mathbf{y}(t_f)\right] + \int_{t_0}^{t_f} l\left[t, \mathbf{y}\left(t\right), \mathbf{u}\left(t\right)\right] \mathrm{d}t \tag{3.2}$$

were the *running cost* l and the *terminal cost* ϕ are given functions. In some cases, one may be interested in constraining functions of the terminal state to have prescribed values, which can be expressed as

$$\psi\left[t_f, \mathbf{y}\left(t_f\right)\right] = 0 \tag{3.3}$$

where the k-vector function $\psi : \mathbb{R} \times \mathbb{R}^n \mapsto \mathbb{R}^k$ is the *final-state-constraint function*. The particular case in which some state variables are prescribed at the final time is subsumed in the more general case addressed by Eq. (3.3).

In summary, the optimal control problem can be stated as follows:

$$\begin{aligned}
\text{Minimize} \quad & J(\mathbf{y}, \mathbf{u}) = \phi\left[t_f, \mathbf{y}(t_f)\right] + \int_{t_0}^{t_f} l\left[t, \mathbf{y}\left(t\right), \mathbf{u}\left(t\right)\right] \mathrm{d}t \\
\text{subject to} \quad & \dot{\mathbf{y}} = \mathbf{f}\left[t, \mathbf{y}\left(t\right), \mathbf{u}\left(t\right)\right], \qquad \forall t \in [t_0, t_f] \\
& \mathbf{u}(t) \in U, \qquad \forall t \in [t_0, t_f] \\
& \mathbf{y}(t_0) = \mathbf{y}_0 \\
& \psi\left[t_f, \mathbf{y}\left(t_f\right)\right] = 0
\end{aligned} \tag{3.4}$$

An *optimal process*, also called an *extremal*, is a process $(\mathbf{y}^*, \mathbf{u}^*)$ defined on the interval $[t_0, t_f]$ satisfying the constraints of Eq. (3.4) and verifying $J(\mathbf{y}^*, \mathbf{u}^*) \leq J(\mathbf{y}, \mathbf{u})$, for any other process $(\mathbf{y}, \mathbf{u})$ satisfying the aforementioned constraints, as well as $\|\mathbf{y} - \mathbf{y}^*\| \leq \epsilon$, for some $\epsilon > 0$. In this definition, $\|\mathbf{z}\|$ means the relevant supremum norm, that is, $\sup_{t \in [t_0, t_f]} |\mathbf{z}(t)|$.

Although an optimal control problem stated as in Eq. (3.4) is quite general, additional considerations can be made.

First, the final time t_f can be either specified, that is, a given parameter, or unspecified, that is, an unknown parameter whose optimal value will result from solving the optimal control problem. Although it does not imply any change in the problem formulation, it has a direct impact in the statement of the necessary conditions for optimality. Moreover, in the case of t_f unspecified, the definition of an optimal process has to be slightly modified as follows. An optimal process (equivalently, an extremal), is a process $(\mathbf{y}^*, \mathbf{u}^*)$ defined on the interval $[t_0, t_f]$, satisfying the constraints of Eq. (3.4) and verifying $J(\mathbf{y}^*, \mathbf{u}^*) \leq J(\mathbf{y}, \mathbf{u})$, for any other process $(\mathbf{y}, \mathbf{u})$ defined on the interval $[t_0, \tau_f]$ and satisfying the aforementioned constraints, as well as $|t_f - \tau_f| \leq \epsilon$ and $\|\mathbf{y} - \mathbf{y}^*\| \leq \epsilon$, for some $\epsilon > 0$.

Second, constraints that apply at intermediate points or over the whole path $t \in [t_0, t_f]$, rather than just at the end points, may also be considered. In particular, one may have integral constraints, equality or inequality constraints of functions of the control and state variables, interior point constraints, and discontinuities in the dynamics function or variables at interior points.

3.1.2 Necessary Conditions for Optimality

In this section, necessary conditions for a process $(\mathbf{y}, \mathbf{u})$ to be the solution of the optimal control problem (3.4) are presented, with a formulation based on the works of Ross [58] and Clarke [24]. These conditions are known as Pontryagin Maximum Principle, or simply Maximum Principle. In these thesis, sufficient conditions for optimality are not considered.

The Maximum Principle is a set of necessary conditions for optimality which, as Hestenes [36] pointed out, is equivalent to the conditions of Euler-Lagrange, Weierstrass and Legendre-Clebsch in the classical theory of the calculus of variations. Nevertheless, the Maximum Principle extends those conditions in a twofold way, to optimal control problems, and to problems in which the control is constrained to be in a specified control set (i.e., in the presence of control variable inequality constraints).

Let first define the Hamiltonian and the endpoint Lagrangian of the problem (3.4) as functions $H^\eta : [t_0, t_f] \times \mathbb{R}^n \times \mathbb{R}^m \times \mathbb{R}^n \mapsto \mathbb{R}$, and $E^\eta : [t_0, t_f] \times \mathbb{R}^n \times \mathbb{R}^k \mapsto \mathbb{R}$, respectively, given by

$$H^\eta(t, \mathbf{y}, \mathbf{u}, \lambda) = \eta l\,(t, \mathbf{y}, \mathbf{u}) + \lambda^T \mathbf{f}\,(t, \mathbf{y}, \mathbf{u}) \tag{3.5}$$

and

$$E^\eta\,[t_f, \mathbf{y}(t_f), \nu] = \eta\phi\,[t_f, \mathbf{y}(t_f)] + \nu^T \psi\,[t_f, \mathbf{y}\,(t_f)] \tag{3.6}$$

Then, assuming classical regularity of the functions involved (see Clarke [24]), the Maximum Principle can be stated as follows:

Let $(\mathbf{y}^*, \mathbf{u}^*)$ be an optimal process of the problem (3.4), where U is bounded. Then there exist an n-vector function with continuous components $\lambda : [t_0, t_f] \mapsto \mathbb{R}^n$, a scalar $\eta \geq 0$, and a multipliers vector $\nu \in \mathbb{R}^k$ satisfying the following conditions:

1) The *non-triviality condition*, that is, $(\eta, \lambda(t), \nu) \neq 0$, $\forall t \in [t_0, t_f]$.

2) The *adjoint dynamics equation*, given by

$$\dot{\lambda}(t) = -\frac{\partial H^\eta}{\partial \mathbf{y}}\,[t, \mathbf{y}^*(t), \mathbf{u}^*(t), \lambda(t)]\,, \quad \forall t \in [t_0, t_f] \tag{3.7}$$

3) The *Hamiltonian minimization condition*, which states that for the control to be optimal it must globally minimize the Hamiltonian, and hence

$$\mathbf{u}^*\,[t, \mathbf{y}^*(t), \lambda(t)] = \arg\min_{\mathbf{u} \in U} H^\eta\,[t, \mathbf{y}^*(t), \mathbf{u}, \lambda(t)]\,, \quad \forall t \in [t_0, t_f] \tag{3.8}$$

4) The *transversality conditions*, stated as

$$\lambda(t_f) = \frac{\partial E^\eta}{\partial \mathbf{y}(t_f)}\,[t_f, \mathbf{y}^*(t_f), \nu] \tag{3.9}$$

to which one has to add, if the final time is unspecified, another transversality condition called the *Hamiltonian value condition* and given by

$$H^\eta\,[t_f, \mathbf{y}^*(t_f), \mathbf{u}^*(t_f), \lambda(t_f)] = -\frac{\partial E^\eta}{\partial t_f}\,[t_f, \mathbf{y}^*(t_f), \nu] \tag{3.10}$$

Furthermore, the minimized Hamiltonian $\mathcal{H}^\eta : [t_0, t_f] \times \mathbb{R}^n \times \mathbb{R}^n \mapsto \mathbb{R}$, defined as

$$\mathcal{H}^\eta(t, \mathbf{y}, \lambda) = \min_{\mathbf{u} \in U} H^\eta(t, \mathbf{y}, \mathbf{u}, \lambda) \tag{3.11}$$

evolves according to the *Hamiltonian evolution equation*, given by

$$\dot{\mathcal{H}}^{\eta}\left[t, \mathbf{y}^{*}(t), \lambda(t)\right] = \frac{\partial H^{\eta}}{\partial t}\left[t, \mathbf{y}^{*}(t), \mathbf{u}^{*}(t), \lambda(t)\right], \quad \forall t \in [t_0, t_f] \tag{3.12}$$

If the problem is autonomous, Eq. (3.12) reduces to the *Hamiltonian constancy condition* stating that, for some constant $\overline{\mathcal{H}}$, one has

$$H^{\eta}\left[t, \mathbf{y}^{*}(t), \mathbf{u}^{*}(t), \lambda(t)\right] = \overline{\mathcal{H}}, \quad \forall t \in [t_0, t_f] \tag{3.13}$$

Moreover, if the final time is unspecified, the Hamiltonian value condition provides $\overline{\mathcal{H}} = 0$.

In these necessary conditions, λ is known as *adjoint* or *costate*, whereas the components of the constant vector ν are referred to as the *final-state Lagrange multipliers*. The *cost multiplier* η is introduced to include the *abnormal case*, in which $\eta = 0$. The abnormal case arises when the constraints are so restrictive as to identify the optimal solution regardless of the running cost $l\left[t, \mathbf{y}\left(t\right), \mathbf{u}\left(t\right)\right]$ and the terminal cost $\phi\left[\mathbf{y}(t_f), t_f\right]$. For the *normal case*, the constancy and non-negativity of η leads to consider $\eta = 1$ without loss of generality, as η simply scales the Hamiltonian; this is called the *normality condition*.

The Hamiltonian minimization condition, whose solution is symbolically stated in the form of Eq. (3.8), can be posed as a problem in itself, given by (see Ross [58])

$$\begin{aligned} &\text{Minimize} \quad H^{\eta}\left(t, \mathbf{y}, \mathbf{u}, \lambda\right) \\ &\text{subject to} \quad \mathbf{u} \in U \end{aligned} \tag{3.14}$$

for every $t \in [t_0, t_f]$.

The convexity condition for problem (3.14) is given by

$$\frac{\partial^2 H^{\eta}}{\partial \mathbf{u}^2}\left[t, \mathbf{y}^{*}(t), \mathbf{u}^{*}(t), \lambda(t)\right] \geq 0, \quad \forall t \in [t_0, t_f] \tag{3.15}$$

which is known as the *Legendre-Clebsch condition*.

Furthermore, when the optimal control is interior to the set U (i.e. $\mathbf{u}^{*}(t) \in intU$, $\forall t \in [t_0, t_f]$), the stationarity condition for problem (3.14) is given by

$$\frac{\partial H^{\eta}}{\partial \mathbf{u}}\left[t, \mathbf{y}^{*}(t), \mathbf{u}^{*}(t), \lambda(t)\right] = 0, \quad \forall t \in [t_0, t_f] \tag{3.16}$$

which is known as the *Euler-Lagrange condition*. This equation allows for the determination of $\mathbf{u}^{*}$, provided that the Hessian of the Hamiltonian $H^{\eta}_{\mathbf{uu}}\left(t, \mathbf{y}, \mathbf{u}, \lambda\right)$ is not singular. In a more general case in which the control constraints may be active in some portions of the optimal process, (3.14) is a nonlinear programming problem. In particular, when $\mathbf{u}$ is scalar (namely u) and the set U is given by $U = \{u \in \mathbb{R} : u_{min} \leq u \leq u_{max}\}$, the Karush-Kuhn-Tucker conditions applied to the problem (3.14) provide:

$$\begin{cases} u^{*}(t) = u_{max} & \text{if} \quad \dfrac{\partial H^{\eta}}{\partial u}\left[t, \mathbf{y}^{*}(t), u^{*}(t), \lambda(t)\right] \leq 0 \\ \dfrac{\partial H^{\eta}}{\partial u}\left[t, \mathbf{y}^{*}(t), u^{*}(t), \lambda(t)\right] = 0 & \text{if} \quad u_{min} < u^{*} < u_{max} \\ u^{*}(t) = u_{min} & \text{if} \quad \dfrac{\partial H^{\eta}}{\partial u}\left[t, \mathbf{y}^{*}(t), u^{*}(t), \lambda(t)\right] \geq 0 \end{cases} \tag{3.17}$$

for every $t \in [t_0, t_f]$.

According to the Maximum Principle, once the optimal control is obtained, then it can be substituted into the state and adjoint differential equations, leading to a $2n$ system of ordinary differential equations with boundary conditions given by the combination of prescribed initial state, final-state constraint and transversality conditions. Boundary conditions add up to $2n+k$ equations, but with k additional unknown final-state multipliers that can be eliminated (in principle) form these, leading to $2n$ boundary conditions for a $2n$ system that, hence, can be solved (again, in principle) in order to obtain an extremal. Note that if the final time is unspecified one has an additional unknown t_f and an additional transversality condition (the Hamiltonian value condition), which lead to $2n+1$ boundary conditions for a $2n$ system with 1 unknown parameter.

In the subsequent sections, only the normal case is considered, and H and E are written for H^1 and E^1, respectively.

3.1.3 Singular Optimal Control

According to Bell and Jacobson [4], a singular optimal process is one for which the Legendre-Clebsch necessary condition (3.15) is not satisfied with strict inequality, or equivalently, the $m \times m$ determinant $|H_{\mathbf{uu}}|$ vanishes at any point along it. In this thesis only the case in which the Hamiltonian is a linear function on $\mathbf{u}$ is considered, as it is the most common case in which singular optimal problems arise in applications (see Bryson [15]). In that case, the derivative $H_{\mathbf{u}}(t, \mathbf{y}, \lambda)$, commonly known as the *switching function* $S(t, \mathbf{y}, \lambda)$, does not depend on $\mathbf{u}$ and represents the vector of coefficients of these linear terms. In this section, a scalar control is considered ($m = 1$, $\mathbf{u} = u$) and the set U is given by $U = \{u \in \mathbb{R} : u_{min} \leq u \leq u_{max}\}$.

In singular optimal control problems, the switching function may vanish over a finite time interval, that is, $S(t, \mathbf{y}, \lambda) = 0$ for $t \in [\tau_1, \tau_2] \subseteq [t_0, t_f]$, defining a portion of the optimal process referred to as a *singular arc*. If that happens, the optimal control along the singular arc, known as *singular control* $u_{sing}(t, \mathbf{y}, \lambda)$, is not determined by the Hamiltonian minimization condition. This can be understood by particularizing Eq. (3.14) for a singular optimal problem with a scalar control, which gives

$$u^* = \begin{cases} u_{max} & \text{if} \quad S[t, \mathbf{y}^*(t), \lambda(t)] < 0 \\ u_{sing}[t, \mathbf{y}^*(t), \lambda(t)] & \text{if} \quad S[t, \mathbf{y}^*(t), \lambda(t)] = 0 \quad \text{over a finite time interval} \\ u_{min} & \text{if} \quad S[t, \mathbf{y}^*(t), \lambda(t)] > 0 \end{cases} \tag{3.18}$$

for every $t \in [t_0, t_f]$. The singular control is determined, instead, by the requirement that the switching function remains zero on the singular arc, which implies that also the time derivatives of the switching function must vanish.

Thus, on one hand, there is one equation defining the singular control

$$\frac{\mathrm{d}^{2\xi} S}{\mathrm{d}t^{2\xi}}(t, \mathbf{y}, u_{sing}, \lambda) = 0 \tag{3.19}$$

where ξ is the order of the singular arc. Note that, in general, the order of the singular arc is ξ when the lowest-order time derivative in which u appears explicitly is of order 2ξ, as defined in Ref. [4]. Kelley et al. [40] demonstrate that u cannot first appear in an odd-order derivative; hence the order ξ is an integer number.

On the other hand, 2ξ equations have to be satisfied along the singular arc

$$\begin{aligned} &S\left[t, \mathbf{y}^*(t), \lambda(t)\right] = 0 \\ &\frac{\mathrm{d}^j S}{\mathrm{d}t^j}\left[t, \mathbf{y}^*(t), \lambda(t)\right] = 0 \qquad \text{for } j = 1, ..., 2\xi - 1 \end{aligned} \tag{3.20}$$

for every $t \in [\tau_1, \tau_2]$. As a consequence, singular arcs are not possible at any point of the $(t, \mathbf{y}, \lambda)$ space of dimension $2n + 1$, but they are restricted to a manifold, referred to as a *singular surface* (see Bryson and Ho [15]). The singular surface is in fact the locus of possible points in the aforementioned space on which optimal paths can lie, as well as a switching boundary for the optimal control (see Ben-Asher [6]).

For singular optimal problems of autonomous systems, a remark regarding the dimension of the singular surface can be made. The Hamiltonian constancy condition adds, in general, an extra equation (which makes $2\xi + 1$ equations defining the singular arc) and an extra unknown parameter $\overline{\mathcal{H}}$. Thus, the singular surface can be seen to belong to a uniparametric family of surfaces of dimension $2(n - \xi) - 1$. If the final time is unspecified, there is no unknown, since $\overline{\mathcal{H}} = 0$, so that one simply has a singular surface of dimension $2(n - \xi) - 1$.

Hence, for $n = 3$ and $\xi = 1$, the previous analysis shows that, in general, the singular arc is defined by three equations involving an unknown parameter, which define a uniparametric family of singular surfaces of dimension 3. As a consequence, it may not be possible to define a singular surface exclusively contained in the state space, but those three equations are enough to define the three adjoints along the singular arc in terms of the state variables, and thus, in combination with Eq. (3.19), one obtains a feedback control law (control variable as function of the state variables) that can be directly used to guide the aircraft along the optimal path.

3.1.3.1 Additional Necessary Conditions for Optimality

A remarkable consequence of the singularity of H_{uu} is that additional necessary conditions for optimality must be satisfied in order both, for a singular extremal to be minimizing, and for the junctions between singular and nonsingular arcs to be optimal.

On one hand, the *generalized Legendre-Clebsch condition* (see Kelley et al. [40]), also known as Kelley-Contensou test, establishes that for the singular control to be optimal one must have

$$(-1)^{\xi} \frac{\partial}{\partial u}\left(\frac{\mathrm{d}^{2\xi} S}{\mathrm{d}t^{2\xi}}\right) \geq 0 \tag{3.21}$$

In particular, when $\xi = 1$, this necessary condition for the optimality of the singular control reduces to

$$-\frac{\partial \ddot{S}}{\partial u} \geq 0 \tag{3.22}$$

On the other hand, McDanell and Powers [45] prove that, for the optimality of junctions between singular and nonsingular arcs, the following necessary condition must be satisfied: the sum of the order of the singular arc (ξ) and the lowest-order time derivative of the control which is discontinuous at the junction (ζ) must be an odd integer if the strengthened generalized Legendre-Clebsch condition is satisfied at the junction and if the control is piecewise analytic in a neighborhood of the junction. In particular, this necessary condition is satisfied

when the order of the singular arc is $\xi = 1$, and the lowest-order time derivative of the control which is discontinuous at the junction is $\zeta = 0$ (that is, the control itself is discontinuous at the junction).

Moreover, one has that at the junctions where the control variable were discontinuous, the adjoint variables, the Hamiltonian and the switching function should all be continuous in order for the Weierstrass-Erdman corner conditions to be satisfied (see Ref. [15]).

3.1.4 Optimal Control for Switched Systems

Switched systems usually refer to the class of hybrid systems in which there are no discontinuities (jumps) in the state at the switching times (see Xu and Antsaklis [83]). Therefore, a switched control system consists of an indexed set of dynamical control subsystems, whose elements are formed by the couple $(\mathbf{f}_q, U_q)$, and a set of constraints in the endpoints of the state trajectories (state continuity).

In the previous definition, $\mathbf{f}_q : [t_0, t_f] \times \mathbb{R}^n \times \mathbb{R}^{m_q} \mapsto \mathbb{R}^n$ and $U_q \subset \mathbb{R}^{m_q}$ are the dynamics function and the control set, respectively, in the phase $q \in Q$, where Q is the set of possible discrete phases.

The input for a switched control system comprises the three following elements: the phase sequence (also referred to as the switching sequence) $\sigma = (q_1, ..., q_N)$, where $q_j \in Q$ for $j = 1, ..., N$ and N is the number of phases considered; the sequence of switching times $\tau = (t_0, ..., t_N)$, where $t_N = t_f$ and the number of switchings is $N - 1$; and the sequence of control functions at each phase, $\mathbf{u}_{q_j}$. If the phase sequence is $\sigma = (q_1, ..., q_N)$ and the sequence of switching times is $\tau = (t_0, ..., t_N)$, the dynamical control subsystem q_j is active during the time interval $[t_{j-1}, t_j)$ ($[t_{N-1}, t_N]$ if $j = N$).

According to Branicky et al. [12], the nature of the discrete phenomenon underlying the switching law leads to define different types of switchings for hybrid systems: autonomous switching, autonomous impulse, controlled switching and controlled impulse. For switched systems, in which state discontinuities are not allowed, only autonomous switching and controlled switching can happen. A switching is said to be autonomous if it takes place when the state enters a prescribed manifold in the state space, whereas it is said to be controlled if it takes place in response to a control command. In this thesis, only the case in which one is allow to pick among the set of control subsystems is considered; hence, the subsequent formulation is restricted to controlled switchings.

The control in the phase q_j is an m_{q_j}-vector function on $[t_{j-1}, t_j)$ with values in U_{q_j}, whereas the state in the phase q_j corresponding to the control $\mathbf{u}_{q_j}$ refers to a solution $\mathbf{y}_{q_j}$ of the IVP given by

$$\begin{aligned} &\dot{\mathbf{y}}_{q_j} = \mathbf{f}_{q_j}[t, \mathbf{y}_{q_j}(t), \mathbf{u}_{q_j}(t)], \qquad \forall t \in [t_{j-1}, t_j) \\ &\mathbf{y}_{q_j}(t_{j-1}) = \mathbf{y}_{q_j, j-1} \end{aligned} \tag{3.23}$$

The initial value $\mathbf{y}_{q_j,j-1}$ is given by $\mathbf{y}_{q_1,0} \doteq \mathbf{y}_0$ for $j = 1$, where $\mathbf{y}_0$ is the prescribed initial value, and by

$$\mathbf{y}_{q_j,j-1} = \lim_{t \to t_{j-1}} \mathbf{y}_{q_{j-1}}(t) \tag{3.24}$$

for $j = 2, ..., N$. As a consequence, the state $\mathbf{y} : [t_0, t_f] \mapsto \mathbb{R}^n$, defined as $\mathbf{y}(t) = \mathbf{y}_{q_j}(t)$,

$\forall t \in [t_{j-1}, t_j)$ ($[t_{N-1}, t_N]$ if $j = N$) for $j = 1, ..., N$, is an n-vector function with continuous components.

The cost functional $J(\mathbf{y}, \mathbf{u}_1, ..., \mathbf{u}_N)$ is defined by

$$J(\mathbf{y}, \mathbf{u}_1, ..., \mathbf{u}_N) = \phi\left[t_f, \mathbf{y}(t_f)\right] + \sum_{j=1}^{N} \int_{t_{j-1}}^{t_j} l_{q_j}\left[t, \mathbf{y}\left(t\right), \mathbf{u}_{q_j}\left(t\right)\right] \mathrm{d}t \tag{3.25}$$

were the running cost in the phase q_j, l_{q_j}, and the terminal cost ϕ are given functions. Note that no switching cost is considered in this thesis. A final-state constraint as Eq. (3.3) can also be taken into account.

In this thesis, only multiphase optimal control problems in the sense of Soler et al. [67] are considered. These are optimal control problems of switched dynamical control systems in which the number of switchings (equivalently the number of phases N) and the phase sequence σ (the sequence of active dynamical subsystems) are predefined.

In summary, the multiphase optimal control problem can be stated as follows:

$$\begin{aligned}
\text{Minimize} \quad & J(\mathbf{y}, \mathbf{u}_1, ..., \mathbf{u}_N) = \phi\left[t_f, \mathbf{y}(t_f)\right] + \sum_{j=1}^{N} \int_{t_{j-1}}^{t_j} l_{q_j}\left[t, \mathbf{y}\left(t\right), \mathbf{u}_{q_j}\left(t\right)\right] \mathrm{d}t \\
\text{subject to} \quad & \dot{\mathbf{y}} = \mathbf{f}_{q_j}[t, \mathbf{y}_{q_j}\left(t\right), \mathbf{u}_{q_j}\left(t\right)], \quad \forall t \in [t_{j-1}, t_j), \quad j = 1, ..., N \\
& \mathbf{u}_{q_j}(t) \in U_{q_j}, \quad \forall t \in [t_{j-1}, t_j), \quad j = 1, ..., N \\
& \mathbf{y}(t_0) = \mathbf{y}_0 \\
& \psi\left[t_f, \mathbf{y}\left(t_f\right)\right] = 0 \\
\text{for a given} \quad & \sigma = (q_1, ..., q_N), \quad q_j \in Q, \quad j = 1, ..., N
\end{aligned} \tag{3.26}$$

The concept of optimal process or extremal can be readily extended to multiphase optimal control problems. An optimal multiprocess is a multiprocess $(\mathbf{y}^*, \mathbf{u}_1^*, ..., \mathbf{u}_N^*)$ defined on the interval $[t_0, t_f]$ satisfying the constraints of Eq. (3.26) and verifying $J(\mathbf{y}^*, \mathbf{u}_1^*, ..., \mathbf{u}_N^*) \leq J(\mathbf{y}, \mathbf{u}_1, ..., \mathbf{u}_N)$, for any other multiprocess $(\mathbf{y}, \mathbf{u}_1, ..., \mathbf{u}_N)$ satisfying the aforementioned constraints, as well as $\|\mathbf{y} - \mathbf{y}^*\| \leq \epsilon$, for some $\epsilon > 0$.

3.1.5 Necessary Conditions for Optimality in Switched Systems

In this section, necessary conditions for a multiprocess $(\mathbf{y}, \mathbf{u}_1, ..., \mathbf{u}_N)$ to be the solution of the multiphase optimal control problem (3.26) are presented, with a formulation based on the previous one in 3.1.1. These conditions are known as Hybrid Maximum Principle. In this thesis, sufficient conditions for optimality are not considered.

The Hybrid Maximum Principle is a set of first order necessary conditions for optimality relating to how to select continuous variables in a hybrid optimal control problem in such a way that optimizes the cost function for a fixed choice of the switching sequence. Several formulations of the Hybrid Maximum Principle can be found in works of Sussmann [73], Riedinger [54], Caines [19] and Shaikh and Caines [62]), among others. In this thesis, the Hybrid Maximum Principle is both, rewritten in terms of the formulation in Section 3.1.1, and particularized to multiphase optimal control problems introduced in Section 3.1.4, in order to obtain a Multiphase Maximum Principle.

Let first define the Hamiltonian at the phase $q_j \in Q$ of the problem (3.26) as a function $H_{q_j} : [t_{j-1}, t_j) \times \mathbb{R}^n \times \mathbb{R}^{m_{q_j}} \times \mathbb{R}^n \mapsto \mathbb{R}$, ($[t_{N-1}, t_N]$ if $j = N$) given by

$$H_{q_j}(t, \mathbf{y}, \mathbf{u}_{q_j}, \lambda) = l_{q_j}\left(t, \mathbf{y}, \mathbf{u}_{q_j}\right) + \lambda^T \mathbf{f}_{q_j}\left(t, \mathbf{y}, \mathbf{u}_{q_j}\right) \tag{3.27}$$

and second, the end endpoint Lagrangian of the problem (3.26) as a function $E : [t_0, t_f] \times \mathbb{R}^n \times \mathbb{R}^k \mapsto \mathbb{R}$ given by

$$E\left[t_f, \mathbf{y}(t_f), \nu\right] = \phi\left[t_f, \mathbf{y}(t_f)\right] + \nu^T \psi\left[t_f, \mathbf{y}\left(t_f\right)\right] \tag{3.28}$$

Note that the superscript η is no longer used because only the normal case is considered. Then, assuming classical regularity of the functions involved, the Multiphase Maximum Principle can be stated as follows.

Let $(\mathbf{y}^*, \mathbf{u}_1^*, ..., \mathbf{u}_N^*)$ be an optimal multiprocess of the problem (3.26), where U_q is bounded for any $q \in Q$, the phase sequence is defined as $\sigma = (q_1, ..., q_N)$, with $q_j \in Q$ for $j = 1, ..., N$, and N is the number of phases considered. Then there exist a piecewise continuous function $\lambda : [t_0, t_f] \mapsto \mathbb{R}^n$ and a multipliers vector $\nu \in \mathbb{R}^k$ satisfying the following conditions:

1) The non-triviality condition, that is, $(\lambda(t), \nu) \neq 0$, $\forall t \in [t_0, t_f]$.

2) The adjoint dynamics equation, given by

$$\dot{\lambda}(t) = -\frac{\partial H_{q_j}}{\partial \mathbf{y}}\left[t, \mathbf{y}^*(t), \mathbf{u}_{q_j}^*(t), \lambda(t)\right], \quad \forall t \in [t_{j-1}, t_j) \tag{3.29}$$

($[t_{N-1}, t_N]$ if $j = N$) for $j = 1, ..., N$.

3) The switching conditions regarding the adjoint variables, which state that since the states are continuous at the switching points t_j, and only controlled switchings are considered, the adjoint function verifies

$$\lambda(t_j^-) = \lambda(t_j^+) \tag{3.30}$$

for $j = 1, ..., N-1$. Hence, λ is a continuous functions for all $t \in [0, t_f]$. Note that some authors classify these conditions as transversality conditions at the switching instants, because they are associated to the constraints ensuring the state continuity at the switching points.

4) The Hamiltonian continuity condition, which states that, since the transition times t_j are not specified, the Hamiltonian is continuous at the switching instants t_j:

$$H_{q_j}\left[t_j, \mathbf{y}^*\left(t_j\right), \mathbf{u}_{q_j}^*\left(t_j\right), \lambda\left(t_j\right)\right] = H_{q_{j+1}}\left[t_j, \mathbf{y}^*\left(t_j\right), \mathbf{u}_{q_{j+1}}^*\left(t_j\right), \lambda\left(t_j\right)\right] \tag{3.31}$$

for $j = 1, ..., N-1$, where the left-hand side is defined as

$$H_{q_j}\left[t_j, \mathbf{y}^*\left(t_j\right), \mathbf{u}_{q_j}^*\left(t_j\right), \lambda\left(t_j\right)\right] = \lim_{t \to t_j} H_{q_j}\left[t, \mathbf{y}^*\left(t\right), \mathbf{u}_{q_j}^*\left(t\right), \lambda\left(t\right)\right] \tag{3.32}$$

because, with the formulation considered, H_{q_j} is not defined for $t = t_j$ and $j = 1, ..., N-1$.

5) The Hamiltonian minimization condition, which states that for the control to be optimal it must globally minimize the Hamiltonian, and hence

$$\mathbf{u}_{q_j}^*\left[t, \mathbf{y}^*(t), \lambda(t)\right] = \arg \min_{\mathbf{u}_{q_j} \in U_{q_j}} H_{q_j}\left[t, \mathbf{y}^*(t), \mathbf{u}_{q_j}, \lambda(t)\right] \tag{3.33}$$

for $j = 1, ..., N-1$.

6) The transversality conditions, stated as Eq. (3.9)

$$\lambda(t_f) = \frac{\partial E}{\partial \mathbf{y}(t_f)}\left[t_f, \mathbf{y}^*(t_f), \nu\right] \tag{3.34}$$

to which one has to add, if the final time is unspecified, the so called Hamiltonian value condition, given by

$$H_{q_N}\left[t_f, \mathbf{y}^*(t_f), \mathbf{u}^*_{q_N}(t_f), \lambda(t_f)\right] = -\frac{\partial E}{\partial t_f}\left[t_f, \mathbf{y}^*(t_f), \nu\right] \tag{3.35}$$

Furthermore, the minimized Hamiltonian at the phase $q_j \in Q$, $\mathcal{H}_{q_j} : [t_0, t_f]\times\mathbb{R}^n\times\mathbb{R}^n \mapsto \mathbb{R}$, defined as

$$\mathcal{H}_{q_j}(t, \mathbf{y}, \lambda) = \min_{\mathbf{u}_{q_j}\in U_{q_j}} H_{q_j}(t, \mathbf{y}, \mathbf{u}_{q_j}, \lambda) \tag{3.36}$$

evolves according to the Hamiltonian evolution equation, given by

$$\dot{\mathcal{H}}_{q_j}\left[t, \mathbf{y}^*(t), \lambda(t)\right] = \frac{\partial H_{q_j}}{\partial t}\left[t, \mathbf{y}^*(t), \mathbf{u}^*_{q_j}(t), \lambda(t)\right], \quad \forall t \in [t_{j-1}, t_j) \tag{3.37}$$

($[t_{N-1}, t_N]$ if $j = N$). If the problem is autonomous, Eq. (3.37) reduces to the Hamiltonian piecewise-constancy condition stating that, for some constant $\overline{\mathcal{H}}_j$, one has

$$H_{q_j}\left[t, \mathbf{y}^*(t), \mathbf{u}^*_{q_j}(t), \lambda(t)\right] = \overline{\mathcal{H}}_j, \quad \forall t \in [t_{j-1}, t_j) \tag{3.38}$$

($[t_{N-1}, t_N]$ if $j = N$) for $j = 1, ..., N$. Moreover, if the final time as well as the transition times t_j are unspecified, the Hamiltonian value condition provides $\overline{\mathcal{H}}_j = 0$ for $j = 1, ..., N$.

3.2 Equations of Motion

To describe the aircraft motion, the model adopted considers the aircraft as a point-mass with three degrees of freedom, commonly used for trajectory prediction, as indicated by Slattery and Zhao [66]. The equations describe the movement of the aircraft center of mass, considered as a mass-varying body, and are uncoupled from the rotational equations by assuming that the aircraft rotational rates are small and the control surface deflections do not affect forces.

The scalar equations of motion are formulated based on the following general assumptions:

1. The Earth is considered plane, non-rotating and an approximate inertial reference frame. The acceleration of gravity is constant and acting perpendicular to the surface of the Earth. (Flat Earth model.)
2. The aircraft is a symmetric rigid body.
3. The flight takes place in a vertical plane.
4. The aircraft performs a symmetric flight (no sideslip) with all forces (thrust, aerodynamic force and weight) acting at the center of gravity and lying in the plane of symmetry.
5. The wind velocity field is steady and contained in the flight plane.

These assumptions are appropriate for subsonic, transport aircraft. Under all these assumptions the scalar equations of motion are (see Miele et al. [48] and Jackson et al. [39]):

$$\begin{aligned}
\dot{V} &= \frac{T\cos\epsilon - D - mg\sin\gamma}{m} - (\dot{w}_x\cos\gamma + \dot{w}_h\sin\gamma) \\
\dot{\gamma} &= \frac{T\sin\epsilon + L - mg}{mV} + \frac{1}{V}(\dot{w}_x\sin\gamma - \dot{w}_h\cos\gamma) \\
\dot{m} &= -cT \\
\dot{h} &= V\sin\gamma + w_h \\
\dot{x} &= V\cos\gamma + w_x
\end{aligned} \tag{3.39}$$

where

$$\begin{aligned}
\dot{w}_x &= \frac{\partial w_x}{\partial x}(V\cos\gamma + w_x) + \frac{\partial w_x}{\partial h}(V\sin\gamma + w_h) \\
\dot{w}_h &= \frac{\partial w_h}{\partial x}(V\cos\gamma + w_x) + \frac{\partial w_h}{\partial h}(V\sin\gamma + w_h)
\end{aligned} \tag{3.40}$$

In these equations, V is the aerodynamic speed; γ is the aerodynamic path angle (or velocity pitch angle); m is the aircraft mass; h is the altitude; x is the horizontal distance travelled; g is the gravity acceleration; w_x and w_h are the horizontal and vertical wind velocities, respectively; D is the aerodynamic drag; L is the aerodynamic lift; T is the thrust; ϵ is the thrust angle-of-attack; c is the specific fuel consumption; and t is the time.

In addition to the previous assumptions, some supplementary hypotheses are considered in the applications of this thesis:

1. The thrust is parallel to the aerodynamic velocity, that is, $\epsilon = 0$.
2. An altitude-dependent, horizontal wind is considered, that is, $w_h = 0$ and $w = w_x(h)$.
3. The aerodynamic path angle is very small, that is, $\gamma \ll 1$, which leads to $\sin\gamma \approx \gamma, \cos\gamma \approx 1, \sin^2\gamma \approx 0$.
4. The normal acceleration $\dfrac{V\dot{\gamma}}{g}$ is negligible.

Under these supplementary assumptions, the scalar equations of motion (3.39) become

$$\begin{aligned}
\dot{V} &= \frac{T - D}{m} - g\gamma - V\frac{\mathrm{d}w}{\mathrm{d}h}\gamma \\
\dot{m} &= -cT \\
\dot{h} &= V\gamma \\
\dot{x} &= V + w
\end{aligned} \tag{3.41}$$

In these equations, the drag is a general known function $D(V, m, h)$, which takes into account the remaining equation of motion $L = mg$; the thrust $T(V, h)$ is given by $T(V, h) = \pi T_M(V, h)$ where π models the throttle setting and $T_M(V, h)$ is a general known function; and the specific fuel consumption is also a general known function $c(V, h)$. The aerodynamic and propulsion models considered in this thesis, which provide $D(V, m, h)$, $T(V, h)$ and $c(V, h)$, are described in Appendix B, along with the Earth model providing gravity and atmosphere models. In

particular, a general aircraft performance model corresponding to a Boeing 767-300ER (a typical twin-engine, wide-body, transport aircraft) is considered. In these equations, there is an independent variable, t; four states, V, m, h and x; and two controls, γ and π, both of which are bounded ($\gamma_{min} \leq \gamma \leq \gamma_{max}$ and $0 \leq \pi_{min} \leq \pi \leq \pi_{max} = 1$, respectively).

Additional constraints can be imposed to the aircraft motion in order to model the existence of different flight phases. A *flight phase* is defined by one additional flight constraint. A change from one flight phase to another implies a switch in the structure of the dynamics, constraints sets, etc., governing the evolution of the continuous variables (states and controls). In particular, three types of flight phases are considered in this thesis: climb, cruise, and unpowered descent. During climb, one has the additional constraint that π is a known parameter $\pi = \pi_{cl}$; hence, in this phase there are four states, V, m, h and x, and one control, γ. During cruise, one has the additional constraint of flying at constant altitude ($\gamma = 0$), that is, the altitude is a parameter; thus, in this phase there are three states, V, m and x, and one control, π. During unpowered descent, one has the additional constraint that $\pi = 0$, that is, the mass is a parameter; hence, in this phase there are three states, V, h and x, and one control, γ.

Particularization of the equations of motion for each flight phase (by taking into account the additional constraint) leads to different equations of motion and control definition. However, when changing from one flight phase to another the state remains continuous. These characteristics indicate that the controlled aircraft motion in a trajectory composed of climb, cruise and descent phases is a switched control system. Moreover, the optimization of the controlled aircraft motion in a trajectory composed of a prescribed series of climb, cruise and descent phases is a multiphase optimal control problem.

3.3 Computation of Optimal Aircraft Trajectories

In all the phases corresponding to a multiphase trajectory to be optimized, there is one control variable which appears linearly in the equations of motion as well as in the performance indices to be optimized (this is shown in the following chapters). As a consequence, the Hamiltonian of the problem is also linear on the control variable, which leads to a singular optimal control problem.

When addressing a flight phase, it is assumed that the initial and final points of the path are given. In that case, the optimal path is expected to be of the bang-singular-bang type, that is, formed by three arcs: one initial bang arc (with the control being at its maximum or minimum value) to go from the initial point to the singular arc, the singular arc, and a final bang arc (again, with the control being at its maximum or minimum value) to go from the singular arc to the final point.

The remark regarding the dimension of the singular surface with $n = 3$ and $\xi = 1$ applies to all the problems to be solved, even to the optimization of a climb phase (in which $n = 4$) because neither the dynamics function nor the performance index depend on x, and the final value of x is not specified. Therefore, in order to solve the singular optimal control problems considered in this thesis, an indirect numerical method is implemented, because it has the great advantage of providing feedback control laws, that can be directly used to guide the aircraft along the optimal path. This feedback control law and the expression of

the singular surface (in which singular arcs must lie) are obtained thanks to the application of the necessary conditions for optimality (as seen in Section 3.1).

As already mentioned, optimizing global trajectories implies not only addressing each flight phase, but also taking into account the interactions among them as well as looking for a global objective. The aim for a global objective is achieved by considering a global performance index, which is split into the contributions of each phase and particularized to the additional constraint imposed at each phase. The interactions are taken into account by appropriately imposing the transversality conditions and by enforcing state and adjoint continuity at the switching points.

Therefore, an optimal global trajectory cannot be obtained by simply piecing individually optimized phases together, not even when each phase is optimized with a performance index suitable for a global objective, because the transversality conditions do not provide the same results for the evolution of the adjoints. However, conclusions regarding the optimal control and optimal path structure for a single-phase optimal trajectory also apply at each phase of an optimal multiphase trajectory. As a consequence, besides trajectories involving a series of flight phases, trajectories involving only one flight phase are also optimized. These are the auxiliary problems analyzed in Chapters 4, 5 and 6.

In order to explain the numerical method developed in this thesis to compute optimal aircraft trajectories, the general case in which the trajectory is composed of a predefined sequence of phases is considered throughout this section. Note that the general case includes applications in which the trajectory only contains one phase.

3.3.1 Indirect Numerical Method

Assuming the control law has already been obtained the optimization problem becomes a multipoint boundary-value problem for which a numerical resolution procedure must be defined. Knowing the structure of the solution allows one to define an efficient numerical procedure (see Maurer [44]). In this thesis, an *indirect multiple shooting method* is implemented, which includes:

1. The definition of some unknown parameters.
2. A procedure to compute the candidates for optimal trajectory phases for given values of that unknown parameters.
3. An iterative procedure to find the value of the unknown parameters that satisfy some closing equations.

On one hand, the procedure to compute the candidates for optimal trajectory phases includes, for each phase, integration of the state equations with either $u = u_{min}$ or $u = u_{max}$ from the initial point (with known initial values) until the singular arc is reached (which defines the first junction point), integration of the state equations with $u = u_{sing}$ from the first junction point until the second one is reached, and integration of the state equations with either $u = u_{min}$ or $u = u_{max}$ from the second junction point until the final point (with known final values) is reached (see Franco and Rivas [31]). This procedure may also include integration of the adjoint equations along the trajectory phases in order to apply

some necessary conditions for optimality (transversality conditions and continuity of the adjoints at the switching instants). The computation of the adjoints also allows, once the iterative method has converged, to check both, whether the assumed structure for the control is correct, and whether the generalized Legendre-Clebsch condition for the singular arc to be minimizing is satisfied.

To solve the IVP posed at any trajectory segment, the ODE systems are solved by using MATLAB's *ode45* (see Shampine and Reichelt [63]), which is a method based on a pair of explicit Runge-Kutta formulae, the Dormand-Prince pair. This method is suitable for non-stiff problems with medium to quite stringent integration tolerances, and is therefore the method of choice. The other codes for non-stiff problems in MATLAB's ODE suite, *ode23* and *ode113*, are not preferred in this thesis.

On the other hand, to find the values of the unknown parameters, a set of nonlinear equations must be solved, which includes those necessary conditions for optimality and terminal constraints not explicitly imposed to obtain the candidates for optimal trajectory phases. In this thesis, the systems of nonlinear equations are solved by using MATLAB's *fsolve*, starting the iteration with appropriate initial values selected specifically for each application. By default, MATLAB's *fsolve* applies a trust-region dogleg algorithm, whose implementation is based on the dogleg method described by Powell [52].

In summary, this thesis proposes a methodology for aircraft trajectory optimization that exploits the singular character of the problem. With this approach, assuming a prescribed solution structure in terms of phase sequence and sequence of singular and bang arcs within each phase, the problem of finding the optimal control is transformed into the problem of finding the values of some unknowns such that the necessary conditions for optimality as well as the initial and final conditions are satisfied, that is, the problem of solving a nonlinear system of equations.

4 Fuel-Optimal Climb

4.1 Introduction

For commercial transport aircraft, minimizing fuel consumption is of prime importance, both economically and environmentally (because CO_2 emissions are directly related to fuel burnt). In the context of minimum-fuel global trajectories (from take-off to landing) the horizontal distance travelled during the climb affects the cruise distance. Thus, to be able to compare different climb trajectories which in general cover different horizontal distances, the fuel consumption up to a common reference distance could be considered, for example by including a horizontal segment at the final altitude (as done in Ref. [82]). However, in this chapter to take this point into consideration, a different approach is followed: only the climb segment is considered, and a performance index is defined in which fuel consumption is minimized, but penalizing small values of the climb distance, so that the actual objective is to minimize the contribution of the climb to the global-trajectory fuel consumption (as done in Ref. [49]).

In this chapter this fuel-optimal climb problem is addressed in the case of fixed engine rating and in the presence of altitude-dependent horizontal winds, so that wind-shear effects can be analyzed. The aircraft mass is not taken as constant but considered as a state variable, and a general aircraft performance model is considered (general compressible drag polar, and general thrust and specific fuel consumption models dependent on speed and altitude). The two main objectives of this chapter are: 1) to optimize the climb in the presence of altitude-dependent winds; and 2) to assess the optimality of the climb procedure, commonly used in practice, defined by segments with constant calibrated air speed (CAS) and constant Mach number (CAS/Mach climb).

The optimization analysis is made using the theory of singular optimal control, which has the great advantage of providing feedback control laws (control variables as functions of the state variables), that can be directly used to guide the aircraft along the optimal path. The control variable is the aerodynamic path angle (γ). The initial and final speeds and altitudes are given, so that the structure chosen for the optimal control is of the bang-singular-bang type, with the optimal paths formed by a singular arc and two minimum-γ arcs joining the singular arc with the given initial and final points. In the analysis of the climb made in this chapter the singular arc cannot be obtained in terms of the state variables alone, which makes the numerical procedure to solve the singular optimal control problem more involved than in another applications, such as maximum-range or minimum-cost cruise at constant altitude and maximum-range unpowered descents.

Despite their theoretical interest, optimal solutions may not be flyable according to present-day air traffic procedures and regulations. However, they represent best performance and can be used either as references to design improved flight procedures or to assess the optimality of flight procedures commonly used in practice, as for example the CAS/Mach procedure. In Franco et al. [34], a CAS/Mach procedure, composed of four segments (initial and final horizontal accelerations, constant-CAS climb and constant-Mach climb), is optimized using parametric optimization theory (see Fletcher [29]), with the same objective of minimizing the contribution of the climb to the global-trajectory fuel consumption; the optimization parameters are the climb CAS and Mach. In this chapter the optimality of CAS/Mach climbs is analyzed by comparing results from Ref. [34] with the optimal ones. The comparison of the results with the optimal ones shows that the integral performance of the optimized CAS/Mach procedure is very close to optimal, that is, the fuel consumption, the flight time, the horizontal distance travelled and, especially, the minimum performance index are very close to the optimum values.

Results are presented for a model of a Boeing 767-300ER, for linear wind profiles, characterized by two parameters: the average wind speed and the speed-profile slope or wind shear, and for $\gamma_{min} = 0$ so that the initial and final arcs are horizontal segments, as in the optimized CAS/Mach procedure, with which the optimum results are to be compared. The influence of the two wind parameters and of the initial aircraft weight on the results is analyzed. The strong effect of the wind shear is described.

The outline of the chapter is as follows: the problem is formulated in Section 4.2, including equations of motion, performance index, application of the necessary conditions for optimality and obtention of the singular surface and the singular control; the numerical procedure is explained in Section 4.3; some results are presented in Section 4.4, both for the optimal and the optimized CAS/Mach procedure, along with the comparison between the two procedures; and finally, a summary of the main results and conclusions is included in Section 4.5.

4.2 Problem Formulation

In this section, the fuel-optimal climb problem is formulated. First, the optimal control problem is stated by defining the equations of motion (along with the initial and final conditions) and the performance index considered. Second, because an indirect numerical method is considered for the resolution of the problem, the necessary conditions for optimality are included. Then, the optimal trajectories are described, including the equations defining the singular arc and the singular control (which is a feedback control law).

4.2.1 Equations of Motion

The equations of motion (3.41) particularized to a climb phase, in which one has the additional constraint that π is a known parameter $\pi = \pi_{cl}$, reduce to

$$\begin{aligned} \dot{V} &= \frac{T - D}{m} - g\gamma - V\frac{\mathrm{d}w}{\mathrm{d}h}\gamma \\ \dot{m} &= -cT \\ \dot{h} &= V\gamma \\ \dot{x} &= V + w \end{aligned} \tag{4.1}$$

In this problem there are four states, V, m, h and x, and one control, γ. The initial values of speed, mass, altitude and distance (V_i, m_i, h_i, x_i), and the final values of speed and altitude (V_f, h_f) are given. The final value of mass (m_f), distance (x_f), and flight time (t_f) are unspecified.

4.2.2 Performance Index

In the study of minimum-fuel climbs in the context of the analysis of global trajectories (from take off to landing), one must take into account that the horizontal distance travelled during the climb affects the cruise distance and the associated fuel consumption. If one compares a minimum-fuel climb trajectory with another one less steep, in which the horizontal distance is larger, even though the fuel consumption during the climb in the former case is smaller, to have a fair comparison of fuel consumption one should consider the extra fuel consumed to cover the same distance as in the latter case. To take this point into consideration in the analysis of climb performance, it is common in the literature (see for example Ref. [82]) to define a procedure in which the climb to the given final altitude is followed by a horizontal segment which ends when an arbitrarily given horizontal distance is travelled.

In this thesis a different approach is followed. Only the climb phase is considered, and the fuel consumption during the climb is minimized but penalizing small values of the climb distance. Hence the following performance index is considered

$$J \doteq m_F - K x_f = -\int_{m_i}^{m_f} \mathrm{d}m - K \int_0^{x_f} \mathrm{d}x, \tag{4.2}$$

which can be also written as follows, using the equations of motion (4.1),

$$J = \int_0^{t_f} \left[cT - K(V + w)\right] \mathrm{d}t, \tag{4.3}$$

where $m_F \doteq m_i - m_f$ is the fuel consumed during the climb, x_f is the climb horizontal distance, and the positive parameter K is a cost factor that defines the tradeoff between fuel consumption and horizontal distance. Obviously, $K = 0$ corresponds to the minimum-fuel problem, and $K > 0$ leads to optimal climbs with larger horizontal distance, but at the expense of a larger fuel consumption. One can see that this cost factor plays a role similar to the one played by the well-known cost index used by airlines, which defines the tradeoff between fuel consumption and flight time.

Although one could consider K just as a penalty factor and fix its value arbitrarily, in this cahpter to choose a value for K the following physical interpretation given in Ref. [49] is considered: if K is defined as an average fuel consumption per unit distance in cruise flight, and if two different climbs with horizontal distances x_{f_1} and $x_{f_2} > x_{f_1}$ are considered, then $K(x_{f_2} - x_{f_1})$ can be seen as an estimation of the decrease in fuel consumption during the cruise due to the reduction in cruise distance. Therefore, K is defined as follows

$$K \doteq -\left(\frac{\mathrm{d}m}{\mathrm{d}x}\right)_{cr} \tag{4.4}$$

expression that must be evaluated at the start of the cruise phase, under some given reference conditions.

The optimal climb problem reduces to minimize the performance index given by Eq. (4.3) subject to the constraints defined by the equations of motion (4.1).

4.2.3 Necessary Conditions for Optimality

The Hamiltonian of this problem is given by

$$H = cT + \lambda_V \left(\frac{T-D}{m} - g\gamma - Vw'\gamma \right) - \lambda_m cT + \lambda_h V\gamma + (\lambda_x - K)(V+w) \tag{4.5}$$

where $()'$ denotes derivative with respect to h, and λ_V, λ_m, λ_h and λ_x are the adjoint variables.

Assuming that the normality and non-triviality conditions are satisfied, the necessary conditions for optimality are summarized next (see Chapter 3):

1) The equations defining the adjoints:

$$\begin{aligned}
\dot{\lambda}_V &= -\frac{\partial H}{\partial V} = -\frac{\lambda_V}{m}\left(\frac{\partial T}{\partial V} - \frac{\partial D}{\partial V} - m\gamma w'\right) - (1-\lambda_m)\left(T\frac{\partial c}{\partial V} + c\frac{\partial T}{\partial V}\right) - \lambda_h\gamma \\
&\quad + K - \lambda_x \\
\dot{\lambda}_m &= -\frac{\partial H}{\partial m} = \frac{\lambda_V}{m}\left(\frac{T-D}{m} + \frac{\partial D}{\partial m}\right) \\
\dot{\lambda}_h &= -\frac{\partial H}{\partial h} = -\frac{\lambda_V}{m}\left(\frac{\partial T}{\partial h} - \frac{\partial D}{\partial h} - Vm\gamma w''\right) - (1-\lambda_m)\left(T\frac{\partial c}{\partial h} + c\frac{\partial T}{\partial h}\right) \\
&\quad + w'(K - \lambda_x) \\
\dot{\lambda}_x &= -\frac{\partial H}{\partial x} = 0
\end{aligned} \tag{4.6}$$

The last equation leads to constant λ_x.

2) The transversality conditions: First, because the final distance x_f is not specified, one has

$$\lambda_x(t_f) = 0 \tag{4.7}$$

which leads to

$$\lambda_x(t) = 0 \tag{4.8}$$

Second, because the final mass $m(t_f)$ is not specified,

$$\lambda_m(t_f) = 0 \tag{4.9}$$

Third, because the final time is not specified,

$$H(t_f) = 0 \tag{4.10}$$

3) The Hamiltonian minimization condition: For the control to be optimal it is necessary that it globally minimize the Hamiltonian. The Hamiltonian is linear in γ, so that it can be written as

$$H = \overline{H} + S\gamma \tag{4.11}$$

with

$$\begin{aligned}
\overline{H} &= \frac{\lambda_V}{m}(T-D) + (1-\lambda_m)cT - K(V+w) \\
S &= \lambda_h V - \lambda_V(g + Vw')
\end{aligned} \tag{4.12}$$

where Eq. (4.8) has been taken into account, and S is the switching function. As a consequence, this is a singular optimal control problem. The Hamiltonian minimization condition for singular optimal control problems has a special form given by Eq. (3.18), which in this case defines the optimal control as follows

$$\gamma = \begin{cases} \gamma_{max} & \text{if} \quad S < 0 \\ \gamma_{min} & \text{if} \quad S > 0 \\ \gamma_{sing} & \text{if} \quad S = 0 \quad \text{over a finite time interval} \end{cases} \tag{4.13}$$

where γ_{sing} is the singular control (yet to be determined), which satisfies $\gamma_{min} < \gamma_{sing} < \gamma_{max}$. Trajectory segments defined by γ_{sing} are singular arcs.

As indicated in Chapter 3, in singular optimal control problems there arise additional conditions that must be satisfied in order both, for a singular arc to be minimizing, and for the junctions between singular and nonsingular arcs to be optimal. These additional necessary condition for optimality are analyzed below in Section 4.2.4.2.

Finally, because the Hamiltonian is not an explicit function of time (as the problem is autonomous), the Hamiltonian constancy condition applies, and using Eq. (4.10) one gets

$$H(t) = 0 \tag{4.14}$$

along the optimal trajectory.

4.2.4 Optimal Trajectories

In general the optimal trajectory will be composed of singular arcs (with γ_{sing}) and arcs with γ_{min} or γ_{max}, commonly referred to as bangs; whether one has γ_{min} or γ_{max} is defined by the sign of the switching function S. In this problem the solution is expected to be of the bang-singular-bang type, that is, a singular arc and two minimum/maximum-γ arcs joining the singular arc with the given initial and final points. This bang-singular-bang structure is suggested by the results in Miele [47], where it is shown that the minimum-fuel climb is defined by a central path and two initial and final branches to join that path with the initial and final conditions. Although the underlying aerodynamic and propulsive models might affect the structure of the solution, for the smooth models considered in this thesis, the bang-singular-bang structure is plausible, and hence it is the one analyzed in this chapter. Since the initial and final speeds are given, there is a physical criterium to decide whether one has γ_{min} or γ_{max}, just by comparing those speeds with the speeds that correspond to the singular arc for the initial and final altitudes and masses.

Although called optimal trajectories, they are in fact extremals, that is, trajectories that satisfy the necessary conditions for optimality.

4.2.4.1 Singular Arc

The singular arc is defined by the following three equations

$$H = 0, \quad S = 0, \quad \dot{S} = 0 \tag{4.15}$$

where the function $\dot{S}$ is given by

$$\begin{aligned}\dot{S} =& \frac{\lambda_V g}{m}\left[(1+\frac{Vw'}{g})\frac{\partial T}{\partial V} - \frac{V}{g}\frac{\partial T}{\partial h} - (1+\frac{Vw'}{g})\frac{\partial D}{\partial V} + \frac{V}{g}\frac{\partial D}{\partial h} - \frac{w'}{g}(T-D)\right] \\ &+ (1-\lambda_m)\, gcT\left[(1+\frac{Vw'}{g})\frac{1}{T}\frac{\partial T}{\partial V} - \frac{V}{gT}\frac{\partial T}{\partial h} + (1+\frac{Vw'}{g})\frac{1}{c}\frac{\partial c}{\partial V} - \frac{V}{gc}\frac{\partial c}{\partial h}\right] \\ &+ \frac{\lambda_h}{m}(T-D) - gK\end{aligned} \tag{4.16}$$

(note that the terms in the control variable γ have cancelled out of this equation). Moreover, because $H = 0$ one also has $\overline{H} = 0$.

Hence, the three equations that define the singular arc ($\overline{H} = S = \dot{S} = 0$) lead to

$$\begin{aligned}\frac{\lambda_V}{m}(T-D) + (1-\lambda_m)\, cT - (V+w)K &= 0 \\ \lambda_h V - \lambda_V g(1+\frac{Vw'}{g}) &= 0 \\ \frac{\lambda_V g}{m}\left[(1+\frac{Vw'}{g})\frac{\partial T}{\partial V} - \frac{V}{g}\frac{\partial T}{\partial h} - (1+\frac{Vw'}{g})\frac{\partial D}{\partial V} + \frac{V}{g}\frac{\partial D}{\partial h} - \frac{w'}{g}(T-D)\right] & \\ + (1-\lambda_m)\, gcT\left[(1+\frac{Vw'}{g})\frac{1}{T}\frac{\partial T}{\partial V} - \frac{V}{gT}\frac{\partial T}{\partial h} + (1+\frac{Vw'}{g})\frac{1}{c}\frac{\partial c}{\partial V} - \frac{V}{gc}\frac{\partial c}{\partial h}\right] & \\ + \frac{\lambda_h}{m}(T-D) - gK &= 0\end{aligned} \tag{4.17}$$

which define the three adjoints λ_V, λ_m and λ_h along the singular arc in terms of the state variables, namely

$$\begin{aligned}\lambda_V &= f_V(V,m,h) \\ \lambda_m &= f_m(V,m,h) \\ \lambda_h &= f_h(V,m,h)\end{aligned} \tag{4.18}$$

Contrary to other cases (such as cruise and descent problems), in this climb problem it is not possible to obtain an expression for the singular arc in terms of the state variables alone. However, in the case $K = 0$ it is possible, because the system of equations (4.17) is homogeneous, and, therefore, to have a nontrivial solution one must have

$$\begin{aligned}\left(1+\frac{Vw'}{g}\right)\left(\frac{V}{T}\frac{\partial T}{\partial V} - \frac{V}{D}\frac{\partial D}{\partial V}\right) - \frac{V^2}{g}\left(\frac{1}{T}\frac{\partial T}{\partial h} - \frac{1}{D}\frac{\partial D}{\partial h}\right) & \\ + \left(\frac{T}{D}-1\right)\left[1 - \left(1+\frac{Vw'}{g}\right)\frac{V}{c}\frac{\partial c}{\partial V} + \frac{V^2}{gc}\frac{\partial c}{\partial h}\right] &= 0\end{aligned} \tag{4.19}$$

which defines a singular surface in the (V,m,h) space, namely $f(V,m,h) = 0$.

In the case of no wind ($w = 0$), even in the case of constant wind ($w' = 0$), Eq. (4.19) reduces to

$$\left(\frac{V}{T}\frac{\partial T}{\partial V} - \frac{V}{D}\frac{\partial D}{\partial V}\right) - \frac{V^2}{g}\left(\frac{1}{T}\frac{\partial T}{\partial h} - \frac{1}{D}\frac{\partial D}{\partial h}\right) + \left(\frac{T}{D}-1\right)\left(1 - \frac{V}{c}\frac{\partial c}{\partial V} + \frac{V^2}{gc}\frac{\partial c}{\partial h}\right) = 0 \tag{4.20}$$

which is the same result obtained by Miele [47] for the cental pattern of his solution, even though it is obtained under the assumption of constant aircraft mass.

4.2.4.2 Optimal Singular Control

Because the function $\ddot{S}$ depends linearly on the control variable γ (note that $\dot{S}$ does not depend on γ), the order of the singular arc is $\xi = 1$. Let $\ddot{S} = A(V,m,h) + B(V,m,h)\gamma$, where

$$\begin{aligned} A =& \frac{\lambda_V g}{m^2 V^2} A_1(V,m,h) + \frac{\lambda_h}{m^2 V} A_2(V,m,h) + \frac{(1-\lambda_m)\, gc}{mV^2} A_3(V,m,h) \\ &+ \frac{Kg}{mV} A_4(V,m,h) \\ B =& \frac{\lambda_V g^2}{mV^2} B_1(V,m,h) + \frac{\lambda_h g}{mV} B_2(V,m,h) + \frac{(1-\lambda_m)\, g^2 c}{V^2} B_3(V,m,h) \end{aligned} \tag{4.21}$$

with known functions A_1, A_2, A_3, A_4, B_1, B_2, and B_3 (these functions are included in Appendix C), and with the adjoints $\lambda_V, \lambda_m, \lambda_h$ given by Eqs. (4.18). Therefore, because one also has $\ddot{S} = 0$ (where $S = \dot{S} = 0$), the singular control is given by

$$\gamma_{sing} = -\frac{A(V,m,h)}{B(V,m,h)} \tag{4.22}$$

The generalized Legendre-Clebsch condition for the optimality of the singular control, Eq. (3.21), reduces in this case ($\xi = 1$ and $u = \gamma$) to $-\dfrac{\partial \ddot{S}}{\partial \gamma} \geq 0$, which leads to

$$B(V,m,h) \leq 0 \tag{4.23}$$

It can be shown numerically that $B < 0$ for all the cases considered in this Chapter, so that the strengthened generalized Legendre-Clebsch condition ($-\dfrac{\partial \ddot{S}}{\partial \gamma} > 0$) is satisfied.

The McDanell-Powers necessary condition for the optimality of junctions between singular and nonsingular arcs (see Chapter 3) is shown to be satisfied, because the order of the singular arc is $\xi = 1$ and the lowest-order time derivative of the control which is discontinuous at the junction is $\zeta = 0$ (that is, the control itself is discontinuous at the junction). Moreover, although the control variable is discontinuous at the junctions, the Weierstrass-Erdman corner conditions are satisfied because the adjoint variables, the Hamiltonian and the switching function are all continuous.

4.3 Numerical Procedure

In this section the numerical procedure used to solve the optimal climb is described. In Fig. 4.1 a sketch of the expected optimal path (bang-singular-bang) is presented (the particular case of two γ_{min} arcs is depicted). Knowing the structure of the solution allows one to define an efficient numerical procedure (see Maurer [44]), as follows.

The first bang starts with the initial values V_i, m_i, h_i and x_i. Let $\lambda_{V,1}$ be the value of the adjoint λ_V at the beginning of the singular arc (point 1 in Fig. 4.1). If $\lambda_{V,1}$ were known, the state equations (4.1) could be integrated until the singular arc were reached, that is until $\lambda_{V,1} = f_V(V_1, m_1, h_1)$ were satisfied. Also, if the altitude at the end of the singular arc h_2 were known, the state equations could be integrated along the singular arc (from point 1 to point 2 in Fig. 4.1), and then, using Eqs. (4.18), λ_V, λ_m and λ_h could be obtained at point

2. Finally, the state equations and the adjoint equations (4.6) could be integrated along the second bang, which starts at the singular arc (point 2) and ends when the value $V = V_f$ is reached. At the final point one has two additional conditions, $h(t_f) = h_f$ and $\lambda_m(t_f) = 0$, which are to be used to define $\lambda_{V,1}$ and h_2; this task is performed by means of an iterative procedure.

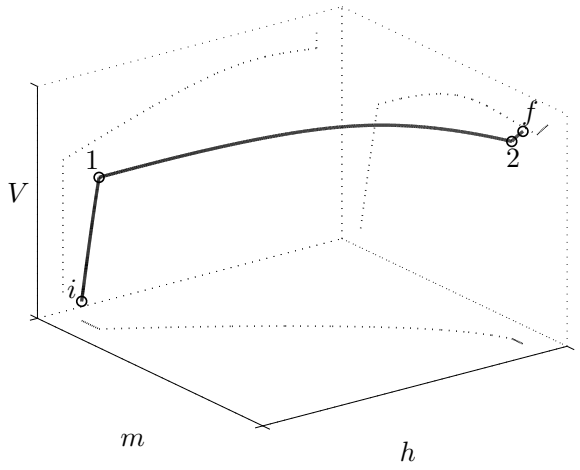

Figure 4.1: Sketch of the optimal climb path.

The iterative procedure must be started with an initial guess for the two unknowns. First, the initial guess for h_2 is $h_2^{[0]} = h_f$, because the second bang arc has very small length. Second, an initial guess for $\lambda_{V,1}$ can be obtained by considering $\lambda_{m,1} \approx 0$ in $\overline{H} = 0$, which gives $\lambda_{V,1} \approx -\left.\dfrac{m\left[cT - K\left(V+w\right)\right]}{T-D}\right|_1$. As the state variables at 1 are unknown, the previous expression can be approximated by evaluating the variables at i, so that the initial guess is $\lambda_{V,1}^{[0]} = -\left.\dfrac{m\left[cT - K\left(V+w\right)\right]}{T-D}\right|_i$. These initial guesses lead to convergence in all cases considered in this chapter.

4.3.1 Iterative Procedure

The following iterative procedure is used in the numerical resolution.

Step 0. Guess values $\lambda_{V,1}^{[n]}$ and $h_2^{[n]}$.

Step 1. Integrate the state equations (4.1) with either $\gamma = \gamma_{min}$ or $\gamma = \gamma_{max}$ from the initial point (with known initial values V_i, m_i, h_i, x_i) until the singular arc is reached (point 1), that is, until V_1, m_1, h_1 and $\lambda_{V,1}^{[n]}$ satisfy $\lambda_{V,1}^{[n]} = f_V(V_1, m_1, h_1)$; at that point one also has x_1. The value γ_{min} or γ_{max} is chosen depending on whether one has $V_i < V_a$ or $V_i > V_a$, where V_a is defined by $\lambda_{V,1}^{[n]} = f_V(V_a, m_i, h_i)$, that is, the speed that corresponds in the singular arc to the initial mass m_i and altitude h_i.

Step 2. Integrate the state equations (4.1) with $\gamma = \gamma_{sing}$ from point 1 (with known starting values V_1, m_1, h_1, x_1) until the altitude $h_2^{[n]}$ is reached. At the end of the integration

along the singular arc one also has V_2, m_2 and x_2; $\lambda_{V,2}$, $\lambda_{m,2}$ and $\lambda_{h,2}$ are obtained from Eqs. (4.18).

Step 3. Integrate the state equations (4.1) and the adjoint equations (4.6) with either $\gamma = \gamma_{min}$ or $\gamma = \gamma_{max}$ from point 2 (with known starting values $V_2, m_2, h_2^{[n]}, x_2, \lambda_{V,2}, \lambda_{m,2}, \lambda_{h,2}$) until the speed V_f is reached. The value γ_{min} or γ_{max} is chosen depending on whether one has $V_f > V_2$ or $V_f < V_2$. At the final point one also obtains the final values $h_f^{[n]}$ and $\lambda_{m,f}^{[n]}$, which in general are different from h_f and 0, respectively; in such case, one must iterate on the guessed values $h_2^{[n]}$ and $\lambda_{V,1}^{[n]}$, which is done as described next.

The procedure defined by steps 1 to 3 defines a function $\mathbf{g} : \mathbb{R}^2 \mapsto \mathbb{R}^2$, $\left(h_2^{[n]}, \lambda_{V,1}^{[n]}\right) \mapsto \left(h_f^{[n]}, \lambda_{m,f}^{[n]}\right)$, so that one searches for the values h_2 and $\lambda_{V,1}$ that satisfy $\mathbf{g}\left(h_2, \lambda_{V,1}\right) = (h_f, 0)$. If one defines the function $\mathbf{G} = \mathbf{g}\left(h_2, \lambda_{V,1}\right) - (h_f, 0)$ one searches for the zero of $\mathbf{G}\left(h_2, \lambda_{V,1}\right)$. The resolution of this system of equations is performed using MATLAB's *fsolve*, starting the iteration with the values $h_2^{[0]}$ and $\lambda_{V,1}^{[0]}$ defined above, and stopping when $h_f^{[n]} = h_f$ and $\lambda_{m,f}^{[n]} = 0$ to within some prescribed tolerance.

Once the problem is integrated, one has the final optimum values of the distance travelled x_f, the flight time t_f and the aircraft mass m_f which defines the fuel consumption $m_F = m_i - m_f$.

4.3.2 Control Structure Optimality

It still remains to check whether the assumed structure for the control (bang-singular-bang) is correct. That is, one must check that $S > 0$ for $\gamma = \gamma_{min}$ and that $S < 0$ for $\gamma = \gamma_{max}$. This requires the computation of S along the extremal path just computed. Since $S = \lambda_h V - \lambda_V \left(g + V w'\right)$, one must compute λ_V and λ_h.

Because of the resolution procedure previously explained, λ_V and λ_h have already been computed along the final bang. To compute them along the initial bang, one can integrate backwards the state equations (4.1) and the adjoint equations (4.6) from point 1 (with known starting values $V_1, m_1, h_1, x_1, \lambda_{V,1}, \lambda_{m,1}, \lambda_{h,1}$) until the initial point is reached. Note that $\lambda_{V,1}$, $\lambda_{m,1}$ and $\lambda_{h,1}$ are obtained from Eqs. (4.18).

The numerical results show that the control structure is correct in all cases presented in Section 4.4.

4.4 Results

The aircraft model considered in this thesis for the numerical applications (corresponding to a Boeing 767-300ER) is described in Appendix B, and the atmosphere model is the International Standard Atmosphere (ISA).

For the wind model, linear profiles are considered, with the absolute value of the wind speed increasing with altitude (see Ref. [50]). The profiles are defined as follows

$$w(h) = \bar{w} + \Delta w \frac{h - \bar{h}}{h_f - \bar{h}} \tag{4.24}$$

where $\bar{w}$ is the average wind, Δw is the wind-shear parameter and $\bar{h} = (h_i + h_f)/2$ is the

average altitude. For given values of h_i and h_f, Δw defines the wind shear $\frac{\mathrm{d}w}{\mathrm{d}h}$, and, in particular, $\Delta w = 0$ defines a uniform wind profile. Note that the average wind speed $\bar{w}$ satisfies

$$\bar{w} = \frac{1}{h_f - h_i} \int_{h_i}^{h_f} w(h)\mathrm{d}h \tag{4.25}$$

and, also, since the wind profiles are linear, $\bar{w}$ is the wind speed at the average altitude, that is, $\bar{w} = w(\bar{h})$. In the following, both tailwinds (TW) and headwinds (HW) are considered, with the linear profiles defined as follows: for TW one has $\bar{w} > 0$ and $\Delta w \geq 0$, and for HW $\bar{w} < 0$ and $\Delta w \leq 0$.

Results are presented for the case of initial and final γ_{min}-arcs, which require that the initial and final speeds be sufficiently low and high, respectively. In particular, $\gamma_{min} = 0$ has been considered so that the initial and final arcs are horizontal segments, as in the optimized CAS/Mach procedure, with which the optimum results are compared.

The initial conditions (corresponding to a hypothetical departure fix) are $CAS_i = 250$ kt, $h_i = 10000$ ft, and the final conditions (corresponding to the initial cruise conditions) are $M_f = 0.80$, $h_f = 33000$ ft. The average altitude is $\bar{h} = 21500$ ft. The value of K follows from Eq. (4.4) evaluated at the final climb conditions (start of the cruise) M_f and h_f, for $W_f = 1670$ kN, without wind, and using a quasi-steady cruise formulation; the value obtained is $K = 6.27$ kg/km. The throttle setting has been fixed to $\pi = 0.75$, so that typical performance is obtained for the range of parameters considered in the application.

To analyze the wind effects on the optimal trajectories, the initial aircraft weight is $W_i = 1700$ kN, the average wind ranges from -30 kt to 30 kt, and the absolute value of the wind-shear parameter ranges from 0 to 20 kt. In the analysis of the effect of the initial aircraft weight on the results, no wind is considered, and W_i ranges from 1650 kN to 1750 kN.

Results from Franco et al. [34] corresponding to optimized CAS/Mach climbs for the same performance index, aircraft and atmosphere models, wind model, as well as initial and final conditions are reproduced here. For completeness, a detailed description of this CAS/Mach climb procedure is included in Appendix D.

The outline of this section is as follows: the effects of the average wind speed (Section 4.4.1), the wind-shear parameter (Section 4.4.2), and the aircraft weight (Section 4.4.3) on the optimal and optimized trajectories as well as on the optimal control and the aerodynamic path angle are analyzed; then, the optimal and optimized climbs are compared in terms of global variables, which are also analyzed in Section 6.4.2.

4.4.1 Effect of the Average Wind Speed

The optimal and optimized CAS/Mach speed profiles $V(h)$ are represented in Fig. 4.2, for different values of the average wind speed ($\bar{w}$ ranging from -30 kt to 30 kt) and for a wind-shear parameter $\Delta w = 0$. The climb trajectories start and end with horizontal accelerations. In the optimal climbs, these horizontal segments correspond to the γ_{min}-arcs, from the given initial point to the singular arc, and from the singular arc to the given final point; and in the optimized CAS/Mach climbs, they correspond to the initial and final horizontal accelerations from the given initial speed to the optimum CAS_c, and from the optimum M_c to the final speed. In the optimal climbs, along the singular arc the speed increases, reaches a maximum

and then slowly decreases; and in the optimized CAS/Mach climbs, the speed increases during the CAS segment and decreases during the Mach segment, as expected. Qualitatively one has the same behavior in both cases. The influence of $\bar{w}$ is clear: as $\bar{w}$ increases, the speed decreases, so that for TW one has speeds smaller than for HW.

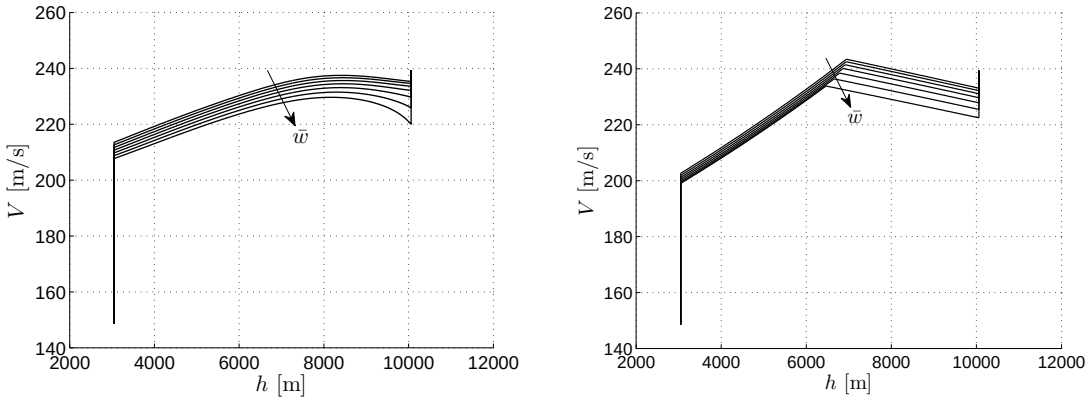

(a) (b)

Figure 4.2: Speed profiles for $\bar{w} = -30, -20, -10, 0, 10, 20, 30$ kt and $\Delta w = 0$. (a) Optimal climbs, (b) Optimized CAS/Mach climbs.

The CAS and Mach profiles, $CAS(h)$ and $M(h)$, are represented in Figs. 4.3 and 4.4. One can see that the first part of the optimal trajectory is not at constant CAS, but rather the CAS decreases, and as a consequence the increase of the aerodynamic speed during the constant-CAS segment is stronger than during the first part of the optimal trajectory (see Fig. 4.2). On the other hand, during the last part of the optimal trajectory the variation of the Mach number is small, so that the constant-Mach segment is somewhat close to the optimal trajectory (closer than the constant-CAS segment).

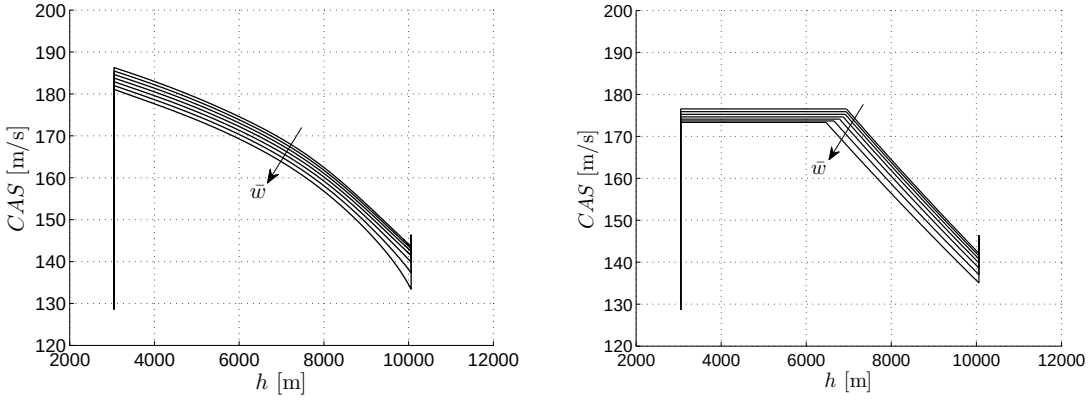

(a) (b)

Figure 4.3: CAS profiles for $\bar{w} = -30, -20, -10, 0, 10, 20, 30$ kt and $\Delta w = 0$. (a) Optimal climbs, (b) Optimized CAS/Mach climbs.

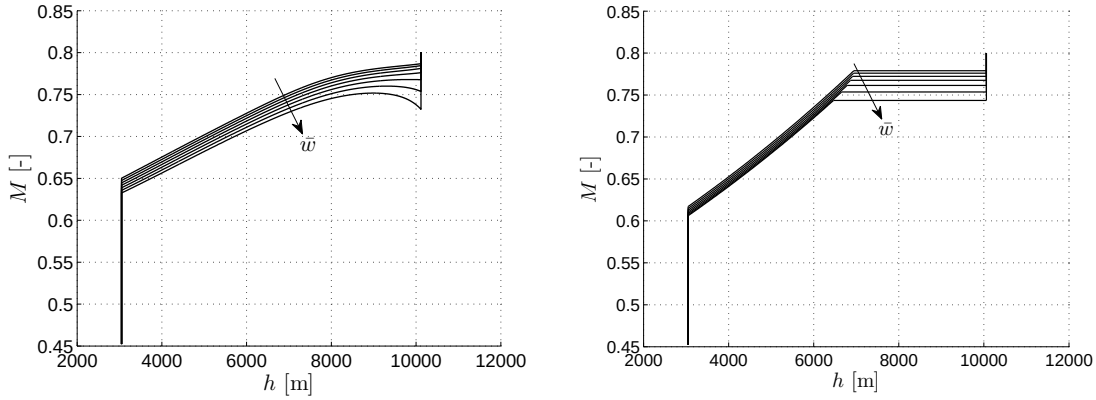

(a) (b)

Figure 4.4: Mach-number profiles for $\bar{w} = -30, -20, -10, 0, 10, 20, 30$ kt and $\Delta w = 0$. (a) Optimal climbs, (b) Optimized CAS/Mach climbs.

The optimal control and the aerodynamic path angle in the CAS/Mach climbs $\gamma(h)$ are represented in Fig. 4.5 for the same values of $\bar{w}$ as before and $\Delta w = 0$. It is discontinuous: for the optimal trajectories, one has the two arcs with $\gamma_{min} = 0$ (hardly seen in the figure) and the singular arc, and for the optimized CAS/Mach trajectories, one has the four constitutive segments (the initial and final ones hardly seen). Note that in the CAS/Mach climbs there is an increase in γ at the transition altitude between the segments with constant CAS and constant Mach, as required to decelerate the aircraft. As one can see, the average wind speed has very little influence both on the singular optimal control (except near the final bang) and on the path angle of the optimized CAS/Mach climbs.

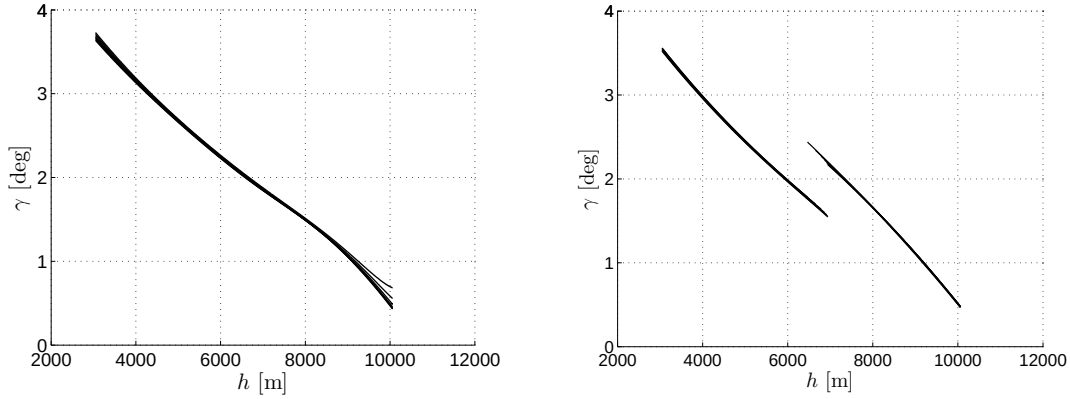

(a) (b)

Figure 4.5: Path-angle profiles for $\bar{w} = -30, -20, -10, 0, 10, 20, 30$ kt and $\Delta w = 0$. (a) Optimal climbs, (b) Optimized CAS/Mach climbs.

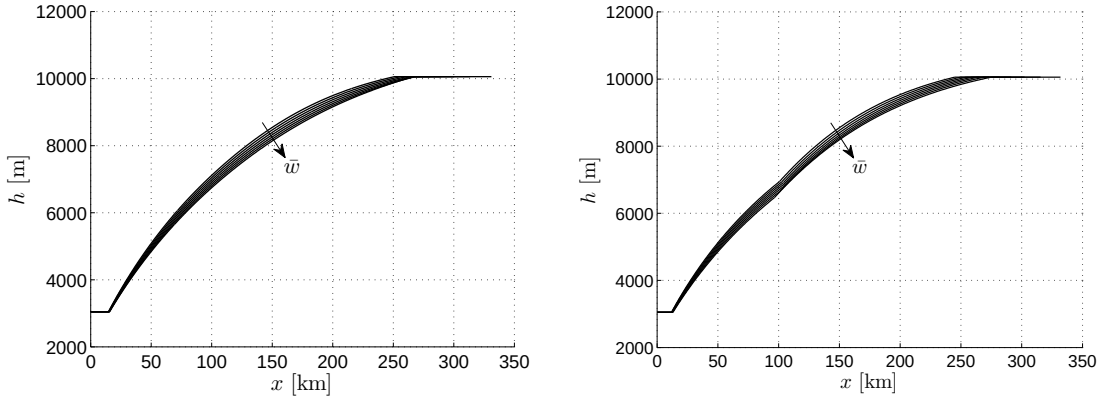

(a) (b)

Figure 4.6: Flight paths for $\bar{w} = -30, -20, -10, 0, 10, 20, 30$ kt and $\Delta w = 0$. (a) Optimal climbs, (b) Optimized CAS/Mach climbs.

The flight paths $h(x)$ are represented in Fig. 4.6, where one can see that there is a big qualitative agreement between the optimal and optimized CAS/Mach climbs. Note the slope discontinuity at the transition altitude between the constant-CAS and constant-Mach segments.

4.4.2 Effect of the Wind Shear

The optimal and optimized CAS/Mach speed profiles $V(h)$ are represented in Fig. 4.7, for different values of the wind-shear parameter ($|\Delta w|$ ranging from 0 kt to 20 kt), and for two values of the average wind ($\bar{w} = 30$ kt TW and $\bar{w} = -30$ kt HW).

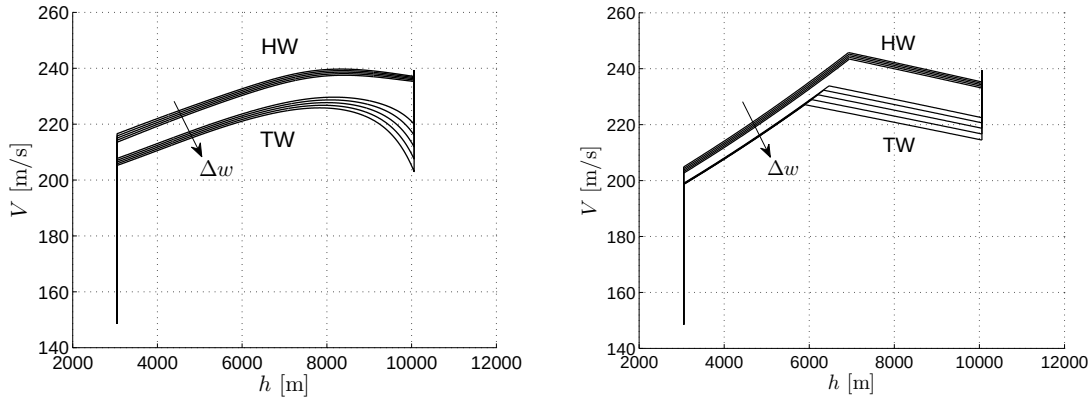

(a) (b)

Figure 4.7: Speed profiles for TW ($\bar{w} = 30$ kt, $\Delta w = 0, 5, 10, 15, 20$ kt) and HW ($\bar{w} = -30$ kt, $\Delta w = 0, -5, -10, -15, -20$ kt). (a) Optimal climbs, (b) Optimized CAS/Mach climbs.

As before, the speed increases, reaches a maximum and then slowly decreases; in the optimal trajectories the speed decrease is very weak for HW and quite strong for TW. The influence of Δw on the profiles is relatively small, except with TW at higher altitudes, when the speed decreases. The effect of Δw can be seen as a reinforcement of the average wind effects: as Δw increases, the speed decreases (note that, for HW, when Δw increases $|\Delta w|$ decreases). The behavior of the CAS and Mach profiles in this case follows the same trends already shown in Figs. 4.3 and 4.4, and are not represented for that reason.

The optimal control and the aerodynamic path angle in the CAS/Mach climbs $\gamma(h)$ are represented in Fig. 4.8 for the same values of $\bar{w}$ and Δw as before. They show the same discontinuities as before. The wind shear has a small influence on γ, although somewhat larger than the influence of the average wind speed.

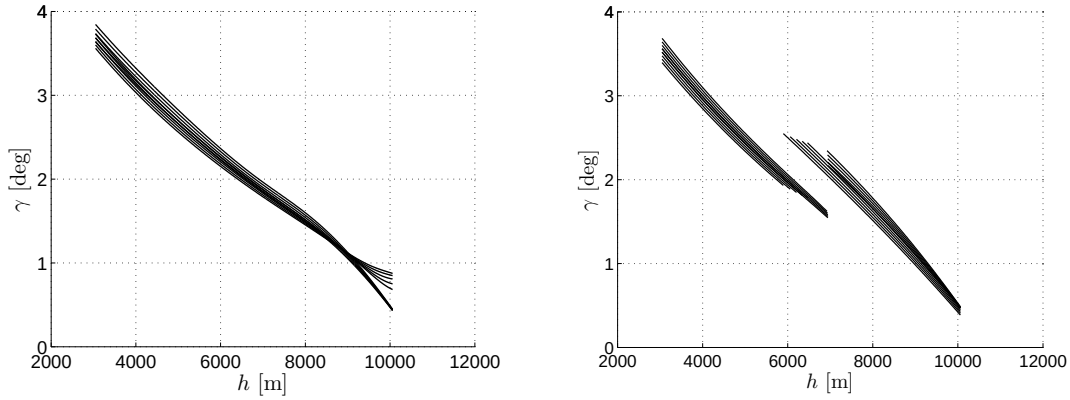

Figure 4.8: Path-angle profiles for TW ($\bar{w} = 30$ kt, $\Delta w = 0$, 5, 10, 15, 20 kt) and HW ($\bar{w} = -30$ kt, $\Delta w = 0, -5, -10, -15, -20$ kt). (a) Optimal climbs, (b) Optimized CAS/Mach climbs.

The corresponding flight paths are shown in Fig. 4.9, where again there is a big qualitative agreement between the optimal and optimized CAS/Mach climbs, except in the case of TW at high altitudes.

4.4.3 Effect of the Initial Aircraft Weight

The optimal and optimized CAS/Mach speed profiles $V(h)$ are represented in Fig. 4.10, for different values of the initial aircraft weight (W_i ranging from 1650 kN to 1750 kN) and for no wind ($\bar{w} = 0$ and $\Delta w = 0$). The optimal and optimized CAS/Mach profiles have the same structure as before: the speed increases, reaches a maximum and then slowly decreases. The influence of W_i on the profiles is clear: as the initial aircraft weight increases, the speed along the singular arc and the constant-CAS and constant-Mach segments slightly increases. As before, the CAS and Mach profiles in this case are not represented.

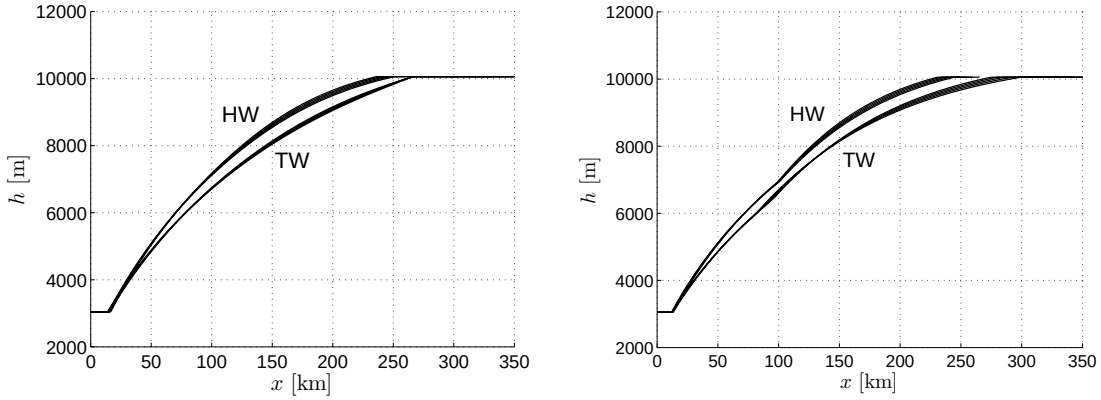

(a) (b)

Figure 4.9: Flight paths for TW ($\bar{w} = 30$ kt, $\Delta w = 0, 5, 10, 15, 20$ kt) and HW ($\bar{w} = -30$ kt, $\Delta w = 0, -5, -10, -15, -20$ kt). (a) Optimal climbs, (b) Optimized CAS/Mach climbs.

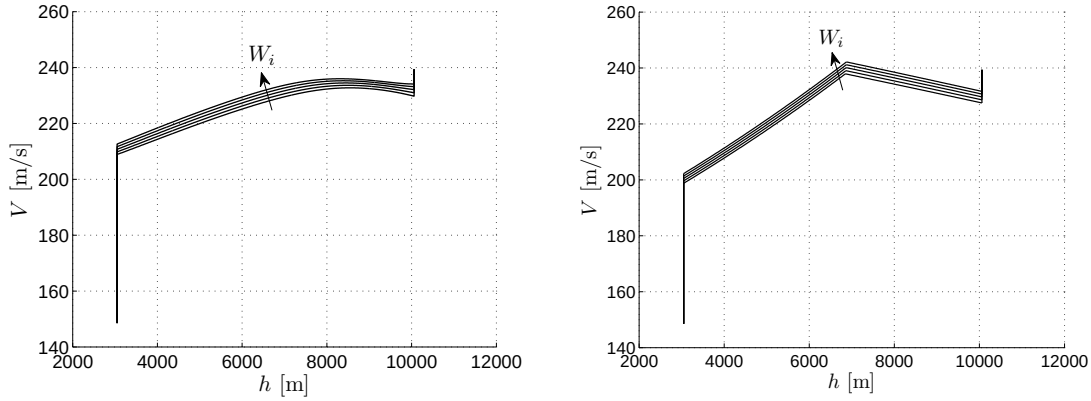

(a) (b)

Figure 4.10: Speed profiles for $W_i = 1650$, 1675, 1700, 1725 and 1750 kN. (a) Optimal climbs, (b) Optimized CAS/Mach climbs.

The optimal control and the aerodynamic path angle in the CAS/Mach climbs $\gamma(h)$ are represented in Fig. 4.11 for the same values of the initial aircraft weight as before and no wind, showing the same discontinuities as before. The initial aircraft weight has a clear influence on γ: as W_i increases, the control slightly decreases.

The corresponding flight paths are shown in Fig. 4.12, where again there is a big qualitative agreement between the optimal and optimized CAS/Mach climbs.

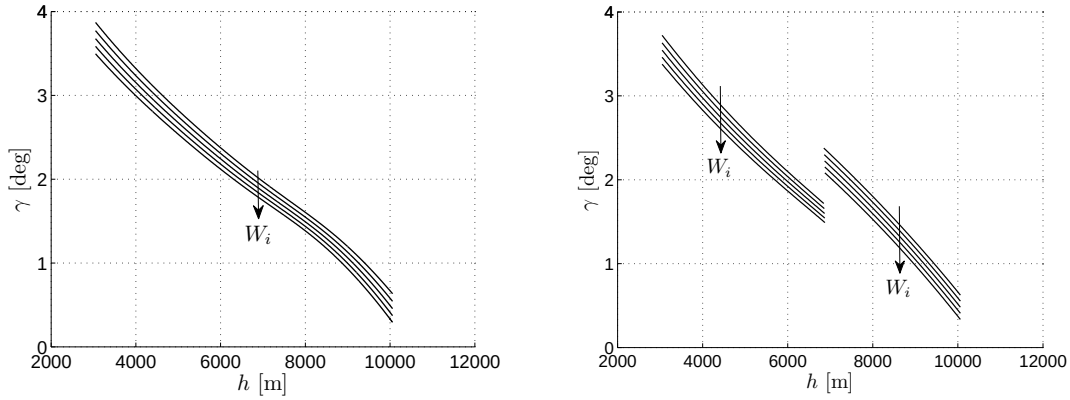

(a) (b)

Figure 4.11: Path-angle profiles for $W_i = 1650$, 1675, 1700, 1725 and 1750 kN. (a) Optimal climbs, (b) Optimized CAS/Mach climbs.

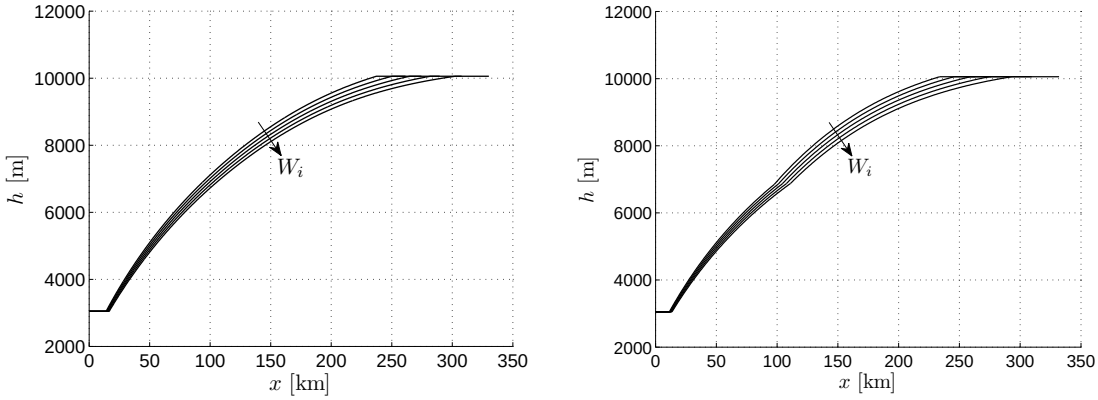

(a) (b)

Figure 4.12: Flight paths for $W_i = 1650$, 1675, 1700, 1725 and 1750 kN. (a) Optimal climbs, (b) Optimized CAS/Mach climbs.

4.4.4 Comparison and Analysis of Global Variables

Besides the comparison made between the flight profiles in the previous sections, now the optimized CAS/Mach climbs are compared with the optimal climbs in terms of fuel consumption, flight time and range, global variables which are also analyzed in this section, along with the minimum performance index.

In Figs. 4.13, 4.14, 4.15 and 4.16, the fuel consumption, the flight time, the range and the minimum performance index for both problems are represented, first, as functions of the wind-shear parameter for two values of the average wind ($\bar{w} = 30$ kt TW and $\bar{w} = -30$ kt HW) and $W_i = 1700$ kN, and, second, as functions of the average wind for different values of the initial aircraft weight (W_i ranging from 1675 to 1750 kN) and $\Delta w = 0$. One can see that the differences between both sets of results are very small in all cases (less than 88 kg in fuel consumption, less than 1.1 min in flight time, less than 15 km in range and less than 3.1 kg in performance index). Hence, it can be concluded that the performance of the CAS/Mach

procedure is very close to optimal, provided that the optimum values of CAS_c and M_c are used in the climb.

Next the global variables are analyzed. Some numerical values are given in Table 4.1. The results show the following: 1) the stronger the wind shear for TW, the larger the fuel consumption, the flight time, the range and the minimum performance index, although this index is roughly constant; 2) the stronger the wind shear for HW (in absolute value), the smaller the fuel consumption, the flight time, the range and the minimum performance index; 3) the higher the average wind speed, the higher the fuel consumption, the flight time and the range, and the lower the minimum performance index; and 4) the heavier the aircraft, the larger the fuel consumption, the flight time, the range and the minimum performance index. These trends are now quantified (using the values given in Table 4.1).

Table 4.1: Flight variables for different winds and initial aircraft weights (optimum values)

$W_i = 1700\,\text{kN}$				
	$\bar{w} = -30\,\text{kt}$ (HW)		$\bar{w} = 30\,\text{kt}$ (TW)	
	$\Delta w = -20\,\text{kt}$	$\Delta w = 0\,\text{kt}$	$\Delta w = 0\,\text{kt}$	$\Delta w = 20\,\text{kt}$
m_F [kg]	2650.6	2825.3	2992.9	3433.3
t_f [min]	19.06	20.63	23.18	28.12
x_f [km]	243.82	264.59	331.08	399.97
J [kg]	1121.8	1166.3	917.0	925.5
$\Delta w = 0\,\text{kt}$				
	$\bar{w} = -30\,\text{kt}$ (HW)		$\bar{w} = 30\,\text{kt}$ (TW)	
	$W_i = 1650\,\text{kN}$	$W_i = 1750\,\text{kN}$	$W_i = 1650\,\text{kN}$	$W_i = 1750\,\text{kN}$
m_F [kg]	2576.7	3165.9	2735.8	3338.4
t_f [min]	18.70	23.43	21.20	25.99
x_f [km]	237.97	302.83	299.57	375.25
J [kg]	1084.7	1267.2	857.5	985.6

The effect of the average wind speed on the fuel consumption, the flight time, the range and the minimum performance index is quite large, especially the effect on x_f. When $\bar{w}$ increases from -30 kt to 30 kt, the increases in m_F, t_f and x_f (for $\Delta w = 0$ and $W_i = 1700$ kN) are 167.6 kg, 2.55 min and 66.49 km, respectively, that is 5.93%, 12.4%, 25.1%, and the decrease in J is 249.3 kg, that is 21.4%.

The effect of the wind shear on m_F, t_f and x_f in the case of TW ($\bar{w} = 30$ kt) is quite large, although its effect on J is quite small; when Δw increases from 0 to 20 kt, the increases in m_F, t_f and x_f are 440.4 kg, 4.94 min and 68.89 km, respectively, that is 14.7%, 21.3%, 20.8%, whereas the increase in J is of just 8.5 kg, that is 0.93%. In the case of HW ($\bar{w} = -30$ kt) the effect on m_F, t_f and x_f is not so large, and the effect on J is also small although larger than for TW; when Δw increases from -20 kt to 0, the increases in m_F, t_f and x_f are 174.7 kg, 1.57 min and 20.77 km, respectively, that is 6.59%, 8.24%, 8.52%, whereas the increase in J is of 44.5 kg, that is 3.97%.

The effect of the initial aircraft weight, can be quantified as follows: for $\bar{w} = -30$ kt HW, when W_i increases from 1650 kN to 1750 kN, the increases in m_F, t_f, x_f and J are 589.2 kg, 4.73 min, 64.86 km and 182.5 kg, respectively, that is 22.9%, 25.3%, 27.3%, 16.8%; and for $\bar{w} = 30$ kt TW, the increases are 602.6 kg, 4.79 min, 75.68 km and 128.1 kg, respectively, that is 22.0%, 22.6%, 25.3%, 14.9%.

In summary, the influence of the wind profile and of the initial aircraft weight is in general quite large.

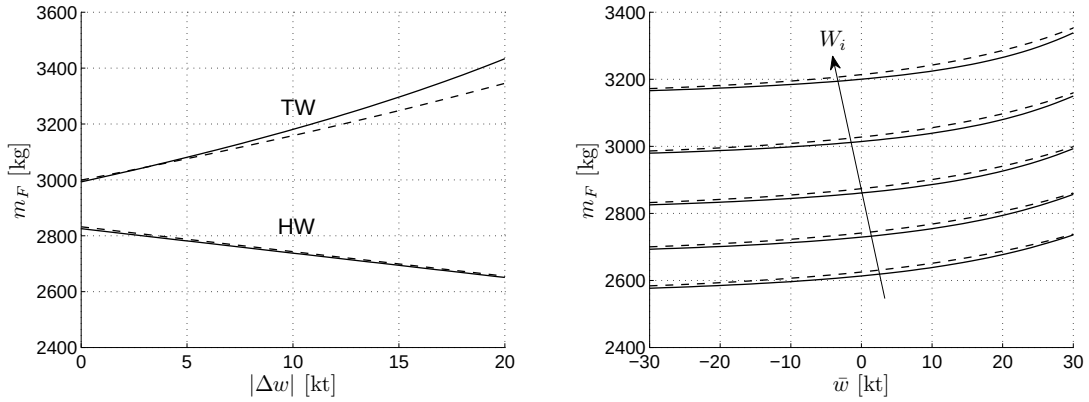

(a) (b)

Figure 4.13: Fuel consumption: (a) vs. wind-shear parameter for TW ($\bar{w} = 30$ kt) and HW ($\bar{w} = -30$ kt), for $W_i = 1700$ kN; (b) vs. average wind speed for $W_i = 1650$, 1675, 1700, 1725 and 1750 kN, for $\Delta w = 0$. Solid lines: optimal climbs. Dashed lines: optimized CAS/Mach climbs.

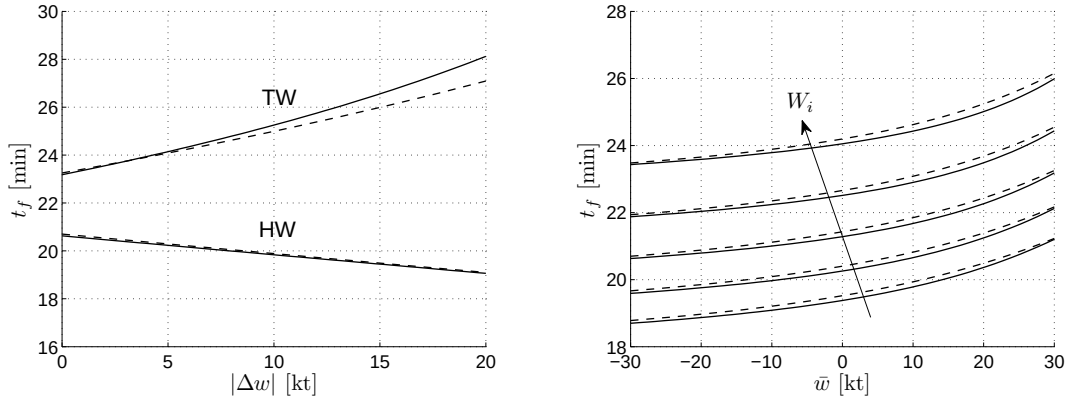

(a) (b)

Figure 4.14: Flight time: (a) vs. wind-shear parameter for TW ($\bar{w} = 30$ kt) and HW ($\bar{w} = -30$ kt), for $W_i = 1700$ kN; (b) vs. average wind speed for $W_i = 1650$, 1675, 1700, 1725 and 1750 kN, for $\Delta w = 0$. Solid lines: optimal climbs. Dashed lines: optimized CAS/Mach climbs.

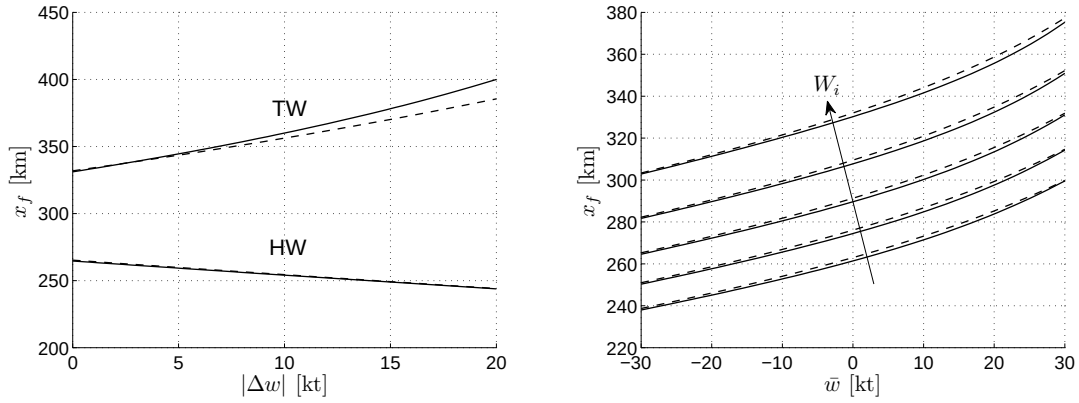

(a) (b)

Figure 4.15: Range: (a) vs. wind-shear parameter for TW ($\bar{w} = 30$ kt) and HW ($\bar{w} = -30$ kt), for $W_i = 1700$ kN; (b) vs. average wind speed for $W_i = 1650$, 1675, 1700, 1725 and 1750 kN, for $\Delta w = 0$. Solid lines: optimal climbs. Dashed lines: optimized CAS/Mach climbs.

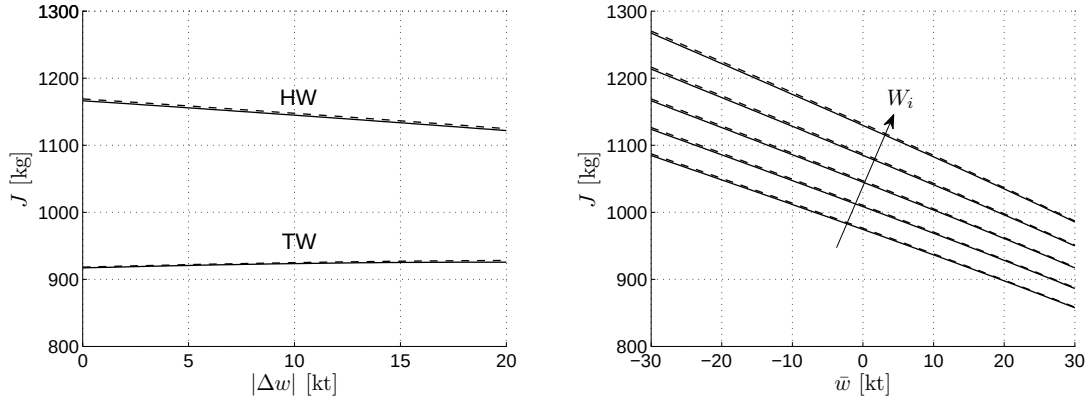

(a) (b)

Figure 4.16: Minimum performance index: (a) vs. wind-shear parameter for TW ($\bar{w} = 30$ kt) and HW ($\bar{w} = -30$ kt), for $W_i = 1700$ kN; (b) vs. average wind speed for $W_i = 1650$, 1675, 1700, 1725 and 1750 kN, for $\Delta w = 0$. Solid lines: optimal climbs. Dashed lines: optimized CAS/Mach climbs.

4.5 Summary

An analysis of fuel-optimal, fixed-rating climb in the presence of altitude-dependent winds has been made, using the theory of singular optimal control. The climb has been optimized to give minimum contribution to the global-trajectory fuel consumption, by means of penalizing small values of the climb distance. The optimal control is of the bang-singular-bang type, and the optimal paths are formed by a singular arc and two minimum/maximum-γ arcs joining the singular arc with the given initial and final points. Results have been presented for the case of initial and final γ_{min}-arcs, in the particular case of $\gamma_{min} = 0$, which lead to two short horizontal acceleration segments at the beginning and end of the optimal trajectory. This analysis has been used to assess the optimality of a CAS/Mach climb procedure composed by four segments (climbs with constant CAS and constant Mach, and initial and final horizontal accelerations), which is defined and optimized in Ref. [34].

This study has been quite general, in the sense that it has been made for a general aircraft model and a general horizontal wind profile, although results have been presented for linear profiles. In the numerical applications, the linear wind profiles have been defined by two parameters: the average wind and the wind shear. The influence of these two parameters on the results and the influence of the initial aircraft weight have been analyzed.

The results have shown that as the average wind increases, the fuel consumption, the flight time and the range increase, being the increase of range quite strong. The result that tailwinds lead to values of fuel consumption and flight time larger than the values for headwinds is not what one usually has, but note that in this chapter the objective has been to minimize the contribution of the climb to the global-trajectory fuel consumption, and that is obtained by flying large horizontal distances (with the corresponding increase in fuel consumption and flight time). The performance index does decrease as the average wind increases, and, hence, one has that tailwinds lead to fuel contributions to the global trajectory smaller than those of headwinds, as one would expect.

Of particular importance in this chapter has been the analysis of the influence of the wind shear on the climb performance. The influence of the wind shear on fuel consumption, flight time and horizontal distance is quite large, especially in the case of tailwinds, influence comparable to that of the average wind, and even larger in the cases of fuel consumption and flight time; in these cases the wind shear reinforces the effects of the average wind. The overall effect of the wind shear on the performance index is however not so large.

The comparison between both sets of results leads to the conclusion that the performance of the optimized CAS/Mach procedure, in terms of global variables such as fuel consumption, flight time and range, is very close to optimal, although the constant-CAS segment is not close to optimal. Clearly, the optimum CAS value represents an average speed that approximates very well, in global terms, the optimal speed law during the first part of the climb. Moreover, the flight paths (altitude vs horizontal distance) also show a very good agreement. From the operational point of view, one can conclude that the use of the CAS/Mach climb in operational practice is justified by the very close comparison with the optimal results.

5 Minimum-Fuel Cruise with Fixed Arrival Time

5.1 Introduction

An important problem in air traffic management (ATM) is the design of aircraft trajectories that meet certain arrival time constraints at given waypoints, for instance at the top of descent, at the initial approach fix, or at the runway threshold (estimated time of arrival). The final-time constraint may be defined, for example, by a flight delay imposed on the nominal (preferred) trajectory. These are four-dimensional (4D) trajectories, which are a key element in the trajectory-based-operations (TBO) concept proposed by SESAR and NextGen for the future ATM system (for example, Bilimoria and Lee [11] analyze aircraft conflict resolution with an arrival time constraint at a downstream waypoint). Also important in ATM is the design of optimal flight procedures that lead to energy-efficient flights. In practice, the airlines consider a cost index (CI) and define the direct operating cost (DOC) as the combined cost of fuel consumed and flight time, weighted by the CI; their goal is to minimize the DOC. When the flight time is fixed, the objective is to minimize fuel consumption.

In the analysis of aircraft trajectories with fixed flight time, wind effects are of primary importance, because changes in wind speed modify the flight time (over a given range), and therefore lead to changes in the speed profiles required to keep the final-time constraint. In this chapter, an analysis of mimimum-fuel cruise with fixed arrival time, at constant altitude, in the presence of horizontal winds, is presented. The problem is unsteady, with variable aircraft mass.

The optimization analysis is made using the theory of singular optimal control, which has the great advantage of providing feedback control laws (control variables as functions of the state variables), that can be directly used to guide the aircraft along the optimal path. The initial and final speeds are given, so that the structure chosen for the optimal control is bang-singular-bang, with the optimal paths formed by a singular arc and two minimum/maximum-thrust arcs joining the singular arc with the given initial and final points. The singular arc in the case of no winds is studied in Franco et al. [30].

The main objective of this chapter is to present a quantitative analysis of the effects of average horizontal winds on the optimal trajectories and control laws that lead to minimum fuel consumption while meeting the final-time constraint. The influence of the initial aircraft weight and the given cruise altitude on the optimal results is also analyzed. From the operational point of view, two applications are studied: first, the fuel penalties associated to

mismodeled winds are estimated, that is, the cost of meeting the given time of arrival under mismodeled winds is quantified; and, second, the cost of flight delays imposed on a nominal optimal path is quantified as well.

The optimal trajectories define speed laws in which the Mach number varies along the singular arc. These optimal solutions, which are a reference for optimal performance, are used to assess the optimality of the standard constant-Mach cruise procedure commonly used in practice (according to air traffic regulations). The comparison with optimal results shows that the performance of the constant-Mach cruise is very close to optimal.

Results are presented for a model of a Boeing 767-300ER, with a general aircraft performance model (general compressible drag polar, and general thrust and specific fuel consumption models dependent on speed and altitude), and for constant winds, which represent average winds along the cruise.

The outline of the chapter is as follows: the problem is formulated in Section 5.2, including optimal control problem statement, application of the necessary conditions for optimality and obtention of the singular surface and the singular control; the numerical procedure is explained in Section 5.3; some results are presented in Section 5.4, both for the optimal and the constant-Mach problems, along with the comparison between the two procedures; and finally, a summary of the main results and conclusions is included in Section 5.5.

5.2 Problem Formulation

In this section, the problem of minimum-fuel cruise with fixed arrival time is formulated. First, the optimal control problem is stated by defining the equations of motion (along with the initial and final conditions) and the performance index considered. Second, because an indirect numerical method is considered for the resolution of the problem, the necessary conditions for optimality are included. Then, the optimal trajectories are describe, including equations defining the singular arc (a uniparametric family of surfaces in the state space) and the singular control (which is a feedback control law).

5.2.1 Optimal Control Problem

The equations of motion (3.41) particularized to a cruise phase, in which one has the additional constraint of flying at constant altitude ($\gamma = 0$), reduces to

$$\begin{aligned} \dot{V} &= \frac{T - D}{m} \\ \dot{m} &= -cT \\ \dot{x} &= V + w \end{aligned} \tag{5.1}$$

In this problem there are three states, V, m and x, and one control, π. The initial values of speed, mass and distance (V_i, m_i, x_i), and the final values of speed and distance (V_f, x_f) are given. The final value of aircraft mass (m_f) is unspecified, whereas the flight time (t_f) is fixed. The altitude h, which plays the role of a parameter, is a given constant.

The objective is to minimize the fuel consumption for a given range, that is, to minimize

the following performance index

$$J = \int_0^{t_f} cT \, \mathrm{d}t \tag{5.2}$$

The optimal cruise problem considered reduces to minimize the performance index given by Eq. (5.2) subject to the constraints defined by the equations of motion (5.1).

5.2.2 Necessary Conditions for Optimality

The Hamiltonian of this problem is given by

$$H = c\pi T_M + \frac{\lambda_V}{m}(\pi T_M - D) - \lambda_m c\pi T_M + \lambda_x (V + w) \tag{5.3}$$

where λ_V, λ_m and λ_x are the adjoint variables. Note that H is linear in the control variable, so that it can be written as

$$H = \overline{H} + S\pi \tag{5.4}$$

where $\overline{H}$ and the switching function S are given by

$$\begin{aligned} \overline{H} &= -\lambda_V \frac{D}{m} + \lambda_x (V + w) \\ S &= \left[\frac{\lambda_V}{m} - (\lambda_m - 1)c \right] T_M \end{aligned} \tag{5.5}$$

As a consequence, this is a singular optimal control problem.

Assuming that the normality and non-triviality conditions are satisfied, the necessary conditions for optimality are summarized next (see Chapter 3):

1) The equations defining the adjoints:

$$\begin{aligned} \dot{\lambda}_V &= -\frac{\partial H}{\partial V} = -\lambda_x + \frac{\lambda_V}{m}\frac{\partial D}{\partial V} - \left[\frac{\lambda_V}{m} - (\lambda_m - 1)c \right] \pi \frac{\mathrm{d}T_M}{\mathrm{d}V} + (\lambda_m - 1)\frac{\mathrm{d}c}{\mathrm{d}V}\pi T_M \\ \dot{\lambda}_m &= -\frac{\partial H}{\partial m} = \frac{\lambda_V}{m}\left[\frac{\pi T_M - D}{m} + \frac{\partial D}{\partial m} \right] \\ \dot{\lambda}_x &= -\frac{\partial H}{\partial x} = 0 \end{aligned} \tag{5.6}$$

Note that the last equation leads to constant λ_x.

2) The transversality condition (associated to m_f being unspecified):

$$\lambda_m(t_f) = 0 \tag{5.7}$$

3) The Hamiltonian minimization condition: For the control to be optimal it is necessary that it globally minimize the Hamiltonian. The Hamiltonian minimization condition for singular optimal control problems has a special form given by Eq. (3.18), which in this case defines the optimal control as follows

$$\pi = \begin{cases} \pi_{max} & \text{if} \quad S < 0 \\ \pi_{min} & \text{if} \quad S > 0 \\ \pi_{sing} & \text{if} \quad S = 0 \quad \text{over a finite time interval} \end{cases} \tag{5.8}$$

where π_{sing} is the singular control (yet to be determined), which satisfies $\pi_{min} < \pi_{sing} < \pi_{max}$. Trajectory segments defined by π_{sing} are singular arcs.

As indicated in Chapter 3, in singular optimal control problems there arise additional conditions that must be satisfied in order both, for a singular arc to be minimizing, and for the junctions between singular and nonsingular arcs to be optimal. These additional necessary condition for optimality are analyzed below in Section 5.2.3.2.

Finally, because the Hamiltonian is not an explicit function of time (as the problem is autonomous), the Hamiltonian constancy condition applies

$$H(t) = \overline{\mathcal{H}} \tag{5.9}$$

where the constant $\overline{\mathcal{H}}$ is unknown.

5.2.3 Optimal Trajectories

In general the optimal trajectory will be composed of singular arcs (with π_{sing}) and arcs with π_{min} or π_{max}; whether one has π_{min} or π_{max} is defined by the sign of the switching function S. In this problem the solution is expected to be of the bang-singular-bang type, as suggested by the results obtained by Bilimoria and Cliff [10], where, using a reduced-order model with different time scales, the trajectory is decomposed into 3 parts: an initial transient, the cruise-dash arc and a terminal transient. Although the underlying aerodynamic and propulsive models might affect the structure of the solution, for the smooth models considered in this thesis, the bang-singular-bang structure is plausible, and hence it is the one analyzed in this chapter. Since the initial and final speeds are fixed, there is a physical criterium to decide whether one has π_{min} or π_{max}, just by comparing those speeds with the speeds that correspond to the singular arc.

Although called optimal trajectories, they are in fact extremals, that is, trajectories that satisfy the necessary conditions for optimality.

5.2.3.1 Singular Arc

The singular arc is defined by the following three equations

$$H = \overline{\mathcal{H}}, \quad S = 0, \quad \dot{S} = 0 \tag{5.10}$$

where the function $\dot{S}$ is given by

$$\begin{aligned} \dot{S} = &- \left[\frac{\lambda_V}{m} - (\lambda_m - 1)c\right] \frac{D}{m} \frac{\mathrm{d}T_M}{\mathrm{d}V} \\ &+ \left[\frac{\lambda_V}{m}\left(\frac{\partial D}{\partial V} + cD - mc\frac{\partial D}{\partial m}\right) - \lambda_x + (\lambda_m - 1)D\frac{\mathrm{d}c}{\mathrm{d}V}\right] \frac{T_M}{m} \end{aligned} \tag{5.11}$$

(note that the terms in the control variable π have cancelled out of this equation).

Hence, the three equations that define the singular arc (5.10) lead to

$$\begin{aligned} -\lambda_V \frac{D}{m} + \lambda_x (V + w) &= \overline{\mathcal{H}} \\ \frac{\lambda_V}{m} - (\lambda_m - 1)c &= 0 \\ \frac{\lambda_V}{m}\left(\frac{\partial D}{\partial V} + cD - mc\frac{\partial D}{\partial m}\right) - \lambda_x + (\lambda_m - 1)D\frac{\mathrm{d}c}{\mathrm{d}V} &= 0 \end{aligned} \tag{5.12}$$

The singular arc is obtained after eliminating the adjoints, λ_V and λ_m, from these equations. One obtains the following expression

$$D\left(\frac{1}{\Omega + V} - c - \frac{1}{c}\frac{\mathrm{d}c}{\mathrm{d}V}\right) - \frac{\partial D}{\partial V} + cm\frac{\partial D}{\partial m} = 0 \tag{5.13}$$

which is a family of singular arcs defined by the family parameter

$$\Omega = w - \frac{\overline{\mathcal{H}}}{\lambda_x} \tag{5.14}$$

This family can be written as $f(m, V, \Omega) = 0$. This is the same family obtained by Franco et al. [30] in the case of no wind, but for a different family parameter. The value of Ω is determined by imposing the final time to be t_f (the numerical procedure is described in Section 5.3). Once Ω is determined, Eq. (5.13) defines a singular line in the (V, m) space.

5.2.3.2 Optimal Singular Control

Because the function $\ddot{S}$ depends linearly on the control variable π (note that $\dot{S}$ does not depend on γ), the order of the singular arc is $\xi = 1$. Let $\ddot{S} = A(V, m) + B(V, m)\pi$, therefore, because one also has $\ddot{S} = 0$ (where $S = \dot{S} = 0$), the singular control is obtained from $A(V, m) + B(V, m)\pi = 0$; one gets the following

$$\pi_{sing} = \frac{D}{T_M}\left(1 + Vc\frac{A_1(V, m)}{B_1(V, m)}\right) \tag{5.15}$$

where $A_1(V, m)$ and $B_1(V, m)$ are given by

$$\begin{aligned} A_1(V, m) &= m\frac{\partial^2 D}{\partial m \partial V} - m^2 c\frac{\partial^2 D}{\partial m^2} - \frac{m}{D}\frac{\partial D}{\partial m}\left(cD + \frac{\partial D}{\partial V} - mc\frac{\partial D}{\partial m}\right) \\ B_1(V, m) &= DV\left(c^2 + 3\frac{dc}{dV} + \frac{1}{c}\frac{d^2 c}{dV^2}\right) + 2\frac{\partial D}{\partial V}\left(Vc + \frac{V}{c}\frac{dc}{dV}\right) \\ &\quad - mV\left(c^2 + 3\frac{dc}{dV}\right)\frac{\partial D}{\partial m} + V\frac{\partial^2 D}{\partial V^2} + m^2 c^2 V\frac{\partial^2 D}{\partial m^2} - 2Vcm\frac{\partial^2 D}{\partial m \partial V} \end{aligned} \tag{5.16}$$

This expression for the optimal singular control depends *implicitly* on the parameter of the family of singular arcs, because V and m are related by the singular arc equation (5.13) which includes the dependence on Ω.

The generalized Legendre-Clebsch condition for the optimality of the singular control, Eq. (3.21), reduces in this case ($\xi = 1$ and $u = \pi$) to $-\dfrac{\partial \ddot{S}}{\partial \pi} \geq 0$, which leads to

$$B(V, m) \leq 0 \tag{5.17}$$

It can be shown numerically that the strengthened generalized Legendre-Clebsch condition ($-\frac{\partial \ddot{S}}{\partial \pi} > 0$) is satisfied for all the cases considered in this Chapter.

The McDanell-Powers necessary condition for the optimality of junctions between singular and nonsingular arcs (see Chapter 3) is shown to be satisfied, because the order of the singular arc is $\xi = 1$ and the lowest-order time derivative of the control which is discontinuous at the junction is $\zeta = 0$ (that is, the control itself is discontinuous at the junction). Moreover, although the control variable is discontinuous at the junctions, the Weierstrass-Erdman corner conditions are satisfied because the adjoint variables, the Hamiltonian and the switching function are all continuous.

5.3 Numerical Procedure

The definition of an efficient numerical procedure to obtain the optimal path is facilitated by the knowledge of the structure of the solution (see Maurer [44]). In this case the expected optimal path is of the bang-singular-bang type, as sketched in Fig. 5.1. Based on this type of path, a procedure is defined to obtain the optimal trajectory.

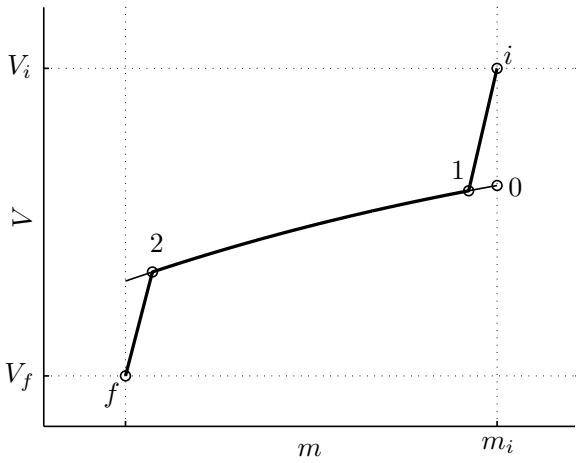

Figure 5.1: Sketch of the optimal cruise path.

The first bang starts with the initial values V_i, m_i, and x_i. Let x_{12} be the distance traveled along the singular arc (between points 1 and 2 in Fig. 5.1). If Ω were known, the state equations (5.1) could be integrated until the singular arc were reached, that is until $f(m_1, V_1, \Omega) = 0$ were satisfied. Also, if x_{12} were known, the state equations could be integrated along the singular arc until the distance $x_{12}^{[n]}$ is traveled (from point 1 to point 2 in Fig. 5.1). Finally, the state equations could be integrated along the second bang, which starts at the singular arc (point 2) and ends when the value $V = V_f$ is reached. At the final point one has two additional conditions, $x = x_f$ and $t = t_f$, which are to be used to define Ω and x_{12}; this task is performed by means of an iterative procedure.

The iterative procedure must be started with an initial guess for the two unknowns. First, the initial guess for Ω is $\Omega^{[0]} = w$, because for t_f unspecified one has $\overline{\mathcal{H}} = 0$. Second, an initial guess for x_{12} is $x_{12}^{[0]} = x_f$, because the two bang arcs have very small length. These initial guesses lead to convergence in all cases considered in this chapter.

5.3.1 Iterative Procedure

The following iterative procedure is used in the numerical resolution.

Step 0. Guess values $\Omega^{[n]}$ and $x_{12}^{[n]}$.

Step 1. Integrate the state equations (5.1) with either $\pi = \pi_{min}$ or $\pi = \pi_{max}$ from the initial point (with known initial values V_i, m_i, x_i) until the singular arc is reached (point 1), that is, until V_1 and m_1 satisfy $f(m_1, V_1, \Omega^{[n]}) = 0$; at that point one also has x_1. The value π_{min} or π_{max} is chosen depending on whether one has $V_i > V_0$ or $V_i < V_0$, where V_0 is defined by $f(m_i, V_0, \Omega^{[n]}) = 0$, that is, the speed that corresponds in the singular arc to the initial mass m_i (point 0 in Fig. 5.1).

Step 2. Integrate the state equations (5.1) with $\pi = \pi_{sing}$ from point 1 (with known initial values V_1, m_1, x_1) until the distance $x_{12}^{[n]}$ is traveled. At the end of the integration along the singular arc one has V_2, m_2, and x_2 (point 2).

Step 3. Integrate the state equations (5.1) with either $\pi = \pi_{min}$ or $\pi = \pi_{max}$ from point 2 (with known initial values V_2, m_2, x_2) until $V = V_f$. The value π_{min} or π_{max} is chosen depending on whether one has $V_f < V_2$ or $V_f > V_2$. At the final point one obtains the final values $x_f^{[n]}$ and $t_f^{[n]}$, which in general are different from x_f and t_f; in such a case, one must iterate on the guessed values $x_{12}^{[n]}$ and $\Omega^{[n]}$, which is done as described next.

The procedure defined by steps 1 to 3 defines a function $\mathbf{g} : \mathbb{R}^2 \mapsto \mathbb{R}^2$, $(x_{12}^{[n]}, \Omega^{[n]}) \mapsto (x_f^{[n]}, t_f^{[n]})$, so that one searches for the values x_{12} and Ω that satisfy $\mathbf{g}\,(x_{12}, \Omega) = (x_f, t_f)$. If one defines the function $\mathbf{G} = \mathbf{g}(x_{12}, \Omega) - (x_f, t_f)$, one searches for the zero of $\mathbf{G}$. The resolution of $\mathbf{G}(x_{12}, \Omega) = \mathbf{0}$ is performed using MATLAB's *fsolve*, starting the iteration with the values $(x_{12}^{[0]}, \Omega^{[0]})$ defined above, and stopping when $x_f^{[n]} = x_f$ and $t_f^{[n]} = t_f$ to within some prescribed tolerance.

Once the problem is integrated, one has the final optimal value of aircraft mass, m_f, which defines the minimum fuel consumption $m_F = m_i - m_f$, for the given values of range and flight time. Note that this procedure for the computation of the optimal path does not require the integration of the adjoint equations.

5.3.2 Control Structure Optimality

It still remains to check whether the assumed structure for the control (bang-singular-bang) is correct. That is, one must check that $S > 0$ for $\pi = \pi_{min}$ and that $S < 0$ for $\pi = \pi_{max}$. This requires the computation of S along the extremal path. Since $S = \left[\dfrac{\lambda_V}{m} - (\lambda_m - 1)c\right] T_M$, one must compute λ_V and λ_m.

First, to obtain λ_V and λ_m along the final bang it is necessary to solve a two-point boundary value problem defined by the corresponding adjoint equations (5.6), in which λ_x is a parametric unknown, with boundary conditions $H(t_2) = \overline{\mathcal{H}}$, $S(t_2) = 0$ and $\lambda_m(t_f) = 0$.

These boundary conditions can be rewritten in terms of λ_V and λ_m, as follows

$$\begin{aligned}\lambda_V(t_2) &= \frac{m_2\lambda_x}{D_2}(V_2+\Omega)\\ \lambda_m(t_2) &= 1+\frac{\lambda_x}{c_2 D_2}(V_2+\Omega)\\ \lambda_m(t_f) &= 0\end{aligned} \tag{5.18}$$

where Ω has been already computed. The resolution of this two-point boundary value problem is performed using MATLAB's *bvp4c*, starting the iteration with the parameter λ_x and the constant distributions of λ_V and λ_m that satisfy Eqs. (5.18), namely

$$\begin{aligned}(\lambda_m)^0 &= 0\\ (\lambda_x)^0 &= -\frac{c_2 D_2}{V_2+\Omega}\\ (\lambda_V)^0 &= -c_2 m_2\end{aligned} \tag{5.19}$$

Once the final bang is integrated, λ_V and λ_m at any point of the singular arc follow from $H=\overline{\mathcal{H}}$ and $S=0$, that is,

$$\begin{aligned}\lambda_V(t) &= \frac{m\lambda_x}{D}(V+\Omega)\\ \lambda_m(t) &= 1+\frac{\lambda_x}{cD}(V+\Omega)\end{aligned} \tag{5.20}$$

Finally, λ_V and λ_m along the initial bang are obtained integrating backwards the first two Eqs. (5.6) from point 1 to point i, with initial conditions $\lambda_V(t_1), \lambda_m(t_1)$ defined by Eqs. (5.20).

The numerical results show that the control structure is correct in all cases presented in Section 5.4.

5.4 Results

The aerodynamic model considered in this thesis for the numerical applications (corresponding to a Boeing 767-300ER) is described in Appendix B, and the atmosphere model is the International Standard Atmosphere.

Results are presented for a cruise flight defined by a range $x_f = 8000$ km, and by initial and final speeds $V_i = 240$ m/s and $V_f = 180$ m/s, corresponding to hypothetical conditions at the end of the climb and the start of the descent (the same values in all cases studied below). Different values of headwind (HW) and tailwind (TW) are considered, corresponding to negative and positive values of w respectively, ranging from -15 to $+15$ m/s; the case of no wind (NW) is included. The flight times range from 8.67 to 10.50 h. The nominal initial aircraft weight is taken to be $W_i = 1600$ kN. In the analysis of the effects of W_i, results are presented for a reference case defined by $w = 0$, $t_f = 9.5$ h and $h = 10000$ m. The nominal cruise altitude is taken to be $h = 10000$ m. In the analysis of the effects of h, results are presented now for a reference case defined by $w = 0$, $t_f = 9.5$ h and $W_i = 1600$ kN.

In the analysis of the effects of cruise altitude on the optimal results, one can take into account the altitude dependence of the wind. For example, in Ref. [21] a linear wind profile

is considered. The theoretical analysis made in this chapter is general and valid for any wind profile, so that results could be presented for any choice of profile. For simplicity, a constant profile is considered (as in Ref. [81]).

The outline of this section is as follows: the optimal trajectories are analyzed in Section 5.4.1 and the minimum fuel consumption in Section 5.4.2; then, two applications are considered: the cost of mismodeled winds is studied in Section 5.4.3, and the cost of flight delays in Section 5.4.4; and, finally, the optimality of the constant-Mach cruise procedure is assessed in Section 5.4.5. Besides the analysis of the wind effects on the optimal results, which is the main objective of this chapter, as already indicated, the effects of the initial aircraft weight and of the cruise altitude are analyzed as well.

5.4.1 Optimal Trajectories and Optimal Control

The optimal trajectories (Mach number as a function of flown distance) are shown in Fig. 5.2a for $t_f = 9.5$ h, $h = 10000$ m, $W_i = 1600$ kN and different values of wind speed (ranging from -15 to 15 m/s). The corresponding optimal controls are shown in Fig. 5.2b. The structure is minimum-thrust arc, singular arc, minimum-thrust arc, in all cases shown except for $w = -10, -15$ m/s, in which cases the optimal trajectory start with a maximum-thrust arc, required to accelerate the aircraft to the high initial singular-arc speed.

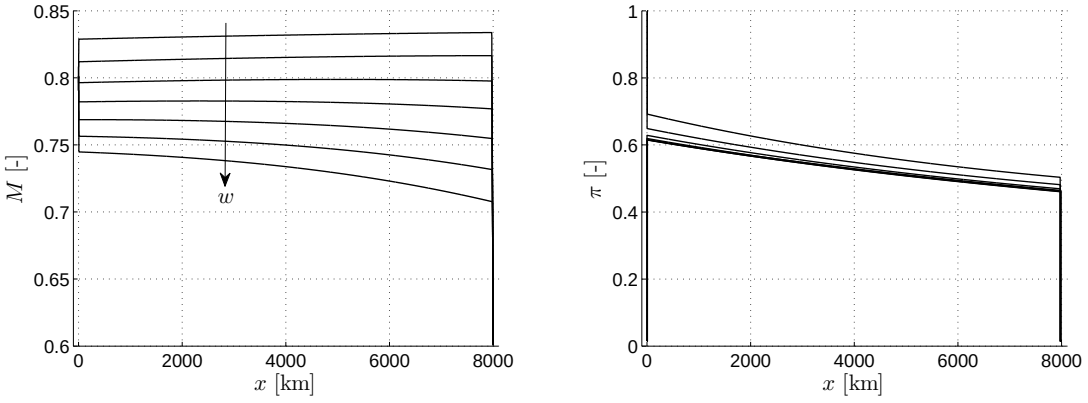

(a) (b)

Figure 5.2: Optimal trajectories and optimal control for $w = -15, -10, -5, 0, 5, 10, 15$ m/s ($t_f = 9.5$ h, $h = 10000$ m, $W_i = 1600$ kN). (a) Optimal trajectories, (b) Optimal control.

The results show that, to meet the given arrival time, the optimal Mach number decreases as the wind speed increases (the optimal cruise speed is larger for HWs than for TWs, as expected); for example, for a HW $w = -10$ m/s the optimal Mach number is $M \approx 0.815$, whereas for a TW $w = 10$ m/s it ranges from 0.756 to 0.732. In general, the optimal trajectory calls for a variation of the Mach number along the cruise (for a given t_f, one has the largest variations of M along the singular arc for the strongest TWs). However, for a given flight time, there is always a range of wind speeds for which the optimal trajectory

along the singular arc is $M \approx const$; for example, as shown in Fig. 5.2a, for $t_f = 9.5$ h and $w = -5$ m/s one has $M \approx 0.798$. The singular control decreases along the singular arc, and its variation with the wind speed is weak.

To analyze the influence of the arrival time, the optimal trajectories for HW $w = -10$ m/s and TW $w = 10$ m/s, and different arrival times (ranging from 9.17 to 10 h) are shown in Fig. 5.3 for $h = 10000$ m and $W_i = 1600$ kN. The corresponding optimal controls are shown in Fig. 5.4.

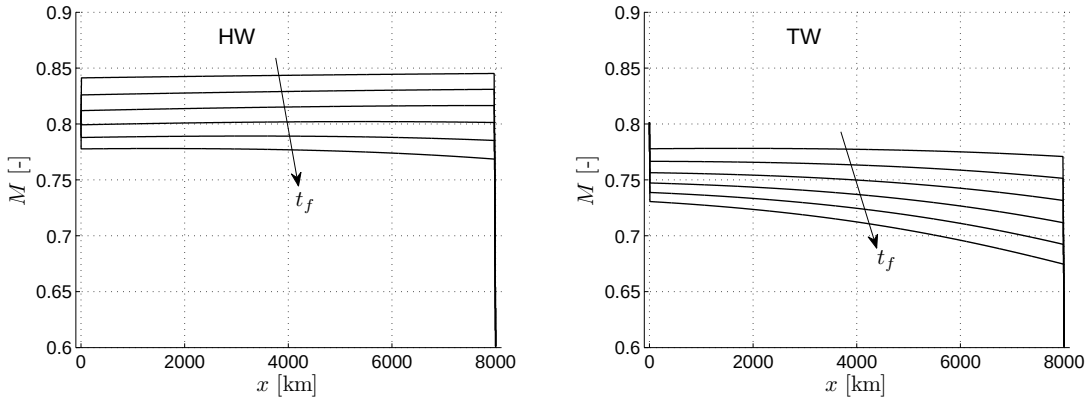

(a) (b)

Figure 5.3: Optimal trajectories for $t_f = 9.17$, 9.33, 9.5, 9.67, 9.83, 10 h ($h = 10000$ m, $W_i = 1600$ kN). (a) HW $w = -10$ m/s, (b) TW $w = 10$ m/s.

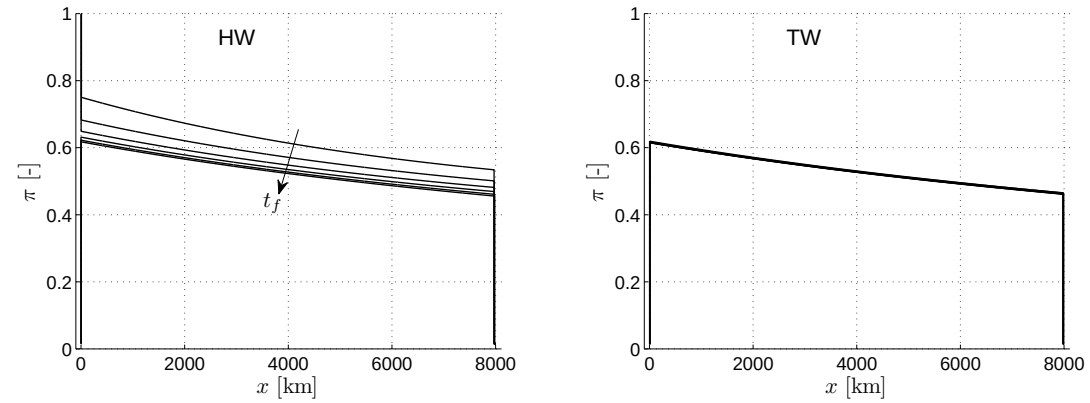

(a) (b)

Figure 5.4: Optimal control for $t_f = 9.17$, 9.33, 9.5, 9.67, 9.83, 10 h ($h = 10000$ m, $W_i = 1600$ kN). (a) HW $w = -10$ m/s, (b) TW $w = 10$ m/s.

As expected, the optimal Mach number decreases as the arrival time increases; and, for the same arrival time, the optimal Mach number is larger in the case of HW. The results also show that the variation of the singular control with the flight time is very small in the case of TW, and somewhat larger in the case of HW. In fact, the results show that for large speeds (say, Mach numbers larger than 0.8) the dependence of the singular control on speed is large, increasing as M increases, whereas for smaller speeds the dependence is very week (this behavior can be seen also in Fig. 5.2b). The reason for this behavior is that the variation of π with M is very shallow at low M (say $0.7< M <0.8$) and increases strongly for $M >0.8$, following the same trend as the aerodynamic drag; note that, as a first approximation, $\pi \approx D/T_M$ (as given by Eq. 5.15), and that the variation of T_M with M at high M is not as strong as the variation of D.

Now, to study the influence of the initial aircraft weight, the optimal trajectories for different values of W_i (ranging from 1500 to 1700 kN) are shown in Fig. 5.5a, for $t_f = 9.5$ h, $w = 0$ and $h = 10000$ m. The corresponding optimal controls are shown in Fig. 5.5b. In this problem in which the final distance and final time are fixed, the speed is so constrained that the influence of the initial aircraft weight on the speed profiles is very small (almost negligible). However, the singular control increases as W_i increases.

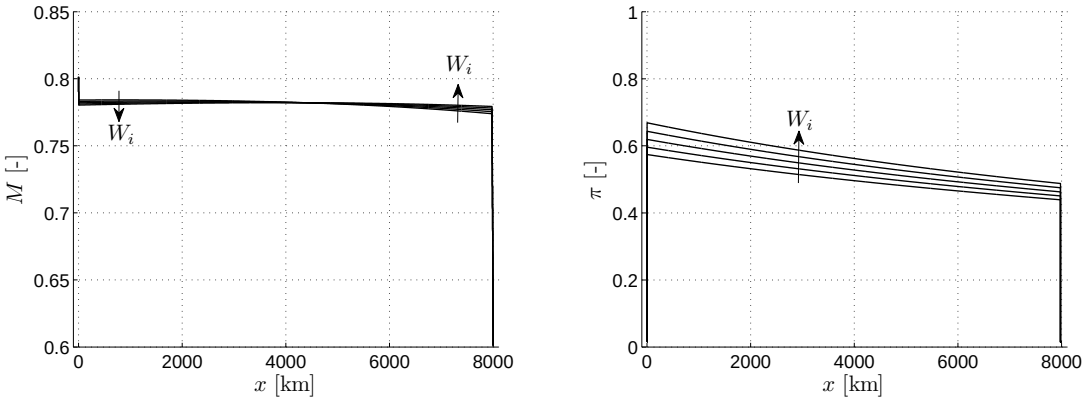

Figure 5.5: Optimal trajectories and optimal control for W_i = 1500, 1550, 1600, 1650, 1700 kN ($t_f = 9.5$ h, $w = 0$, $h = 10000$ m). (a) Optimal trajectories, (b) Optimal control.

Finally, to analyze the influence of the cruise altitude, the optimal trajectories for different values of h (h = 9000, 10000, 11000 m) are shown in Fig. 5.6a, for $t_f = 9.5$ h, $w = 0$ and $W_i = 1600$ kN. The corresponding optimal controls are shown in Fig. 5.6b. One can see that, as the cruise altitude increases, the optimal Mach number increases (result that is related to the corresponding decrease of the speed of sound). The results also show that the singular control increases significantly as the cruise altitude increases.

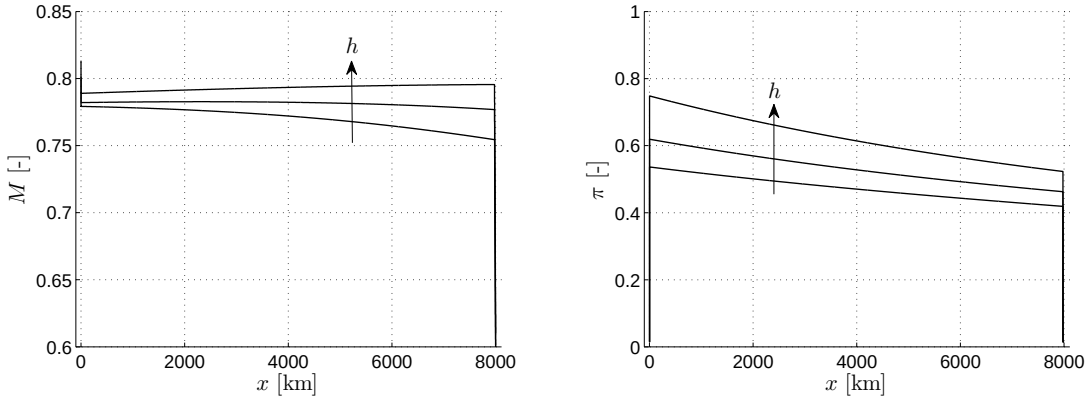

(a) (b)

Figure 5.6: Optimal trajectories and optimal control for $h = 9000, 10000, 11000$ m ($t_f = 9.5$ h, $w = 0$, $W_i = 1600$ kN). (a) Optimal trajectories, (b) Optimal control.

5.4.2 Minimum Fuel Consumption

The minimum fuel consumption as a function of the flight time is shown in Fig. 5.7 for $h = 10000$ m, $W_i = 1600$ kN and different wind speeds (ranging from -15 to 15 m/s). For concretion, some numerical values are given in Table 5.1. As expected, HWs require larger values of fuel consumption, as compared to TWs. This effect can be quantified now, for example, for a flight time of 9.5 h, in the nominal case of no wind the minimum fuel consumption is 39838 kg (see Table 5.1), whereas for a HW $w = -10$ m/s it is 43029 kg and for a TW $w = 10$ m/s it is 38265 kg; hence, one has a difference of 4764 kg between HW and TW, that is an increase of about 12%.

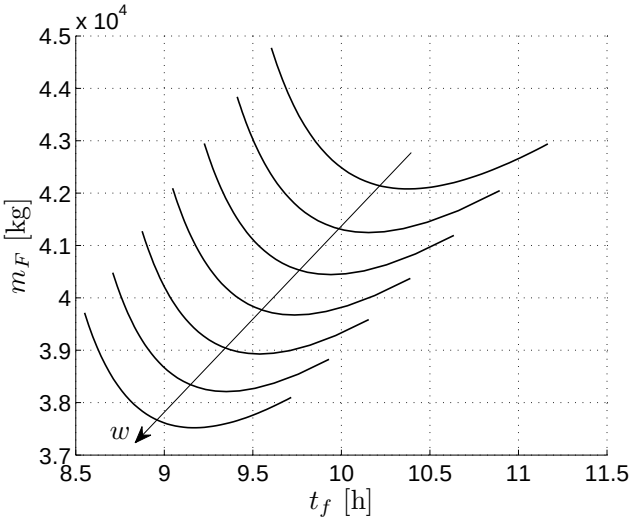

Figure 5.7: Minimum fuel consumption vs flight time for $w = -15, -10, -5, 0, 5, 10, 15$ m/s ($h = 10000$ m, $W_i = 1600$ kN).

Table 5.1: Minimum fuel consumption for different flight times and wind speeds (h = 10000 m, $W_i = 1600$ kN).

	m_F [kg]						
w [m/s]	−15	−10	−5	0	5	10	15
t_f [h]							
8.67	-	-	-	-	-	-	38727
8.83	-	-	-	-	-	39438	37955
9.00	-	-	-	-	40217	38669	37613
9.17	-	-	-	41068	39430	38318	37520
9.33	-	-	42001	40243	39058	38212	37587
9.50	-	43029	41115	39838	38933	38265	37761
9.67	44172	42056	40664	39684	38966	38424	-
9.83	43080	41543	40473	39693	39108	-	-
10.00	42486	41305	40452	39813	-	-	-
10.17	42189	41246	40546	-	-	-	-
10.33	42084	41309	-	-	-	-	-
10.50	42110	-	-	-	-	-	-

All curves in Fig. 5.7 present a minimum. These minima are the solutions of the minimum-fuel problem with *free* final time, that corresponds to $\overline{\mathcal{H}} = 0$, i.e., $\Omega = w$ (in this case one has $H(t) = 0$, because there is an additional necessary condition for optimality that states that $H(t_f) = 0$, see Ref. [15]). The numerical values are given in Table 5.2 (where $m_{F,0}$ is the minimum fuel and $t_{f,0}$ the corresponding optimal flight time). As before, HWs give larger values of minimum fuel consumption, and larger values of flight time, as compared to TWs. For example, for this case of free final time, the difference in minimum fuel consumption between a HW $w = -10$ m/s and a TW $w = 10$ m/s is 3034 kg, and the corresponding difference in flight time is 48 min.

Table 5.2: Minimum fuel consumption and optimal flight time for the free-final-time problem, for different wind speeds ($h = 10000$ m, $W_i = 1600$ kN).

w [m/s]	−15	−10	−5	0	5	10	15
$m_{F,0}$ [kg]	42080	41246	40444	39672	38928	38212	37520
$t_{f,0}$ [h]	10.38	10.15	9.94	9.74	9.54	9.35	9.17

The effect of the initial aircraft weight on the minimum fuel consumption is shown in Fig. 5.8, for different pairs of flight time and wind speeds. In particular three cases are considered: TW ($t_f = 9.17$ h and $w = 10$ m/s), NW ($t_f = 9.5$ h and $w = 0$), and HW ($t_f = 10$ h and $w = -10$ m/s). Even though the influence of the initial aircraft weight on the speed profiles is almost negligible (as shown in Fig. 5.5a), for the fuel consumption the

behaviour is different: one has larger fuel consumption for larger values of W_i, as expected. The minimum fuel consumption increases almost linearly when W_i increases: going from 38781 to 44040 kg for HW, from 37399 to 42489 kg for NW, and from 35942 to 40894 kg for TW, when W_i increases from 1500 to 1700 kN, that is, increases of 5259, 5090, and 4952 kg, respectively (13.56%, 13.61%, and 13.77%); the results give an approximately constant rate of increase of about 2500 kg for each 100 kN.

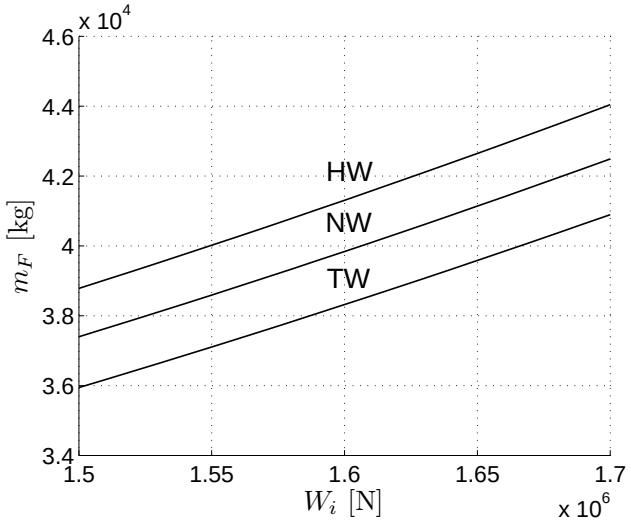

Figure 5.8: Minimum fuel consumption vs initial aircraft weight, for TW ($t_f = 9.17$ h and $w = 10$ m/s), NW ($t_f = 9.5$ h and $w = 0$) and HW ($t_f = 10$ h and $w = -10$ m/s). ($h = 10000$ m.)

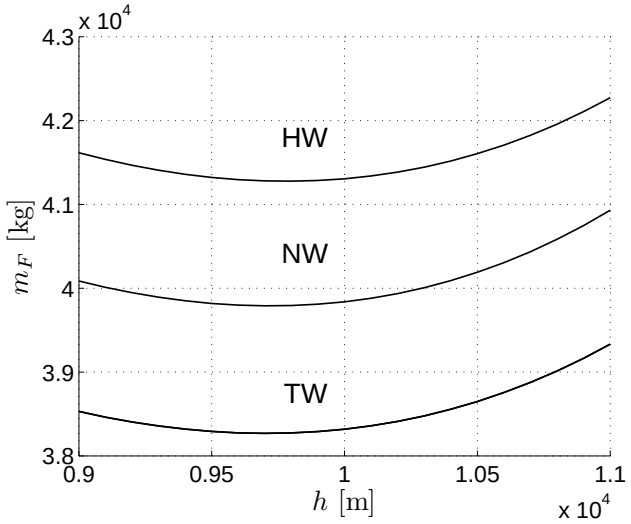

Figure 5.9: Minimum fuel consumption vs altitude, for TW ($t_f = 9.17$ h and $w = 10$ m/s), NW ($t_f = 9.5$ h and $w = 0$), and HW ($t_f = 10$ h and $w = -10$ m/s). ($W_i = 1600$ kN.)

Now, the effect of the cruise altitude on the minimum fuel consumption is shown in Fig. 5.9, for the same pairs of flight time and wind speeds as before: TW ($t_f = 9.17$ h and $w = 10$ m/s), NW ($t_f = 9.5$ h and $w = 0$), and HW ($t_f = 10$ h and $w = -10$ m/s). In each case there is a best altitude that provides lowest minimum fuel consumption. Hence, appropriate selection of cruise altitude implies a reduction in minimum fuel consumption during cruise. For example, in the three cases represented in Fig. 5.9 (HW, NW, TW), cruising at $h = 11000$ m instead of at the best altitudes (9784, 9721 and 9705 m) gives increases in minimum fuel consumption of 996, 1141 and 1064 kg, respectively (2.4%, 2.8%, and 2.7%).

5.4.3 Cost of Mismodeled Winds

In the presence of mismodeled winds, the optimal results are useful in giving an estimation of the fuel penalty that one might have, that is, an estimation of the cost of meeting the given time of arrival under mismodeled winds. The fuel penalty is defined as the difference in fuel consumption between the cases corresponding to the real wind $w + \delta w$ and the mismodeled wind w, that is, $\Delta m_{F,w} = m_F(w + \delta w) - m_F(w)$. The case of negative values of δw is considered, which means HWs stronger (larger in modulus) than expected, and TWs smaller than expected. In the following, the nominal path is that of minimum fuel consumption in the case of free final time: namely, $m_{F,0}$, with flight time $t_{f,0}$ (see Table 5.2); this flight time is to be maintained under the mismodeled wind. The fuel penalty is represented in Fig. 5.10 as a function of δw for different values of wind speed. One has that mismodeled HWs have fuel penalties larger than mismodeled TWs for the same wind speed error (it can be as large as $\Delta m_{F,w} \approx 2400$ kg for $w = -15$ m/s and $\delta w = -10$ m/s); this same result is obtained in Ref. [81], which is explained by the compressible drag increase at the high Mach numbers required to meet the arrival-time constraint in the case of strong HWs.

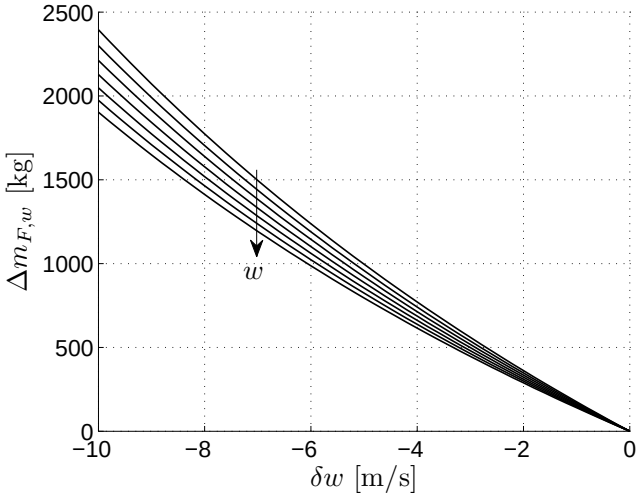

Figure 5.10: Increase in minimum fuel consumption vs mismodeled wind for $w = -15$, -10, -5, 0, 5, 10, 15 m/s ($h = 10000$ m, $W_i = 1600$ kN).

5.4.4 Cost of Flight Delays

The optimal results are also useful in quantifying the cost of a flight delay $\Delta t_f > 0$ imposed on a nominal optimal path with a nominal average wind. Again, the nominal path is that of minimum fuel consumption in the case of free final time: namely, $m_{F,0}$, with flight time $t_{f,0}$. Note that $m_{F,0}$ and $t_{f,0}$ depend on the wind speed (see Table 5.2). The cost of the flight delay is defined as the difference in minimum fuel consumption between the cases corresponding to the path for $t_f = t_{f,0} + \Delta t_f$ and the nominal path, that is, $\Delta m_{F,t} = m_F(t_{f,0} + \Delta t_f) - m_{F,0}$.

The delay cost is represented in Fig. 5.11 as a function of Δt_f for diferent values of wind speed. Obviously, the larger the delay, the larger the cost; for instance, the cost of absorbing a flight delay of 30 minutes in the presence of a TW $w = 15$ m/s is around 500 kg. Moreover, the cost of absorbing a given flight delay is larger in the presence of TWs than in the presence of HWs (the cost increases as w increases); this same result is obtained in Ref. [21], where it is explained by the larger percentage of the nominal flight time that the flight delay Δt_f represents in the case of tailwinds (because in this case the flight times are smaller).

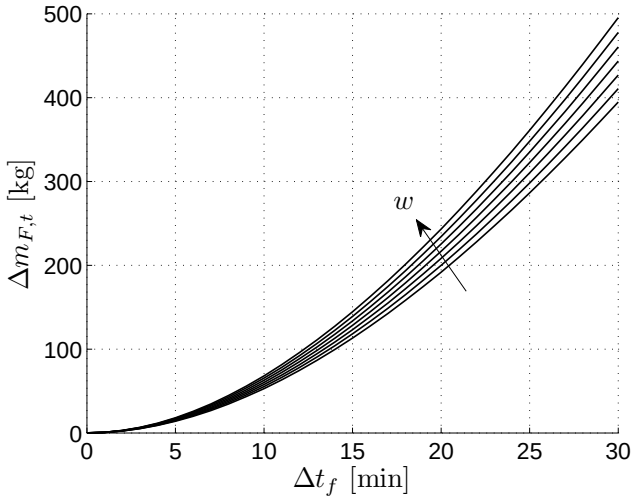

Figure 5.11: Increase in minimum fuel consumption vs flight delay for $w = -15$, -10, -5, 0, 5, 10, 15 m/s ($h = 10000$ m, $W_i = 1600$ kN).

5.4.5 Optimality of Constant-Mach Cruise

In Section 5.4.1 it is shown that the optimal solutions define variable-Mach cruise procedures. Even though these procedures may not be flyable (according to common air traffic control practice), they are a reference for optimum performance, and, therefore, can be used to analyze the optimality of standard flight procedures.

In this section, the optimality of the constant-Mach cruise procedure is analyzed, procedure which is described next. Let M_c be the cruise Mach, hence the cruise speed is $V_c = M_c a(h)$ where $a(h)$ is the speed of sound at the given altitude h. The procedure

considered is formed by three segments, all of them at constant altitude: 1) an initial acceleration/deceleration segment from the given initial speed V_i to the cruise speed V_c, with maximum cruise/idle engine rating, 2) a main cruise segment with constant speed V_c, and 3) a final acceleration/deceleration segment from V_c to the given final speed V_f, with maximum cruise/idle engine rating.

For the initial segment, the equations of motion (5.1) are integrated with initial conditions V_i, m_i and x_i until $V = V_c$; at the end of the segment one has m_1 and x_1. For the cruise segment, because the speed is constant, the equations of motion (5.1) reduce to

$$\begin{aligned} \dot{m} &= -c(V_c, h)D(V_c, m, h) \\ \dot{x} &= V_c + w(h) \end{aligned} \tag{5.21}$$

which are integrated with initial conditions m_1 and x_1 until the distance x_{12} is flown; at the end of the segment one has m_2 and x_2. For the final segment, Eqs. (5.1) are integrated with initial conditions V_c, m_2 and x_2 until $V = V_f$; at the end of the segment one has the final values of aircraft mass, horizontal distance and time, m_3, x_3 and t_3.

The flight distance and the flight time are in general different from x_f and t_f. Hence, one must iterate on the two free variables V_c and x_{12} until $x_3 = x_f$ and $t_3 = t_f$ to within some prescribed tolerance. The iteration is started with the initial guess $V_c = \dfrac{x_f}{t_f} - w$ and $x_{12} = x_f$. Finally, the fuel consumption is $m_F = m_i - m_3$.

The comparison between the optimal and the constant-Mach procedure in the case TW $w = 15$ m/s, $t_f = 9.5$ h, $h = 10000$ m and $W_i = 1600$ kN, is represented in Fig. 5.12, where the initial and final decelerations are not completely represented in order to better compare both trajectories. The constant Mach number obtained in this case is $M_c = 0.7311$, and the corresponding fuel consumption is $(m_F)_c = 37784$ kg, value that one can see is very close to the optimal value $m_F = 37761$ kg.

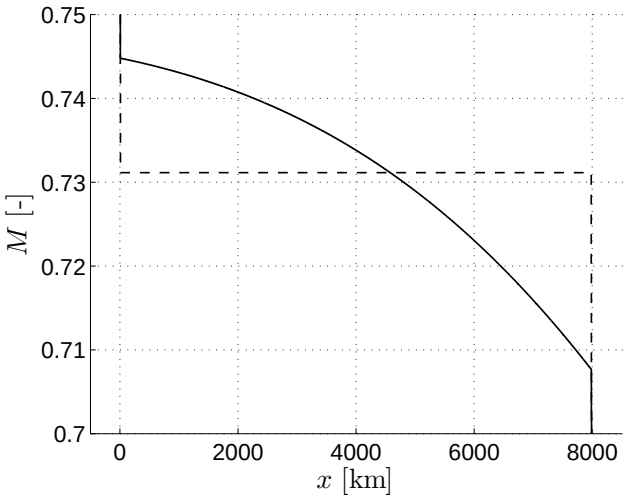

Figure 5.12: Optimal path (solid line) and constant-Mach path (dashed line) for $w = 15$ m/s, $t_f = 9.5$ h, $h = 10000$ m, and $W_i = 1600$ kN.

The constant Mach number M_c is represented in Fig. 5.13 as a function of the wind speed for different values of flight time (ranging from 9.17 to 10 h). One has that M_c decreases as w increases and as t_f increases. The influence of the initial aircraft weight on M_c is found to be negligible, as distance flown and flight time are given. And the influence of the cruise altitude is shown in Fig. 5.14, where M_c is represented as a function of cruise altitude for the same pairs of flight time and wind speeds as above: TW ($t_f = 9.17$ h and $w = 10$ m/s), NW ($t_f = 9.5$ h and $w = 0$), and HW ($t_f = 10$ h and $w = -10$ m/s); one has that M_c increases as h increases (result that is related to the corresponding decrease of the speed of sound). Note that if the initial and final decelerations are not considered, M_c is given by the following relation

$$M_c = \frac{1}{a(h)} \left(\frac{x_f}{t_f} - w \right) \tag{5.22}$$

which gives a very good approximation, because the effect of those decelerations in the global problem is small.

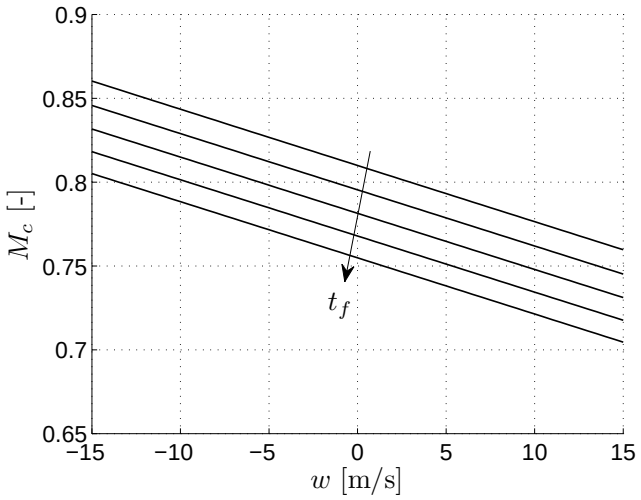

Figure 5.13: M_c vs wind speed for $t_f = 9.17$, 9.33, 9.5, 9.67, 9.83, 10 h ($h = 10000$ m, $W_i = 1600$ kN).

The difference in fuel consumption $\Delta m_{F,c} = (m_F)_c - m_F$ between the optimal and the constant-Mach procedures is represented in Fig. 5.15 as a function of wind speed, for different values of flight time (ranging from 9.17 to 10 h). For concretion, some numerical values are given in Table 5.3. One can see that the differences are always very small (almost negligible in some cases, clearly in those in which the optimal M is almost constant). Hence, one can conclude that the performance of the constant-Mach cruise is always very close to optimal, giving fuel consumptions larger than the optimum by less than 25 kg in all cases considered. As already indicated, for a given t_f (or for a given w) there is always a range of values of w (or t_f) in which the optimal trajectory is $M \approx const$; in these cases the difference between both procedures is negligible ($\Delta m_{F,c} < 1$ kg). The same trends are obtained for different values of W_i and h.

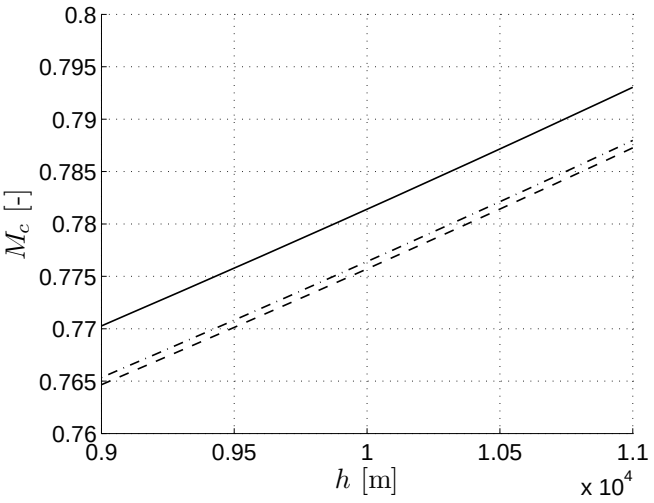

Figure 5.14: M_c vs altitude for TW ($t_f = 9.17$ h and $w = 10$ m/s, dash-dotted line), NW ($t_f = 9.5$ h and $w = 0$, solid line) and HW ($t_f = 10$ h and $w = -10$ m/s dashed line). ($W_i = 1600$ kN.)

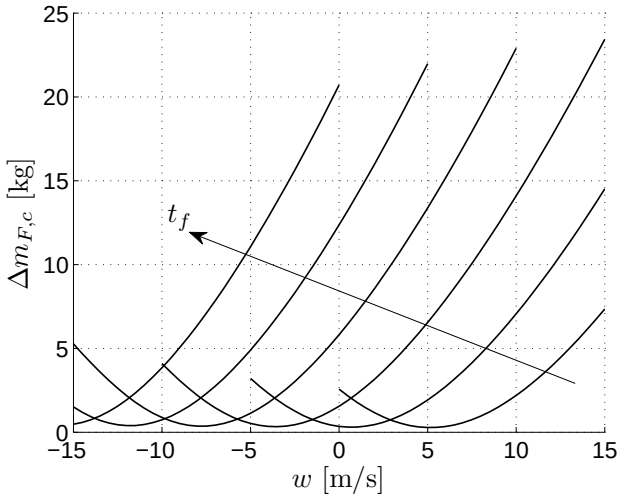

Figure 5.15: Increase in minimum fuel consumption vs wind speed for $t_f = 9.17$, 9.33, 9.5, 9.67, 9.83, 10 h ($h = 10000$ m, $W_i = 1600$ kN).

Table 5.3: Increase in minimum fuel consumption for different flight times and wind speeds ($h = 10000$ m, $W_i = 1600$ kN).

	$\Delta m_{F,c}$ [kg]						
w [m/s]	-15	-10	-5	0	5	10	15
t_f [h]							
8.67	-	-	-	-	-	-	1.7
8.83	-	-	-	-	-	1.9	0.2
9.00	-	-	-	-	2.1	0.3	2.3
9.17	-	-	-	2.6	0.3	2.2	7.3
9.33	-	-	3.2	0.3	1.9	7.1	14.5
9.50	-	4.1	0.5	1.5	6.5	14.1	23.4
9.67	5.3	0.9	1.1	5.8	13.4	22.9	-
9.83	1.5	0.7	4.9	12.4	22.0	-	-
10.00	0.5	3.9	11.1	20.7	-	-	-
10.17	2.7	9.5	19.1	-	-	-	-
10.33	7.8	17.1	-	-	-	-	-
10.50	14.8	-	-	-	-	-	-

5.5 Summary

The problem of minimum-fuel cruise with fixed arrival time have been analyzed, for constant-altitude flight. The analysis of this four-dimensional problem has been made using the theory of singular optimal control. The structure of the optimal control considered has been bang-singular-bang, which is what one expects in this case in which the initial and final values of the speed are given; the optimal trajectories then are formed by a singular arc and two minimum/maximum-thrust arcs that join the singular arc with the given initial and final points. This study has been quite general, in the sense that it has been made for a general aircraft model and a general horizontal wind profile, although results have been presented for constant profiles.

The main objective of this chapter has been the analysis of the effects of average horizontal winds on the optimal problem, both qualitative and quantitatively. The analysis has given, first, the optimal cruise speed and the optimal control required to meet the given flight time in the presence of a given average wind, and second, the corresponding minimum fuel consumption. The influence of the initial aircraft weight and the given cruise altitude on the optimal results has been analyzed as well.

From the operational point of view, if one considers a reference scenario with a given flight time and a nominal average wind, the analysis has allowed to quantify, first, the change in cruise speed required in the case of having a different wind, and second, the fuel penalty associated, that is, the cost of meeting the given flight time under the mismodeled wind. The results have shown that mismodeled headwinds have fuel penalties larger than mismodeled tailwinds for the same wind speed error.

As a second application, the cost of absorbing a flight delay imposed on a nominal optimal path with a nominal average wind has been also quantified: it has been shown that, for a

given delay, the cost in the presence of tailwinds is larger than in the presence of headwinds. Although results have been presented for uniform wind profiles, the analysis has been general, and any other altitude-dependent wind profile could be considered as well.

Despite their theoretical interest, the optimal variable-Mach solutions may not be flyable (according to common air traffic control practice), however, they are a reference for optimal performance and, hence, have been used to assess the optimality of the standard procedure of cruising at constant speed. The results have shown that the performance of this standard constant-Mach procedure is very close to optimal for all values of flight time, wind, aircraft weight and altitude considered in the analysis (in fact, it has been shown that in some cases optimality is obtained by flying at Mach approximately constant).

This page intentionally left blank

6 Maximum-Range Unpowered Descent

6.1 Introduction

As indicated in Chapter 2, in the optimization of the descent flight of commercial aircraft, the objective is to descend and decelerate continuously, so that the economical and environmental impacts are minimized, keeping thrust as low as possible for as long as possible.

In this chapter, an optimization analysis of the descent flight in the presence of altitude-dependent winds, in the case of zero thrust, is presented. The objective is to maximize the aircraft range, so that the unpowered descent can be initiated as far in advance as possible. In this problem the initial and final values of altitude and speed are given; the initial values correspond to cruise conditions, and the final values correspond to the conditions at a hypothetical approach fix within the terminal maneuvering area (TMA). Horizontal altitude-dependent winds are considered, with the acceleration term included in the formulation, so that wind-shear effects can be analyzed. A general compressible drag polar is considered, and no limiting constraint on altitude is imposed. The two main objectives of this chapter are: 1) to optimize the descent in the presence of altitude-dependent winds; and 2) to assess the optimality of a descent procedure, commonly used in practice (a constant-calibrated-airspeed descent).

The analysis is made using the theory of singular optimal control, which has the great advantage of providing feedback control laws (control variables as functions of the state variables), that can be directly used to guide the aircraft along the optimal path. The control variable is the aerodynamic path angle (γ). The initial and final speeds and altitudes are given, so that the structure chosen for the optimal control is of the bang-singular-bang type, with the optimal paths formed by a singular arc and two minimum-γ arcs joining the singular arc with the given initial and final points. For typical cruise and TMA conditions and for $\gamma_{max} > 0$, the initial and final bang arcs correspond to two short climbs, as reported by Rivas et al. [57] in the case of no wind, which is in accordance with the results presented by Bryson et al. [14], and Shapira and Ben-Asher [64, 65].

Despite their theoretical interest, optimal solutions may not be flyable according to present-day air traffic procedures and regulations. However, they represent best performance and can be used either as references to design improved flight procedures or to assess the optimality of flight procedures commonly used in practice, as for example the case of idle-thrust, constant-calibrated-airspeed (CAS) descents considered by Oseguera and Williams [50]. In

Franco et al. [32], a constant-CAS unpowered-descent procedure, composed of three segments (initial and final horizontal decelerations, and descent with constant CAS), is optimized to give maximum range in the presence of altitude-dependent winds using parametric optimization theory (see Fletcher [29]); the optimization parameter is the descent CAS. In this chapter the optimality of constant-CAS unpowered-descents is analyzed by comparing results from Ref. [32] with the optimal ones. The comparison shows that the optimized constant-CAS descent is very close to optimal for all wind profiles considered (this result was shown to hold in the case of no wind by Rivas et al. [57]).

Results are presented for a model of a Boeing 767-300ER, for linear wind profiles (characterized by two parameters, namely, the average wind speed and the profile slope or wind shear), and for $\gamma_{max} = 0$ (so that the initial and final short climbs reported by Rivas et al [57] become horizontal flight segments, as in the constant-CAS procedure with which the optimal results are compared). The influence of the two wind parameters and of the initial aircraft weight on the results is analyzed. For the wind profiles considered, it is shown that the wind shear has a clear effect on the optimal performance, modifying the maximum range in about 4%: increasing for tailwinds and decreasing for headwinds.

The outline of the chapter is as follows: in Section 6.2 the optimal problem is formulated, including equations of motion, performance index, application of the necessary conditions for optimality and obtention of the singular surface and the singular control; the numerical procedure to solve the optimal problem is described in Section 6.3; some results are presented in Section 6.4, both for the optimal and the optimized constant-CAS problems, along with the comparison between the two procedures and the analysis of the effect of the aircraft weight on the results; and finally, a summary of the main results and conclusions is included in Section 6.5.

6.2 Problem Formulation

In this section, the problem of maximum-range unpowered descent is formulated. First, the optimal control problem is stated by defining the equations of motion (along with the initial and final conditions) and the performance index considered. Second, because an indirect numerical method is considered for the resolution of the problem, the necessary conditions for optimality are included. Then, the optimal trajectories are describe, including equations defining the singular arc (a surface in the state space) and the singular control (which is a feedback control law).

6.2.1 Optimal Control Problem

The equations of motion (3.41) particularized to a descent phase, in which one has the additional constraint that $\pi = 0$, reduces to

$$\begin{aligned} \dot{V} &= -\frac{D}{m} - g\gamma - V\frac{\mathrm{d}w}{\mathrm{d}h}\gamma \\ \dot{h} &= V\gamma \\ \dot{x} &= V + w \end{aligned} \tag{6.1}$$

In this problem there are three states, V, h and x, and one control, γ. The initial values of speed, altitude and distance (V_i, h_i, x_i), and the final values of speed and altitude (V_f, h_f) are given. The final value of distance (x_f) and the flight time (t_f) are unspecified. The aircraft mass m, which plays the role of a parameter, is a given constant.

The objective in this problem is to maximize range, that is, to minimize the following performance index

$$J = -\int_0^{t_f} (V + w)\, \mathrm{d}t \tag{6.2}$$

The optimal descent problem considered reduces to minimize the performance index given by Eq. (6.2) subject to the constraints defined by the equations of motion (6.1).

6.2.2 Necessary Conditions for Optimality

The Hamiltonian of this problem is given by

$$H = -(V + w) - \lambda_V \left(\frac{D}{m} + g\gamma + Vw'\gamma \right) + \lambda_h V\gamma + \lambda_x (V + w) \tag{6.3}$$

where $()'$ denotes derivative with respect to h; and λ_V, λ_h and λ_x are the adjoint variables.

Assuming that the normality and non-triviality conditions are satisfied, the necessary conditions for optimality are summarized next (see Chapter 3):

1) The equations defining the adjoints:

$$\begin{aligned}
\dot{\lambda}_V &= -\frac{\partial H}{\partial V} = 1 + \lambda_V \left(\frac{1}{m}\frac{\partial D}{\partial V} + w'\gamma \right) - \lambda_h \gamma - \lambda_x \\
\dot{\lambda}_h &= -\frac{\partial H}{\partial h} = w' + \lambda_V \left(\frac{1}{m}\frac{\partial D}{\partial h} + Vw''\gamma \right) - \lambda_x w' \\
\dot{\lambda}_x &= -\frac{\partial H}{\partial x} = 0
\end{aligned} \tag{6.4}$$

The last equation leads to constant λ_x.

2) The transversality conditions: First, because the final distance x_f is not specified, one has

$$\lambda_x(t_f) = 0 \tag{6.5}$$

which leads, together with the last Eq. (6.4), to

$$\lambda_x(t) = 0 \tag{6.6}$$

Second, because the final time is not specified, one has

$$H(t_f) = 0 \tag{6.7}$$

3) The Hamiltonian minimization condition: For the control to be optimal, it is necessary that it globally minimize the Hamiltonian. The Hamiltonian is linear in γ, so that it can be written as

$$H = \overline{H} + S\gamma \tag{6.8}$$

with

$$\begin{aligned} \overline{H} &= -\left(V + w + \lambda_V \frac{D}{m}\right) \\ S &= \lambda_h V - \lambda_V (g + V w') \end{aligned} \tag{6.9}$$

where equation (6.6) has been taken into account. S is the switching function. As a consequence, this is a singular optimal control problem. The Hamiltonian minimization condition for singular optimal control problems has a special form given by equation (3.18), which in this case defines the optimal control as follows

$$\gamma = \begin{cases} \gamma_{max} & \text{if} \quad S < 0 \\ \gamma_{min} & \text{if} \quad S > 0 \\ \gamma_{sing} & \text{if} \quad S = 0 \text{ over a finite time interval} \end{cases} \tag{6.10}$$

where γ_{sing} is the singular control (yet to be determined), which satisfies $\gamma_{min} < \gamma_{sing} < \gamma_{max}$. The trajectory segments defined by γ_{sing} are singular arcs.

As indicated in Chapter 3, in singular optimal control problems there arise additional conditions that must be satisfied in order both, for a singular arc to be minimizing, and for the junctions between singular and nonsingular arcs to be optimal. These additional necessary condition for optimality are analyzed below in Section 6.2.3.2.

Finally, because the Hamiltonian is not an explicit function of time (as the problem is autonomous), the Hamiltonian constancy condition applies, and using Eq. (6.7) one gets

$$H(t) = 0 \tag{6.11}$$

along the optimal trajectory.

6.2.3 Optimal Trajectories

In general the optimal trajectory will be composed of singular arcs (with γ_{sing}) and arcs with γ_{min} or γ_{max}; whether one has γ_{min} or γ_{max} is defined by the sign of the switching function S. In this problem the solution is expected to be of the bang-singular-bang type, as suggested by the results obtained by Miele [47], Bryson et al. [14], and Shapira and Ben-Asher [64, 65], where it is shown that the maximum-range glide is defined by a central path and two initial and final branches joining that path with the initial and final conditions. Although the underlying aerodynamic and propulsive models might affect the structure of the solution, for the smooth models considered in this thesis, the bang-singular-bang structure is plausible, and hence it is the one analyzed in this chapter. Since the initial and final speeds are given, there is a physical criterium to decide whether one has γ_{min} or γ_{max}, just by comparing those speeds with the speeds that correspond to the singular arc for the initial and final altitudes.

Although called optimal trajectories, they are in fact extremals, that is, trajectories that satisfy the necessary conditions for optimality.

6.2.3.1 Singular Arc

The singular arc is defined by the following three equations

$$H = 0, \quad S = 0, \quad \dot{S} = 0 \tag{6.12}$$

where the function $\dot{S}$ is given by

$$\dot{S} = \frac{\lambda_V}{m}\left[V\frac{\partial D}{\partial h} - g\frac{\partial D}{\partial V} + w'\left(D - V\frac{\partial D}{\partial V}\right)\right] - \lambda_h\frac{D}{m} - g \tag{6.13}$$

(note that the terms in the control variable γ have cancelled out of this equation). Moreover, because $H = 0$ one also has $\overline{H} = 0$.

Hence, the three equations (6.12) that define the singular arc lead to

$$\begin{aligned} V + w + \lambda_V\frac{D}{m} &= 0 \\ \lambda_h V - \lambda_V(g + Vw') &= 0 \\ \frac{\lambda_V}{m}\left[V\frac{\partial D}{\partial h} - g\frac{\partial D}{\partial V} + w'\left(D - V\frac{\partial D}{\partial V}\right)\right] - \lambda_h\frac{D}{m} - g &= 0 \end{aligned} \tag{6.14}$$

The singular arc is obtained after eliminating the adjoints, λ_V and λ_h, from these equations. One obtains the following expression

$$V\frac{\partial D}{\partial h} - (g + Vw')\frac{\partial D}{\partial V} - g\frac{w}{V + w}\frac{D}{V} = 0 \tag{6.15}$$

which defines a singular line in the (V, h) space, namely $f(V, h) = 0$.

Miele [47] obtains, for the case of no wind ($w = 0$), the same expression in equation (6.15) for the central pattern of his solution. Note that, for $w = 0$, if one considers the specific energy $E = gh + \frac{1}{2}V^2$, and makes a change of variables in the problem $(V, h) \to (V, E)$, then one has

$$\frac{\partial D}{\partial V}\Big|_E = \frac{\partial D}{\partial V} - \frac{V}{g}\frac{\partial D}{\partial h} \tag{6.16}$$

so that one can write the expression for the singular arc, given in equation (6.15), as

$$\frac{\partial D}{\partial V}\Big|_E = 0 \tag{6.17}$$

as shown by Rivas et al. [57], which is the result obtained by Bryson et al. [14] for the central part of the maximum-range glide path.

6.2.3.2 Optimal Singular Control

Because the function $\ddot{S}$ depends linearly on the control variable γ, the order of the singular arc is $\xi = 1$. Let $\ddot{S} = A(V, m, h) + B(V, m, h)\gamma$, where

$$\begin{aligned} A(V, h) &= A_1(V, h) + wA_2(V, h) + w'A_3(V, h) \\ B(V, h) &= B_1(V, h) + wB_2(V, h) + w'B_3(V, h) + (w')^2B_4(V, h) + w''B_5(V, h) \end{aligned} \tag{6.18}$$

with

$$
\begin{aligned}
A_1(V,h) &= \frac{V}{m}\left(\frac{\partial D}{\partial h} + V\frac{\partial^2 D}{\partial V \partial h} - g\frac{\partial^2 D}{\partial V^2}\right) \\
A_2(V,h) &= \frac{1}{m}\left(2g\frac{D}{V^2} + V\frac{\partial^2 D}{\partial V \partial h} - g\frac{\partial^2 D}{\partial V^2}\right) \\
A_3(V,h) &= -\frac{V}{m}\left[\frac{\partial D}{\partial V} + (V+w)\frac{\partial^2 D}{\partial V^2}\right] \\
B_1(V,h) &= -\frac{V}{D}\left(V^2\frac{\partial^2 D}{\partial h^2} - 2gV\frac{\partial^2 D}{\partial V \partial h} - g\frac{\partial D}{\partial h} + g^2\frac{\partial^2 D}{\partial V^2}\right) \\
B_2(V,h) &= \frac{1}{D}\left(2g^2\frac{D}{V^2} + g\frac{\partial D}{\partial h} + 2gV\frac{\partial^2 D}{\partial V \partial h} - g^2\frac{\partial^2 D}{\partial V^2} - V^2\frac{\partial^2 D}{\partial h^2}\right) \\
B_3(V,h) &= \frac{V+w}{D}\left[\frac{g}{V}\left(D - V\frac{\partial D}{\partial V}\right) + V\left(\frac{\partial D}{\partial h} - 2g\frac{\partial^2 D}{\partial V^2} + 2V\frac{\partial^2 D}{\partial V \partial h}\right)\right] \\
B_4(V,h) &= -\frac{V+w}{D}V\left(\frac{\partial D}{\partial V} + V\frac{\partial^2 D}{\partial V^2}\right) \\
B_5(V,h) &= \frac{V+w}{D}V^2\frac{\partial D}{\partial V}
\end{aligned}
\tag{6.19}
$$

Therefore, because one also has $\ddot{S} = 0$ (where $S = \dot{S} = 0$), the singular control is given by

$$\gamma_{sing} = -\frac{A(V,h)}{B(V,h)} \tag{6.20}$$

The generalized Legendre-Clebsch condition for the optimality of the singular control, equation (3.21), reduces in this case ($\xi = 1$ and $u = \gamma$) to $-\dfrac{\partial \ddot{S}}{\partial \gamma} \geq 0$, which leads to

$$B(V,h) \leq 0 \tag{6.21}$$

It can be shown numerically that $B < 0$ for all the cases considered in this chapter, so that the strengthened generalized Legendre-Clebsch condition ($-\dfrac{\partial \ddot{S}}{\partial \gamma} > 0$) is satisfied.

For the case of no wind ($w = 0$), the singular control is given by

$$\gamma_{sing} = -\frac{A_1(V,h)}{B_1(V,h)} \tag{6.22}$$

and the generalized Legendre-Clebsch condition by

$$B_1(V,h) \leq 0 \tag{6.23}$$

and, in terms of the variables (V,E), it reduces to

$$\frac{\partial^2 D}{\partial V^2}\Big|_E \geq 0 \tag{6.24}$$

as shown by Rivas et al. [57].

The McDanell-Powers necessary condition for the optimality of junctions between singular and nonsingular arcs (see Chapter 3) is shown to be satisfied, because the order of the singular arc is $\xi = 1$ and the lowest-order time derivative of the control which is discontinuous at the junction is $\zeta = 0$ (that is, the control itself is discontinuous at the junction). Moreover, although the control variable is discontinuous at the junctions, the Weierstrass-Erdman corner conditions are satisfied because the adjoint variables, the Hamiltonian and the switching function are all continuous.

6.3 Numerical Procedure

In this section the numerical procedure used to solve the optimal problem is described. In Fig. 6.1 a sketch of the expected optimal path (bang-singular-bang) is presented (the particular case of two γ_{max} arcs is depicted). Knowing the structure of the solution allows one to define an efficient numerical procedure (see Maurer [44]).

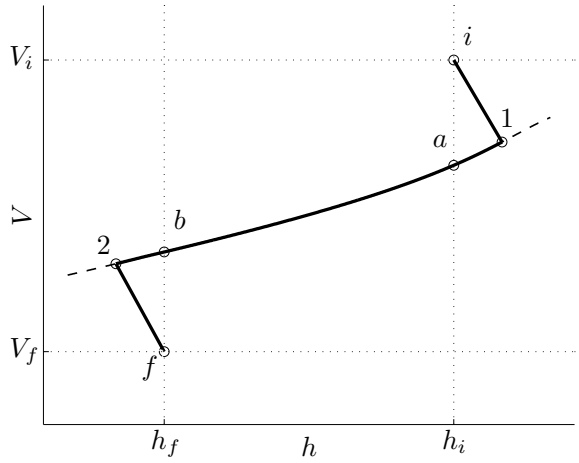

Figure 6.1: Sketch of the optimal descent path.

The following procedure is used in the numerical resolution:

Step 1. Integrate the state equations (6.1) with either $\gamma = \gamma_{min}$ or $\gamma = \gamma_{max}$ from the initial point (with known initial values V_i, h_i, and x_i) until the singular arc is reached (point 1 in Fig. 6.1), that is, until V_1 and h_1 satisfy the singular-arc equation $f(V_1, h_1) = 0$; at that point one also has x_1. The value γ_{min} or γ_{max} is chosen depending on whether one has $V_i < V_a$ or $V_i > V_a$, where V_a is defined by $f(V_a, h_i) = 0$, that is, the speed that corresponds in the singular arc to the initial altitude h_i (point a in Fig. 6.1).

Step 2. Integrate backwards the state equations (6.1) with either $\gamma = \gamma_{min}$ or $\gamma = \gamma_{max}$ from the final point (with known starting values V_f, h_f and an arbitrary value of x, which can be taken as zero), until the singular arc is reached (point 2 in Fig. 6.1), that is, until V_2 and h_2 satisfy $f(V_2, h_2) = 0$; at that point one also has the distance travelled Δx. The value γ_{min} or γ_{max} is chosen depending on whether one has $V_f > V_b$ or $V_f < V_b$, where V_b is defined by $f(V_b, h_f) = 0$, that is, the speed that corresponds in the singular arc to the final altitude h_f (point b in Fig. 6.1).

Step 3. Integrate the state equations (6.1) with $\gamma = \gamma_{sing}$ from point 1 (with known starting values V_1, h_1, and x_1) until the altitude h_2 is reached. At the end of the integration along the singular arc one also has x_2.

Once the problem is integrated, one has the final optimum value of distance $x_f = x_2 + \Delta x$, that is, the maximum range. Note that this procedure for the computation of the optimal path does not require the integration of the adjoint equations.

6.3.1 Control Structure Optimality

It still remains to check whether the assumed structure for the control (bang-singular-bang) is correct. That is, one must check that $S > 0$ for $\gamma = \gamma_{min}$ and that $S < 0$ for $\gamma = \gamma_{max}$. This requires the computation of S along the extremal path just computed. Since $S = \lambda_h V - \lambda_V(g + Vw')$, one must compute λ_V and λ_h. From Eqs. (6.3), (6.6), and (6.11) one has

$$\frac{\lambda_V}{m} = \frac{\lambda_h V\gamma - (V + w)}{D + m(g + Vw')\gamma} \tag{6.25}$$

and therefore, from Eqs. (6.4), and (6.6)

$$\dot{\lambda}_h = w' + \frac{\lambda_h V\gamma - (V + w)}{D + m(g + Vw')\gamma}\left(\frac{\partial D}{\partial h} + mVw''\gamma\right) \tag{6.26}$$

Along the first and final bangs, λ_h is obtained integrating Eq. (6.26) backwards from point 1 and forward from point 2, respectively, starting with the known values, obtained from the first and the second Eqs. (6.14)

$$\begin{aligned} \lambda_{h_1} &= -m\left[1 + \frac{w(h_1)}{V_1}\right]\frac{g + V_1 w'(h_1)}{D(V_1, h_1)} \\ \lambda_{h_2} &= -m\left[1 + \frac{w(h_2)}{V_2}\right]\frac{g + V_2 w'(h_2)}{D(V_2, h_2)} \end{aligned} \tag{6.27}$$

Once λ_h is obtained, λ_V follows from Eq. (6.25).

The numerical results show that the control structure is correct in all cases presented in Section 6.4.

6.4 Results

The aerodynamic model considered in this thesis for the numerical applications (corresponding to a Boeing 767-300ER) is described in Appendix B, and the atmosphere model is the International Standard Atmosphere.

For the wind model, linear profiles are considered, with the absolute value of the wind speed increasing with altitude (see Ref. [50]). The profiles are defined as follows

$$w(h) = \bar{w} + \Delta w\frac{h - \bar{h}}{h_i - \bar{h}} \tag{6.28}$$

where $\bar{w}$ is the average wind, Δw is the wind-shear parameter and $\bar{h} = (h_i + h_f)/2$ is the average altitude. For given values of h_i and h_f, Δw defines the wind shear $\dfrac{\mathrm{d}w}{\mathrm{d}h}$, and, in particular, $\Delta w = 0$ defines a uniform wind profile. Note that the average wind speed $\bar{w}$ satisfies

$$\bar{w} = \frac{1}{h_i - h_f}\int_{h_f}^{h_i} w(h)\mathrm{d}h \tag{6.29}$$

and, also, since the wind profiles are linear, $\bar{w}$ is the wind speed at the average altitude, that is, $\bar{w} = w(\bar{h})$. In the following, both tailwinds (TW) and headwinds (HW) are considered, with the linear profiles defined as follows: for TW one has $\bar{w} > 0$ and $\Delta w \geq 0$, and for HW $\bar{w} < 0$ and $\Delta w \leq 0$.

In this section, besides the state and control variables, the ground path angle γ_g is also analyzed, which is defined (for $\gamma, \gamma_g \ll 1$) by

$$\gamma_g = \gamma \frac{V}{V + w} \tag{6.30}$$

Results are presented for the case of initial and final γ_{max}-arcs, which require that the initial and final speeds be sufficiently high and low respectively, as it is the case in common practice. In particular, $\gamma_{max} = 0$ is considered, so that the initial and final arcs are horizontal decelerations, as in the optimized constant-CAS procedure, with which the optimum results are to be compared. (Results for $\gamma_{max} > 0$ are reported in Ref. [57] in the case of no wind.)

The initial conditions (corresponding to the final cruise conditions) are $M_i = 0.8$, $h_i =$ 33000 ft, and the final conditions (corresponding to a hypothetical approach fix within the TMA) are $CAS_f = 210$ kt, $h_f = 9000$ ft. The average altitude is then $\bar{h} = 21000$ ft. To analyze the wind effects on the optimal trajectories, the average wind ranges from -30 kt to 30 kt, and the wind-shear parameter ranges from 0 to 20 kt. In the analysis of the effect of the aircraft weight on the results, W ranges from 1100 kN to 1300 kN.

Results from Franco et al. [32] corresponding to optimized constant-CAS descents for the same performance index, aircraft and atmosphere models, wind model, as well as initial and final conditions are reproduced here. For completeness, a detailed description of this constant-CAS descent procedure is included in Appendix D.

The outline of this section is as follows. The effects of the average wind speed and the wind-shear parameter on the optimal trajectories as well as on the optimal control is first analyzed in Section 6.4.1; then, the optimal and optimized descent are compared in terms of global variables, which are also analyzed in Section 6.4.2; finally, the effects of the initial aircraft weight on the optimal and optimized results are studied in Section 6.4.3.

6.4.1 Optimal Trajectories and Optimal Control

In this section, the effects of the wind profile on the optimal trajectories are analyzed; first, the effect of the average wind speed, and second, the effect of the wind shear. In all cases the aircraft weight is $W = 1200$ kN.

6.4.1.1 Effect of the Average Wind

The optimal speed and altitude profiles $V(x)$ and $h(x)$ are represented in Fig. 6.2 for different values of the average wind ($\bar{w}$ ranging from -30 to 30 kt) and for a wind-shear parameter $\Delta w = 0$. The speed continuously decreases. Note that for the different values of $\bar{w}$, these profiles end at different values of x; the large influence of $\bar{w}$ on the horizontal distance flown is analyzed in more detail in Section 6.4.2.

The optimal control $\gamma(x)$ and the ground path angle $\gamma_g(x)$ are represented in Fig. 6.3 for the same values of the average wind as before and for $\Delta w = 0$. They are discontinuous (one has the two arcs with $\gamma_{max} = 0$, and the singular arc). The results show that both the optimal control and the ground path angle slightly decrease ($|\gamma|$ and $|\gamma_g|$ increase) along the singular arc. The average wind $\bar{w}$ has very little influence on the singular optimal control, except that it importantly affects the bang-singular and singular-bang switching times. On

the contrary, the influence on the ground path angle is larger; as $\bar{w}$ increases, the ground path angle significantly increases ($|\gamma_g|$ decreases, corresponding to flatter profiles), which is also seen in Fig. 6.2b.

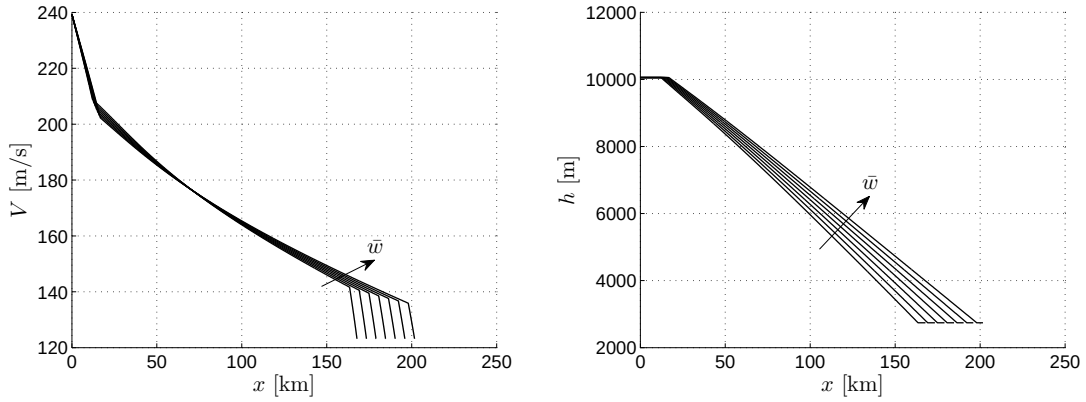

(a) (b)

Figure 6.2: Optimal speed and altitude profiles for $\bar{w} = -30, -20, -10, 0, 10, 20, 30$ kt, and $\Delta w = 0$ ($W = 1200$ kN). (a) $V(x)$, (b) $h(x)$.

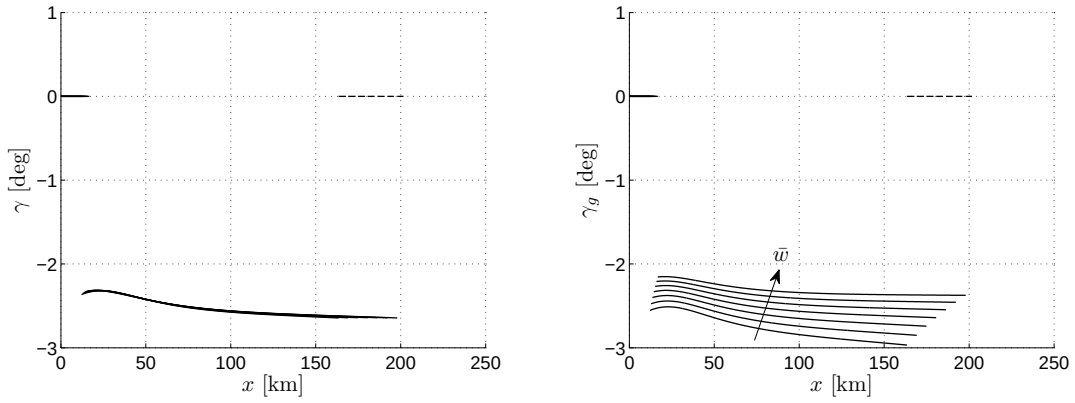

(a) (b)

Figure 6.3: Optimal control $\gamma(x)$ and ground path angle $\gamma_g(x)$ for $\bar{w} = -30, -20, -10, 0, 10, 20, 30$ kt, and $\Delta w = 0$ ($W = 1200$ kN). (a)$\gamma(x)$, (b)$\gamma_g(x)$.

6.4.1.2 Effect of the Wind Shear

The optimal speed and altitude profiles $V(x)$ and $h(x)$ are represented in Fig. 6.4 now for different values of the wind-shear parameter ($|\Delta w|$ ranging from 0 to 20 kt) and for two values of the average wind ($\bar{w} = 30$ kt, TW, and $\bar{w} = -30$ kt, HW). The influence of Δw on the optimal profiles is relatively small.

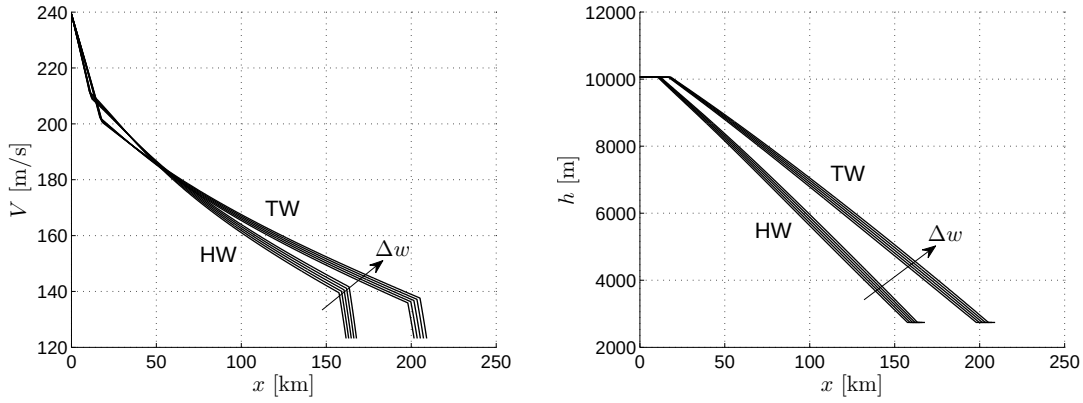

(a) (b)

Figure 6.4: Optimal speed and altitude profiles for TW ($\bar{w} = 30$ kt, $\Delta w = 0$, 5, 10, 15, 20 kt) and HW ($\bar{w} = -30$ kt, $\Delta w = 0$, -5, -10, -15, -20 kt) ($W = 1200$ kN). (a) $V(x)$, (b) $h(x)$.

The optimal control $\gamma(x)$ and the ground path angle $\gamma_g(x)$ are represented in Fig. 6.5 for the same values of Δw and $\bar{w}$ (TW and HW) as before. The results show again that both the optimal control and the ground path angle slightly decrease ($|\gamma|$ and $|\gamma_g|$ increase) along the singular arc. As the wind-shear parameter increases, both $\gamma(x)$ and $\gamma_g(x)$ slightly increase ($|\gamma|$ and $|\gamma_g|$ decrease). The influence of Δw on γ is somewhat larger than the influence of $\bar{w}$. On the contrary, the influence on γ_g is smaller. The influence of Δw on the bang-singular and singular-bang switching times is also smaller than the influence of $\bar{w}$.

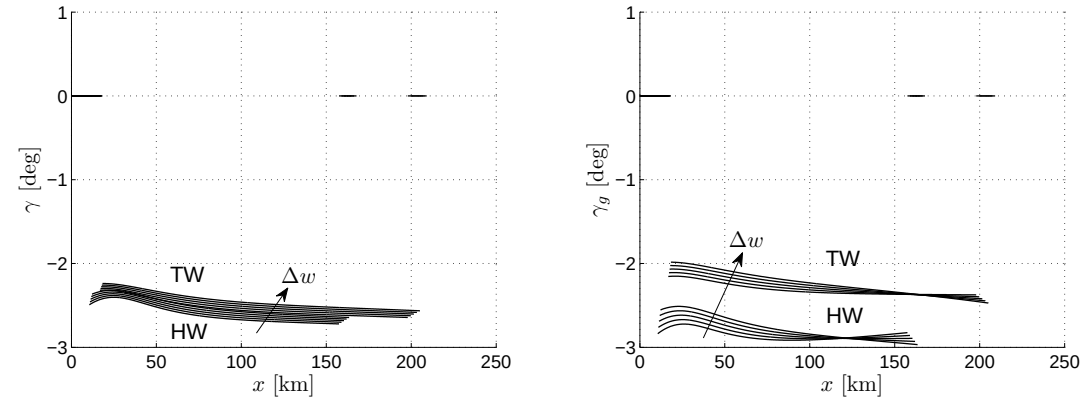

(a) (b)

Figure 6.5: Optimal control $\gamma(x)$ and ground path angle $\gamma_g(x)$ for TW ($\bar{w} = 30$ kt, $\Delta w = 0$, 5, 10, 15, 20 kt) and HW ($\bar{w} = -30$ kt, $\Delta w = 0$, -5, -10, -15, -20 kt) ($W = 1200$ kN). (a)$\gamma(x)$, (b)$\gamma_g(x)$.

6.4.2 Comparison of Optimal and Optimized Constant-Calibrated-Airspeed Descents

In this section the optimized constant-CAS unpowered descents are compared with the optimal descents. The comparison is made in terms of the maximum range and the corresponding flight time, global variables which are also analyzed in this section. In all cases the aircraft weight is $W = 1200$ kN.

The maximum range and the flight time for both problems are represented as functions of the average wind for a wind-shear parameter $\Delta w = 0$ in Fig. 6.6, and as functions of the wind-shear parameter for two values of the average wind ($\bar{w} = 30$ kt, TW, and $\bar{w} = -30$ kt, HW) in Fig. 6.7. One can see that the differences between both sets of results are almost negligible in all cases (less than 45 m in maximum range and less than 0.5 s in flight time).

In the following section, where the effect of the aircraft weight is analyzed, results for speed, altitude, and aerodynamic path angle profiles are presented for optimal and optimized constant-CAS descents, so that the comparison between both sets of results is pursued further. Again the differences are almost negligible. Hence, it can be concluded that the constant-CAS procedure is very close to optimal, provided that the optimum value of CAS_d is used in the descent.

The results (Fig. 6.6) show that the maximum range increases as the average wind speed increases, as expected, going from 167.79 km for $\bar{w} = -30$ kt (HW) to 201.70 km for $\bar{w} = 30$ kt (TW); that is, an increase of 33.91 km (20.2%) when the average wind changes from HW to TW at $|\bar{w}| = 30$ kt. One can also see that the rate of increase of the maximum range is approximately constant: about 0.56 km/kt. On the other hand, the flight time is less sensitive than the maximum range to changes in $\bar{w}$, increasing from 18.03 min to 18.54 min for the same increase in average wind speed as before; that is, an increase of just 0.51 min (2.8%).

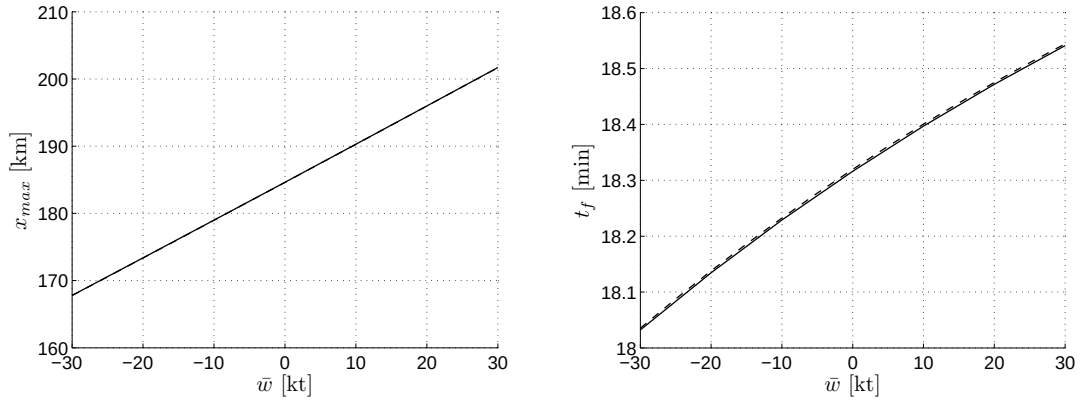

(a) (b)

Figure 6.6: Maximum range and flight time vs. average wind for $\Delta w = 0$ ($W = 1200$ kN). Solid lines: optimal descents. Dashed lines: optimized constant-CAS descents.

The influence of the wind shear on the maximum range is analyzed next (see Fig. 6.7a). For $\bar{w} = 30$ kt (TW), the maximum range increases when Δw increases: going from 201.70 km to 209.10 km when Δw increases from 0 to 20 kt (an increase of 7.40 km, that is 3.67%), with an approximately constant rate of increase of about 0.37 km/kt. On the other hand, for $\bar{w} = -30$ kt (HW), the maximum range decreases when Δw decreases (that is, when $|\Delta w|$ increases): going from 167.79 km to 161.67 km when Δw decreases from 0 to -20 kt (a decrease of 6.12 km, that is 3.65%), with an approximately constant rate of decrease of about 0.31 km/kt.

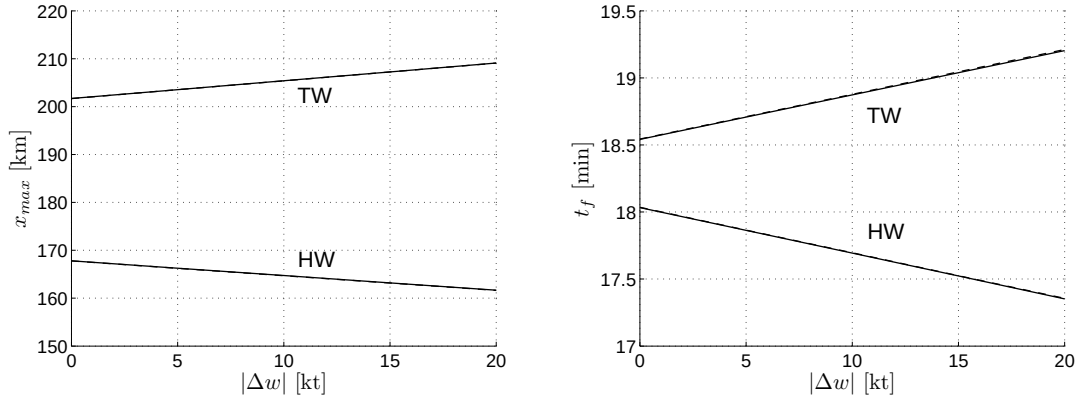

(a) (b)

Figure 6.7: Maximum range and flight time vs. wind-shear parameter for TW ($\bar{w} = 30$ kt) and HW ($\bar{w} = -30$ kt) ($W = 1200$ kN). Solid lines: optimal descents. Dashed lines: optimized constant-CAS descents.

Now the influence of the wind shear on the flight time is studied (see Fig. 6.7b). The trends are analogous to the case of the maximum range. For $\bar{w} = 30$ kt (TW), the flight time increases as Δw increases: going from 18.54 min for $\Delta w = 0$ to 19.20 min for $\Delta w = 20$ kt (an increase of 0.66 min, that is 3.56%), with an approximately constant rate of increase of about 1.99 s/kt. On the other hand, for $\bar{w} = -30$ kt (HW), the flight time decreases when Δw decreases (that is, when $|\Delta w|$ increases): going from 18.03 min for $\Delta w = 0$ to 17.35 min for $\Delta w = -20$ kt (a decrease of 0.68 min, that is 3.78%), with an approximately constant rate of decrease of about 2.04 s/kt.

Comparatively, the wind shear affects equally the maximum range and the flight time.

Hence, one can conclude first that the stronger the TW and the wind shear are, the larger the maximum range and the flight time are, and second that the stronger the HW and the wind shear are, the smaller the maximum range and the flight time are. The maximum range increases from 161.67 km for $(\bar{w}, \Delta w) = (-30, -20)$ kt (HW) to 209.10 km for $(\bar{w}, \Delta w) = (30, 20)$ kt (TW); that is, an increase of 47.43 km (29.3%). And the flight time increases from 17.35 min to 19.20 min for the same winds as before; that is, an increase of 1.85 min (10.7%).

6.4.3 Effects of the Aircraft Weight on the Results

In this section, the effects of the aircraft weight on the results are analyzed, with W ranging from 1100 kN to 1300 kN.

6.4.3.1 Effects on the State and Control Variables

The speed, altitude and aerodynamic path angle profiles ($V(x)$, $h(x)$, and $\gamma(x)$) that correspond to the optimal and the optimized constant-CAS descents are presented in Figs. 6.8, 6.9, and 6.10, respectively, for different values of W, for two values of the average wind ($\bar{w} = 30$ kt, TW, and $\bar{w} = -30$ kt, HW), and for $\Delta w = 0$.

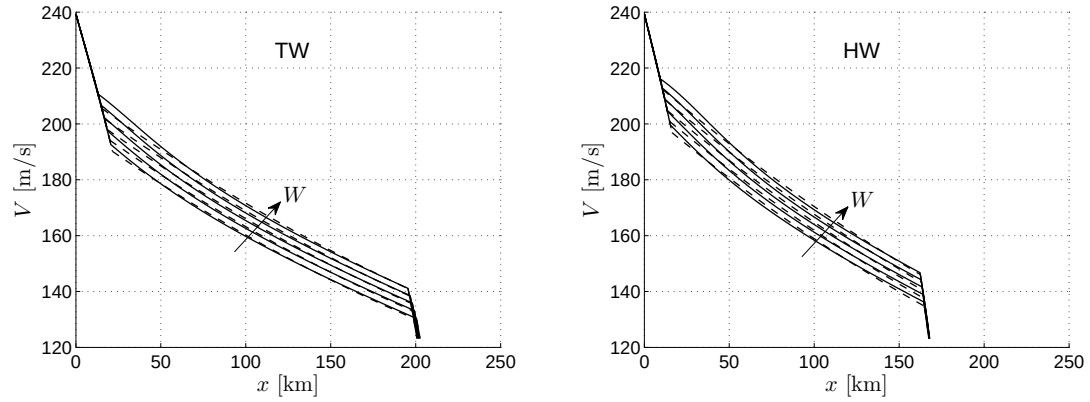

(a) (b)

Figure 6.8: Speed profiles for $\Delta w = 0$ and $W = 1100$, 1150, 1200, 1250, 1300 kN. Solid lines: optimal descents. Dashed lines: optimized constant-CAS descents. a) TW ($\bar{w} = 30$ kt), b) HW ($\bar{w} = -30$ kt).

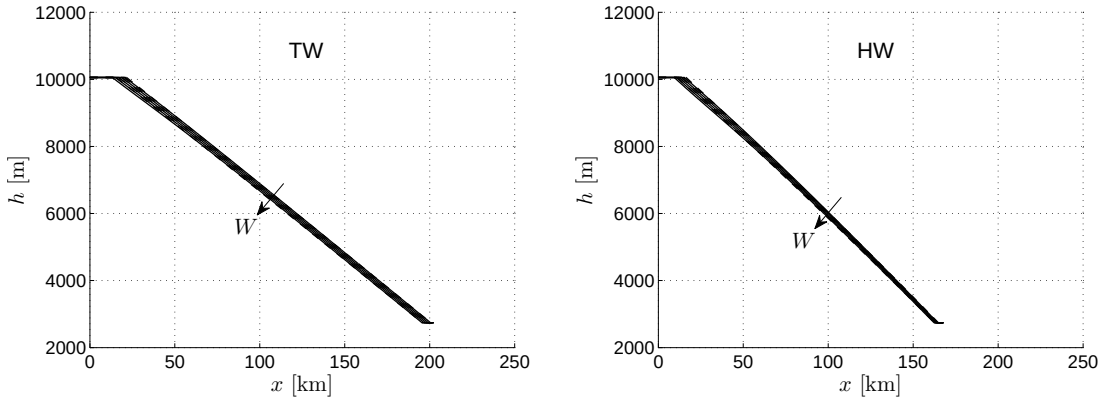

(a) (b)

Figure 6.9: Altitude profiles for $\Delta w = 0$ and $W = 1100$, 1150, 1200, 1250, 1300 kN. Solid lines: optimal descents. Dashed lines: optimized constant-CAS descents. a) TW ($\bar{w} = 30$ kt), b) HW ($\bar{w} = -30$ kt).

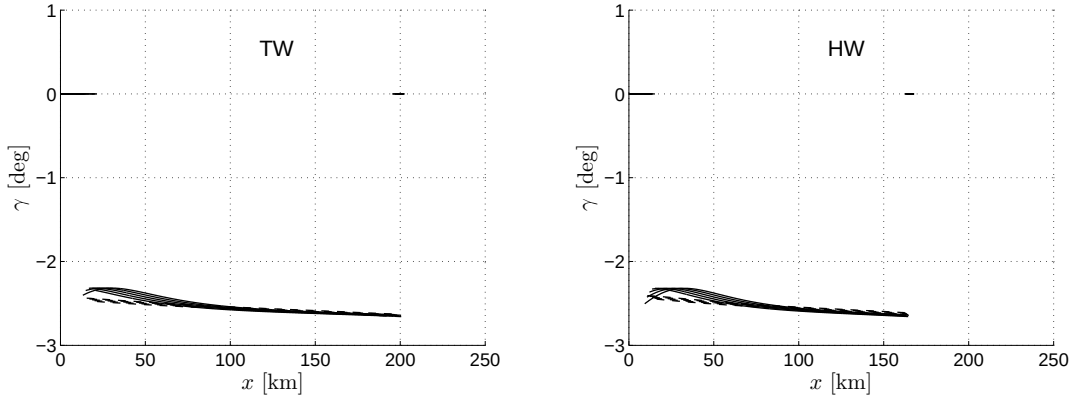

(a) (b)

Figure 6.10: Path angle $\gamma(x)$ for $\Delta w = 0$ and $W = 1100$, 1150, 1200, 1250, 1300 kN. Solid lines: optimal descents. Dashed lines: optimized constant-CAS descents. a) TW ($\bar{w} = 30$ kt), b) HW ($\bar{w} = -30$ kt).

One can see that as the aircraft weight increases, 1) the speed during the singular arc increases, 2) the altitude slightly decreases, and 3) the aircraft weight has very little influence on the singular optimal control. The influence on the ground path angle is not represented graphically because the dependence is very small, as can be inferred from Fig. 6.9.

As it was advanced in the previous section, the differences between the profiles for the optimal and the optimized constant-CAS descents are almost negligible for all weights, showing again that the constant-CAS procedure is very close to optimal.

6.4.3.2 Effects on the Maximum Range and Flight Time

The maximum range and the corresponding flight time for the optimal and for the optimized constant-CAS descents are represented as functions of the aircraft weight in Fig. 6.11 for three values of the average wind ($\bar{w} = 30$ kt, TW; no wind, NW; and $\bar{w} = -30$ kt, HW) and for different values of the wind-shear parameter ($|\Delta w|$ from 0 to 20 kt, in the cases of TW and HW).

The influence of W on the maximum range is very small, for all wind profiles considered. However, the influence of W on the flight time is larger: as the aircraft weight increases, the flight time decreases in an almost linear way. The rate of decrease is roughly independent of the wind condition: about 75 s when W increases from 1100 kN to 1300 kN.

Again, the differences between the optimized constant-CAS results and the optimal results are almost negligible for all weights and wind conditions (less than 30 m in maximum range and less than 0.5 s in flight time).

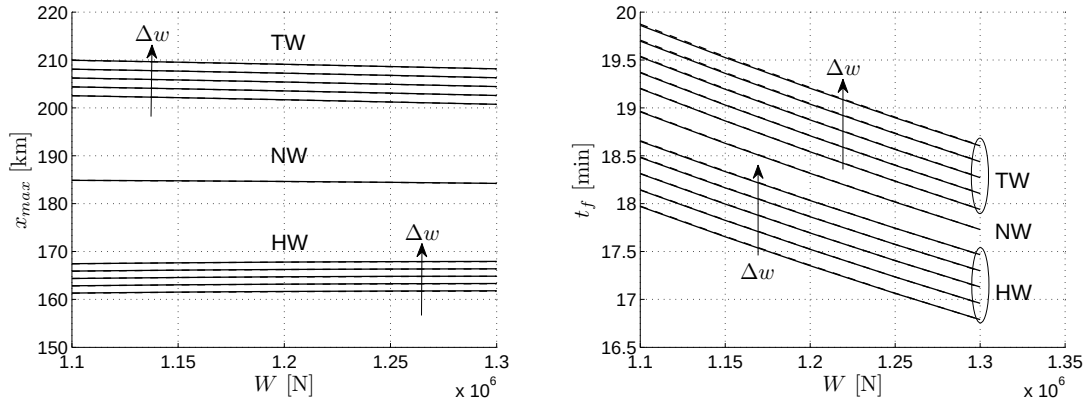

(a) (b)

Figure 6.11: Maximum range and flight time vs. aircraft weight for TW ($\bar{w} = 30$ kt, $\Delta w = 0$, 5, 10, 15, 20 kt), NW ($\bar{w} = \Delta w = 0$), and HW ($\bar{w} = -30$ kt, $\Delta w = 0$, -5, -10, -15, -20 kt). Solid lines: optimal descents. Dashed lines: optimized constant-CAS descents.

6.5 Summary

An analysis of maximum-range, unpowered descent in the presence of altitude-dependent winds has been made, using the theory of singular optimal control. The optimal control is of the bang-singular-bang type, and the optimal paths are formed by a singular arc and two minimum/maximum-γ arcs joining the singular arc with the given initial and final points. Results have been presented for the case of initial and final γ_{max}-arcs, in the particular case of $\gamma_{max} = 0$, which lead to two short horizontal deceleration segments at the beginning and at the end of the optimal trajectory. This analysis has been used to assess the optimality of a constant-CAS, unpowered descent procedure defined by three segments (descent with constant CAS and initial and final horizontal decelerations), which is defined and optimized in Ref. [32].

This study has been quite general, in the sense that it has been made for a general aircraft model and a general horizontal wind profile, although results have been presented for linear profiles. In the numerical applications, the linear wind profiles have been defined by two parameters: the average wind and the wind shear. The influence of these two parameters on the results and the influence of the initial aircraft weight have been analyzed.

The results have shown that the average wind affects strongly the maximum range, as expected, increasing for tailwinds and decreasing for headwinds. Its effect on the flight time is much weaker. The influence of the wind shear has been shown to be moderately large, presenting the same trends as the average wind, that is, increasing the maximum range and the flight time in the case of tailwinds and decreasing them in the case of headwinds. Comparatively, the wind shear affects the flight time more strongly than the average wind; on the contrary, its effect on the maximum range is weaker, but nonetheless important. The effect of the aircraft weight on the results has been analyzed as well. Its effect on the maximum range is very small, and on the flight time is considerably larger, decreasing as the aircraft weight increases.

From the operational point of view, a main conclusion can be drawn: the use of the constant-CAS descent in operational practice, when one aims at starting the unpowered descent as far in advance as possible, is justified by the very close comparison with the optimal results for all wind profiles and aircraft weights considered; that is, the performance of the optimized constant-CAS procedure is expected to be very close to optimal.

This page intentionally left blank

7 Minimum-Fuel Global Trajectory

7.1 Introduction

As indicated in Chapter 2, trajectory optimization is a subject of great importance in air traffic management (ATM). In fact, for commercial transport aircraft, minimizing fuel consumption is of prime importance, both economically and environmentally (because CO_2 emissions are directly related to fuel burnt).

In this chapter, the minimum-fuel global-trajectory problem is analyzed, taking into account altitude-dependent horizontal winds, so that wind-shear effects can be analyzed. The aircraft mass is not taken as constant but considered as a state variable, and a general aircraft performance model is considered (general compressible drag polar, and general thrust and specific fuel consumption models dependent on speed and altitude). Trajectories are considered to be decomposed into several phases of three different types: climb, cruise and descent.

The analysis is made by applying the theory of singular optimal control to a switched dynamical system. This approach has the great advantage of providing feedback control laws (control variables as functions of the state variables), that can be directly used to guide the aircraft along the optimal path. The control variable is the aerodynamic path angle (γ) for climb and descent phases, and the throttle setting (π) for the cruise phase. As in Chapters 4, 5 and 6, the structure chosen for the optimal control in every phase is of the bang-singular-bang type, with the optimal paths formed by a singular arc and two minimum/maximum arcs joining the singular arc with the initial and final switching points.

Results are presented for a model of a Boeing 767-300ER performing a climb-cruise-climb-cruise-descent trajectory, and for linear wind profiles, characterized by two parameters: the average wind speed and the speed-profile slope or wind shear. The influence of the two wind parameters and of the initial aircraft weight on the results is analyzed. The strong effect of the wind shear is described.

The outline of the chapter is as follows: the problem is formulated in Section 7.2, including equations of motion, performance index, application of the necessary conditions for optimality and description of the optimal trajectories; the implemented numerical method is explained in Section 7.3; the particular application considered is defined in Section 7.4; and finally, some results are presented in Section 7.5.

7.2 Problem Formulation

In this section, the problem of minimum-fuel global trajectory is formulated. First, the trajectory optimization problem (consisting of the performance index, the equations of motion and the initial and final conditions) is categorized as a multiphase optimal control problem whose phases are also defined. Second, because an indirect numerical method is considered for the resolution of the switched optimal control problem, the necessary conditions for optimality are included. Then, the optimal flight phases are described, including the equations defining the singular arc and the singular control at each phase. These equations coincide with those obtained for the previous applications in which a single phase is optimized (although in some cases additional considerations must be made).

7.2.1 Optimal Control Problem

Under appropriate assumptions, the equations of motion for a flight in a vertical plane subject to an altitude-dependent horizontal wind $w(h)$ are Eqs. (3.41), which are reproduced here for completeness:

$$\begin{aligned} \dot{V} &= \frac{T-D}{m} - g\gamma - V\frac{dw}{dh}\gamma \\ \dot{m} &= -cT \\ \dot{h} &= V\gamma \\ \dot{x} &= V + w \end{aligned} \tag{7.1}$$

In this problem there are four states, V, m, h and x, and two controls, γ and π. The initial values of speed, mass, altitude and distance (V_i, m_i, h_i, x_i), and the final values of speed, altitude and distance (V_f, h_f, x_f) are given. The final value of mass (m_f), and flight time (t_f) are unspecified. Without loss of generality, $t_i = 0$ and $x_i = 0$ are considered.

In this chapter, minimum-fuel global trajectories with fixed range are analyzed. However, it turns out to be more convenient to consider the equivalent problem of minimizing the following performance index

$$J \doteq (m_i - m_f) - Kx(t_f) = \int_0^{t_f} [cT - K(V+w)]\,\mathrm{d}t, \tag{7.2}$$

with $x(t_f)$ unspecified. For both problems to be equivalent, one has to find the unknown parameter K for which the free-range optimal trajectory travels the assigned final range x_f, as proven next. Let z be a state variable specified at an unspecified final time. The transversality condition of the associated adjoint λ_z is given by $\lambda_z(t_f) = \nu_z$, where ν_z may be regarded as a control parameter that makes the terminal value of z take the specified value (see Bryson and Ho [15]). If now the final value of that state, $z(t_f)$, were unspecified and a linear terminal cost function $-Kz(t_f)$ were considered, the transversality condition on λ_z would be $\lambda_z(t_f) = -K$, and the remaining necessary conditions for optimality would remain unchanged. Hence, both problems are equivalent if $K = -\nu_z$ is chosen, that is, if the cost factor K is chosen so that the terminal value of z is the specified one.

Therefore, the problem can be written as in Eq. (3.4), where $\mathbf{y} = (V, m, h, x)$ is the state vector, $\mathbf{u} = (\gamma, \pi)$ is the control vector, $l(\mathbf{y}, \mathbf{u}) = cT - K(V+w)$ is the running

cost, no terminal cost is considered, $U = \{(\gamma, \pi) \in \mathbb{R}^2 : \gamma_{min} \leq \gamma \leq \gamma_{max} \text{ and } 0 \leq \pi_{min} \leq \pi \leq \pi_{max} = 1\}$ is the control set, $t_i = 0$, $\mathbf{y}_i = (V_i, m_i, h_i, 0)$, $\psi[t_f, \mathbf{y}(t_f)] = (V(t_f), h(t_f)) - (V_f, h_f)$ is the final-state-constraint function, and t_f is unspecified. Note that the initial and final values of the states are the same as before, except for the final value of the distance $x(t_f)$, which is now unspecified.

The global trajectory considered in this chapter is composed of climb, cruise and descent phases in a prespecified phase sequence $\sigma = (q_1, ..., q_N)$. According to Section 3.2, this allows for the optimization of the controlled aircraft motion to be considered as a multiphase optimal control problem. Hence, the problem can be stated as in Eq. (3.26) with some considerations: the running costs l_{q_j} at each phase q_j are particularizations of l according to the type of phase corresponding to q_j; no terminal cost is considered; $Q \doteq \{cl, cr, d\}$ is the set of types of phases, where cl, cr, and d stand for climb, cruise and descent, respectively; and the values of the states at the switching instants (V_j, m_j, h_j, x_j) and the switching instants themselves (t_j) for $j = 1, ..., N-1$ are unspecified. Again, the initial and final values of the states are the same as before, with $x(t_f)$ being unspecified.

In the next subsections, the dynamic state equations $\dot{\mathbf{y}} = \mathbf{f}_q(\mathbf{y}, u_q)$, the control variable u_q, the control constraints $u_{q_{min}} \leq u_q \leq u_{q_{max}}$, the running cost $l_q(\mathbf{y}, u_q)$, and the Hamiltonian $H_q(\mathbf{y}, u_q, \lambda) = l_q(\mathbf{y}, u_q) + \lambda^T \mathbf{f}_q(\mathbf{y}, u_q)$, where $\lambda \in \mathbb{R}^4$ is the adjoint vector, are defined for each $q \in Q$. The Hamiltonian is needed to apply the necessary conditions for optimality, which is done in Section 7.2.2.

7.2.1.1 Climb Phase

During climb ($q = cl$), the additional constraint that π is a known parameter ($\pi = \pi_{cl}$) is considered in this thesis. The equations of motion in this phase are Eqs. (4.1), which are reproduced here for completeness:

$$\begin{aligned} \dot{V} &= \frac{\pi_{cl} T_M - D}{m} - g\gamma - V\frac{dw}{dh}\gamma \\ \dot{m} &= -c\pi_{cl} T_M \\ \dot{h} &= V\gamma \\ \dot{x} &= V + w \end{aligned} \tag{7.3}$$

Now, there is only one control, the aerodynamic path angle $u_{cl} = \gamma$, which is bounded ($\gamma_{min,cl} \leq \gamma \leq \gamma_{max,cl}$). The running cost for the climb phase is $l_{cl}(\mathbf{y}, \gamma) = c\pi_{cl} T_M - K(V + w)$, whereas the Hamiltonian is given by

$$H_{cl} = \lambda_V \left(\frac{\pi_{cl} T_M - D}{m} - g\gamma - V w' \gamma \right) + (1 - \lambda_m) c\pi_{cl} T_M + \lambda_h V \gamma + (\lambda_x - K)(V + w) \tag{7.4}$$

where $()'$ denotes derivative with respect to h, and λ_V, λ_m, λ_h and λ_x are the adjoint variables. Note that H_{cl} is linear on the control variable, so that it can be written as $H_{cl} = \overline{H}_{cl} + S_{cl}\gamma$, where $\overline{H}_{cl}$ and the *climb switching function* S_{cl} are given by

$$\begin{aligned} \overline{H}_{cl} &= \frac{\lambda_V}{m}(\pi_{cl} T_M - D) + (1 - \lambda_m) c\pi_{cl} T_M + (\lambda_x - K)(V + w) \\ S_{cl} &= \lambda_h V - \lambda_V (g + V w') \end{aligned} \tag{7.5}$$

7.2.1.2 Cruise Phase

During cruise ($q = cr$), the additional constraint of flying at constant altitude ($\gamma = 0$) is considered in this thesis. The equations of motion in this phase are Eqs. (5.1), which are reproduced here for completeness:

$$\begin{aligned} \dot{V} &= \frac{\pi T_M - D}{m} \\ \dot{h} &= 0 \\ \dot{m} &= -c\pi T_M \\ \dot{x} &= V + w \end{aligned} \tag{7.6}$$

where the dynamic equation for altitude has been maintained for the sake of consistency, although the altitude is now a constant parameter.

Again, there is only one control, the throttle setting $u_{cr} = \pi$, which is bounded ($0 < \pi_{min} \leq \pi \leq \pi_{max} = 1$). The running cost for the cruise phase is $l_{cr}(\mathbf{y}, \pi) = c\pi T_M - K\,(V + w)$, whereas the Hamiltonian is given by

$$H_{cr} = \frac{\lambda_V}{m}(\pi T_M - D) + (1 - \lambda_m)c\pi T_M + (\lambda_x - K)\,(V + w) \tag{7.7}$$

where λ_V, λ_m and λ_x are the adjoint variables. Note that H_{cr} is linear on the control variable, so that it can be written as $H_{cr} = \overline{H}_{cr} + S_{cr}\pi$, where $\overline{H}_{cr}$ and the *cruise switching function* S_{cr} are given by

$$\begin{aligned} \overline{H}_{cr} &= -\lambda_V \frac{D}{m} + (\lambda_x - K)\,(V + w) \\ S_{cr} &= \left[\frac{\lambda_V}{m} + (1 - \lambda_m)c\right] T_M \end{aligned} \tag{7.8}$$

7.2.1.3 Descent Phase

During descent ($q = d$), the additional constraint of flying unpowered ($\pi = 0$) is considered in this thesis. The equations of motion in this phase are Eqs. (6.1):

$$\begin{aligned} \dot{V} &= -\frac{D}{m} - g\gamma - V\frac{dw}{dh}\gamma \\ \dot{h} &= V\gamma \\ \dot{m} &= 0 \\ \dot{x} &= V + w \end{aligned} \tag{7.9}$$

where dynamic equation for aircraft mass has been maintained for the sake of consistency, although the mass is now a constant parameter.

There is only one control, the aerodynamic path angle $u_d = \gamma$, which is bounded ($\gamma_{min,d} \leq \gamma \leq \gamma_{max,d}$). The running cost for the descent phase is $l_d(\mathbf{y}, \gamma) = -K\,(V + w)$, whereas the Hamiltonian is given by

$$H_d = -\lambda_V \left(\frac{D}{m} + g\gamma + Vw'\gamma\right) + \lambda_h V\gamma + (\lambda_x - K)\,(V + w) \tag{7.10}$$

where λ_V, λ_h and λ_x are the adjoint variables. Note that H_d is linear on the control variable, so that it can be written as $H_d = \overline{H}_d + S_d\gamma$, where $\overline{H}_d$ and the *descent switching function* S_d are given by

$$\begin{aligned} \overline{H}_d &= -\frac{\lambda_V D}{m} + (\lambda_x - K)(V + w) \\ S_d &= \lambda_h V - \lambda_V(g + Vw') \end{aligned} \tag{7.11}$$

7.2.2 Necessary Conditions for Optimality

Assuming that the normality and non-triviality conditions are satisfied, and for a given switching sequence $\sigma = (q_1, ..., q_N)$, with $q_j \in Q$ for $j = 1, ..., N$, the necessary conditions for optimality are summarized next (see Chapter 3):

1) The adjoints are piecewise continuous functions satisfying the following dynamic equations:

$$\begin{aligned} \dot{\lambda}_V &= -\frac{\partial H_{q_j}}{\partial V} \\ \dot{\lambda}_m &= -\frac{\partial H_{q_j}}{\partial m} \\ \dot{\lambda}_h &= -\frac{\partial H_{q_j}}{\partial h} \\ \dot{\lambda}_x &= -\frac{\partial H_{q_j}}{\partial x} \end{aligned} \tag{7.12}$$

along each phase of the optimal trajectory, that is, $\forall t \in [t_{j-1}, t_j)$ ($[t_{N-1}, t_N]$ if $j = N$) for $j = 1, ..., N$. Because H_{q_j} does not depend on x (that is, $\frac{\partial H_{q_j}}{\partial x} = 0$, $\forall q_j$), λ_x is a piecewise constant function.

2) Because the states are continuous at the switching points t_j, and only controlled switchings are considered, the adjoint variables satisfy the following switching conditions:

$$\begin{aligned} \lambda_V(t_j^-) &= \lambda_V(t_j^+) \\ \lambda_h(t_j^-) &= \lambda_h(t_j^+) \\ \lambda_m(t_j^-) &= \lambda_m(t_j^+) \\ \lambda_x(t_j^-) &= \lambda_x(t_j^+) \end{aligned} \tag{7.13}$$

for $j = 1, ..., N-1$. Hence, the adjoints are continuous functions for all $t \in [0, t_f]$. In particular, the last equation (7.13) implies that λ_x is constant. Note that some authors classify these conditions as transversality conditions at the switching instants.

3) The Hamiltonian continuity condition states that, since the transition times t_j are not specified, then the Hamiltonians for the two phases contiguous at t_j satisfy the following equation:

$$H_{q_j}(t_j) = H_{q_{j+1}}(t_j) \tag{7.14}$$

for $j = 1, ..., N-1$. Again, some authors classify these conditions as transversality conditions at the switching instants.

4) The Hamiltonian minimization condition states that for the control to be optimal it is necessary that it minimize the Hamiltonian. In all flight phases considered, the Hamiltonian is linear on the control variable and the control is bounded, that is, $H_{q_j} = \overline{H}_{q_j} + S_{q_j} u_{q_j}$ and $u_{q_j,min} \leq u_{q_j} \leq u_{q_j,max}$, $\forall q_j$. Hence, the minimization of H_{q_j} with respect to u_{q_j} defines the optimal control as follows

$$u_{q_j} = \begin{cases} u_{q_j,max} & \text{if} \quad S_{q_j} < 0 \\ u_{q_j,min} & \text{if} \quad S_{q_j} > 0 \\ u_{q_j,sing} & \text{if} \quad S_{q_j} = 0 \quad \text{over a finite time interval} \end{cases} \tag{7.15}$$

for $j = 1, ..., N$, where $u_{q_j,sing}$ is the singular control (yet to be determined), which satisfies $u_{q_j,min} \leq u_{q_j,sing} \leq u_{q_j,max}$. Trajectory segments defined by $u_{q_j,sing}$ are called singular arcs, whereas trajectory segments defined by $u_{q_j,min}$ or $u_{q_j,max}$ are called bangs.

6) The transversality conditions are the following: First, since the final distance $x(t_f)$ is not specified, one has

$$\lambda_x(t_f) = 0 \tag{7.16}$$

which, along with the result that λ_x is a constant, leads to

$$\lambda_x(t) = 0 \tag{7.17}$$

along the entire optimal trajectory. Second, as the final mass $m(t_f)$ is not specified, one has

$$\lambda_m(t_f) = 0 \tag{7.18}$$

Third, since the final time t_f is not specified, one has

$$H_{q_N}(t_f) = 0 \tag{7.19}$$

Moreover, since the Hamiltonian is not an explicit function of time, one has the first integral that it is constant along each phase of the optimal trajectory, that is,

$$H_{q_j}(t) = \overline{\mathcal{H}}_j \tag{7.20}$$

for $j = 1, ..., N$, where $\overline{\mathcal{H}}_j$ are unknown constant values. This first integral, along with Eqs. (7.19) and (7.14), leads to

$$H_{q_j}(t) = 0 \tag{7.21}$$

for $j = 1, ..., N$.

As indicated in Chapter 3, in singular optimal control problems there arise additional conditions that must be satisfied in order both, for a singular arc to be minimizing, and for the junctions between singular and nonsingular arcs to be optimal. These additional necessary condition for optimality are analyzed below in Section 7.2.3 for each phase.

7.2.3 Optimal Flight Phases

The optimal global trajectory is built up by linking the optimized phases together. Although called optimal trajectories, they are in fact extremals, that is, trajectories that satisfy the necessary conditions for optimality.

In general, each optimal phase $q \in Q$ will be composed of singular arcs (with $u_{q,sing}$) and arcs with $u_{q,min}$ or $u_{q,max}$; whether one has $u_{q,min}$ or $u_{q,max}$ is defined by the sign of the switching function S_q. In this problem, each optimal phase is expected to be of the bang-singular-bang type, that is, a singular arc and two minimum/maximum-u_q arcs joining the singular arc with the initial and final points. Although the underlying aerodynamic and propulsive models might affect the structure of the solution, for the smooth models considered in this thesis, the bang-singular-bang structure is plausible, and hence it is the one analyzed in this chapter.

In the next subsections, the singular arc as well as the singular control are analyzed for the three types of optimal phases considered in this chapter.

7.2.3.1 Singular Arc at a Climb Phase

The singular control is obtained when the switching function is zero ($S_{cl} = 0$) on an interval of time; hence, since $H_{cl} = 0$, one also has $\overline{H}_{cl} = 0$. On that interval of time one has $\dot{S}_{cl} = 0$ as well. The singular arc is defined by the three equations:

$$\overline{H}_{cl} = 0, \qquad S_{cl} = 0, \qquad \dot{S}_{cl} = 0 \tag{7.22}$$

In Chapter 4, the optimization problem of a climb subject to the same equations of motion and considering the same running cost $c\pi_{cl}T_M - K\left(V + w\right)$ is analyzed. Hence, the Hamiltonian and the adjoints dynamic equations are also the same and, as a consequence, the results in Chapter 4 defining the singular arc and the singular control $\gamma_{sing,cl}(V, m, h)$ apply here.

On one hand, it is not possible to obtain an expression for the singular arc in terms of the state variables alone. Instead, the three Eqs. (4.17) define the adjoints λ_V, λ_m and λ_h along the singular arc in the terms of the state variables. On the other hand, the singular feedback control law $\gamma_{sing,cl}(V, m, h)$ is obtained from $\ddot{S}_{cl} = 0$ after eliminating the three adjoints with the equations defining the singular arc; its expression is given by Eq. (4.22).

The generalized Legendre-Clebsch condition for the optimality of the singular control, Eq. (3.21), reduces in this case ($\xi_{cl} = 1$ and $u_{cl} = \gamma$) to $-\dfrac{\partial \ddot{S}_{cl}}{\partial \gamma} \geq 0$, which leads to the same expression as in Chapter 4, that is, Eq. (4.23). It can be shown numerically that the strengthened generalized Legendre-Clebsch condition ($-\dfrac{\partial \ddot{S}_{cl}}{\partial \gamma} > 0$) is satisfied in all the cases considered in this chapter.

The McDanell-Powers necessary condition for the optimality of junctions between singular and nonsingular arcs (see Chapter 3) is shown to be satisfied, because the order of the singular arc is $\xi_{cl} = 1$ and the lowest-order time derivative of the control which is discontinuous at the junction is $\zeta_{cl} = 0$ (that is, the control itself is discontinuous at the junction). Moreover, although the control variable is discontinuous at the junctions, the Weierstrass-Erdman corner conditions are satisfied because the adjoint variables, the Hamiltonian and the switching function are all continuous.

7.2.3.2 Singular Arc at a Cruise Phase

The singular control is obtained when the switching function is zero ($S_{cr} = 0$) on an interval of time; hence, since $H_{cr} = 0$, one also has $\overline{H}_{cr} = 0$. On that interval of time one has $\dot{S}_{cr} = 0$ as well. The singular arc is defined by the three equations:

$$\overline{H}_{cr} = 0, \qquad S_{cr} = 0, \qquad \dot{S}_{cr} = 0 \tag{7.23}$$

In Chapter 5, the optimization problem of a cruise subject to the same equations of motion is analyzed, but a different running cost is considered (namely, $c\pi T_M$) and the final distance and final time are fixed. However, as it has already been shown, a problem with fixed final distance is equivalent to a problem with free final distance and an additional cost $-Kx(t_f)$ just by imposing $\lambda_x(t_f) = -K$. By doing so the Hamiltonian and the adjoints dynamic equations are the same, just by additionally imposing that the constant value of the Hamiltonian equals zero, that is $\overline{\mathcal{H}} = 0$. With this modification, the results in Chapter 5 defining the singular arc and the singular control $\pi_{sing}(V, m, h)$ apply here.

On one hand, the singular arc is defined by the Eq. (5.13), with $\Omega = w$, that is,

$$D\left(\frac{1}{\omega + V} - c - \frac{1}{c}\frac{\mathrm{d}c}{\mathrm{d}V}\right) - \frac{\partial D}{\partial V} + cm\frac{\partial D}{\partial m} = 0 \tag{7.24}$$

On the other hand, the singular feedback control law is obtained from $\ddot{S}_{cr} = 0$, after eliminating the adjoints with the Eqs. (7.23) defining the singular arc; its expression is given by Eq. (5.15).

The generalized Legendre-Clebsch condition for the optimality of the singular control, Eq. (3.21), reduces in this case ($\xi_{cl} = 1$ and $u_{cr} = \pi$) to $-\dfrac{\partial \ddot{S}_{cr}}{\partial \pi} \geq 0$, which leads to the same expression as in Chapter 5, that is, Eq. (5.17). It can be shown numerically that the strengthened generalized Legendre-Clebsch condition ($-\dfrac{\partial \ddot{S}_{cr}}{\partial \pi} > 0$) is satisfied in all the cases considered in this chapter.

The McDanell-Powers necessary condition for the optimality of junctions between singular and nonsingular arcs (see Chapter 3) is shown to be satisfied, because the order of the singular arc is $\xi_{cr} = 1$ and the lowest-order time derivative of the control which is discontinuous at the junction is $\zeta_{cr} = 0$ (that is, the control itself is discontinuous at the junction). Moreover, although the control variable is discontinuous at the junctions, the Weierstrass-Erdman corner conditions are satisfied because the adjoint variables, the Hamiltonian and the switching function are all continuous.

7.2.3.3 Singular Arc at a Descent Phase

The singular control is obtained when the switching function is zero ($S_d = 0$) on an interval of time; hence, since $H_d = 0$, one also has $\overline{H}_d = 0$. On that interval of time one has $\dot{S}_d = 0$ as well. The singular arc is defined by the three equations:

$$\overline{H}_d = 0, \qquad S_d = 0, \qquad \dot{S}_d = 0 \tag{7.25}$$

In Chapter 5, the optimization problem of an unpowered descent subject to the same equations of motion is analyzed, but a different running cost $-(V + w)$ is considered. That

running cost is similar to l_d except for a scaling factor K. Therefore, except for that factor K, the Hamiltonian and the adjoints dynamic equations are also the same and, as a consequence, the results in Chapter 6 defining the singular arc and the singular control $\gamma_{sing,d}(V,m,h)$ apply here.

On one hand, the singular arc is defined by the Eq. (6.15). On the other hand, the singular feedback control law is obtained from $\ddot{S}_d = 0$ after eliminating the three adjoints with the Eqs. (7.25); its expression is given by Eq. (6.20).

The generalized Legendre-Clebsch condition for the optimality of the singular control, Eq. (3.21), reduces in this case ($\xi_d = 1$ and $u_d = \gamma$) to $-\dfrac{\partial \ddot{S}_d}{\partial \gamma} \geq 0$, which leads to the same expression as in Chapter 6, that is, Eq. (6.21). It can be shown numerically that the strengthened generalized Legendre-Clebsch condition ($-\dfrac{\partial \ddot{S}_d}{\partial \gamma} > 0$) is satisfied in all the cases considered in this chapter.

The McDanell-Powers necessary condition for the optimality of junctions between singular and nonsingular arcs (see Chapter 3) is shown to be satisfied, because the order of the singular arc is $\xi_d = 1$ and the lowest-order time derivative of the control which is discontinuous at the junction is $\zeta_d = 0$ (that is, the control itself is discontinuous at the junction). Moreover, although the control variable is discontinuous at the junctions, the Weierstrass-Erdman corner conditions are satisfied because the adjoint variables, the Hamiltonian and the switching function are all continuous.

7.3 Numerical Procedure

In this section the numerical procedure used to solve the problem is described. Knowing the structure of the solution allows one to define an efficient numerical procedure (see Maurer [44]).

The numerical procedure is based on three different phase algorithms intended to obtain a candidate for optimal phase. To apply these phase algorithms one has to guess the values of some unknown parameters. The phase algorithms can be interpreted as blocks that have to be sequentially pieced together, according to the given phase sequence σ, in order to obtain a candidate for optimal trajectory. Finally, the numerical procedure has to iterate on the unknown parameters in order for some necessary conditions for optimality to be satisfied. Note that the numerical procedure also has to obtain the value of K for which the corresponding final value of the horizontal distance travelled $x(t_f)$ is equal to the specified one, x_f.

7.3.1 Algorithm for Optimal Climb

If the phase considered is a climb (that is, $q_j = cl$), the numerical procedure is as follows.

The first bang starts with the following initial values at the point $j-1$: $V(t_{j-1}) = V_{j-1}$, $m(t_{j-1}) = m_{j-1}$, $h(t_{j-1}) = h_{j-1}$, and $x(t_{j-1}) = x_{j-1}$. These initial values are known either because the trajectory at the previous phase has already been obtained (for the general case $j \neq 1$), or because they are the given initial values (for the particular case $j = 1$). Let λ_{V,a_j},

h_{b_j}, and V_j be the values of the adjoint λ_V at the beginning of the singular arc (point a_j), the altitude at the end of the singular arc (point b_j), and the speed at the end of the climb (point j), respectively. If λ_{V,a_j} were known, the state equations (7.3) could be integrated until the singular arc were reached, that is, until $\lambda_{V,a_j} = f_V(V_{a_j}, m_{a_j}, h_{a_j})$ were satisfied (see Eqs. 4.18). Then, using Eqs. (7.22), λ_m and λ_h could be obtained at a_j, so that the adjoint equations (7.12) could be integrated backwards along the first bang. Also, if the altitude h_{b_j} were known, the state equations could be integrated along the singular arc (from point a_j to point b_j), and then, using Eqs. (7.22), λ_V, λ_m and λ_h could be obtained. Finally, if V_j were known, the state equations and the adjoint equations could be integrated along the second bang, which starts at the singular arc (point b_j) and ends when the value $V = V_j$ is reached.

At the end (point j) one has the following final values: $V(t_j) = V_j$, $m(t_j) = m_j$, $h(t_j) = h_j$, $x(t_j) = x_j$, $\lambda_V(t_j^-)$, $\lambda_h(t_j^-)$, and $\lambda_m(t_j^-)$. At the beginning (point $j-1$) one has $\lambda_V(t_{j-1}^+)$, $\lambda_h(t_{j-1}^+)$, and $\lambda_m(t_{j-1}^+)$.

The final values of the states are used as initial values for the next optimal phase calculation ($j \neq N$ in practical cases). The initial (if $j \neq 1$) and final values of the adjoints are used to impose some necessary conditions for optimality and, hence, to define λ_{V,a_j}, h_{b_j}, and V_j. This task is performed by means of an iterative procedure (described in Section 7.3.4), when all phases in σ are already computed.

7.3.2 Algorithm for Optimal Cruise

If the phase considered is a cruise (that is, $q_j = cr$), the numerical procedure is as follows.

The first bang starts with the following initial values at the point $j-1$: $V(t_{j-1}) = V_{j-1}$, $m(t_{j-1}) = m_{j-1}$, and $x(t_{j-1}) = x_{j-1}$, with $h(t_{j-1}) = h_{j-1}$ playing the role of a parameter during this phase ($h = const$). These initial values are known because the trajectory at the previous phase has already been obtained; note that, in practical cases, the first phase from the sequence σ is not a cruise phase ($j \neq 1$). Let x_{b_j} and V_j be the values of the distance travelled at the end of the singular arc (point b_j) and the speed at the end of the cruise (point j), respectively. The state equations (7.6) can be integrated until the singular arc (Eq. 7.24) is reached (point a_j). Then, using the first two Eqs. (7.23), λ_V and λ_m could be obtained at a_j, so that the adjoint equations (7.12) could be integrated backwards along the first bang. If x_{b_j} were known, the state equations could be integrated along the singular arc (from point a_j to point b_j), and then, using the first two Eqs. (7.23), λ_V and λ_m could be obtained. Finally, if V_j were known, the state equations and the adjoint equations could be integrated along the second bang, which starts at the singular arc (point b_j) and ends when the value $V = V_j$ is reached.

At the end (point j) one has the following final values: $V(t_j) = V_j$, $m(t_j) = m_j$, $h(t_j) = h_j = h_{j-1}$, $x(t_j) = x_j$, $\lambda_V(t_j^-)$ and $\lambda_m(t_j^-)$. At the beginning (point $j-1$) one has $\lambda_V(t_{j-1}^+)$ and $\lambda_m(t_{j-1}^+)$. Once the full state as well as the adjoints λ_V and λ_m are known, and in order to obtain the remaining adjoint variable λ_h, one has to integrate its dynamic equation along the entire cruise phase (from $j-1$ to j), starting from $\lambda_h(t_{j-1}^+)$. Note that $\lambda_h(t_{j-1}^-)$ is known from the previous phase (again $j \neq 1$ in practical cases), and the necessary condition $\lambda_h(t_{j-1}^+) = \lambda_h(t_{j-1}^-)$ is imposed.

The final values of the state are used as initial values for the next optimal phase calculation (as $j \neq N$ in practical cases). The initial (as $j \neq 1$ in practical cases) and final values of some of the adjoints are used to impose some necessary conditions for optimality and, hence, to define x_{b_j} and V_j. This task is performed by means of an iterative procedure (described in Section 7.3.4), when all phases in σ are already computed.

7.3.3 Algorithm for Optimal Descent

If the phase considered is a descent (that is, $q_j = d$), the numerical procedure is as follows.

The first bang starts with the following initial values at the point $j-1$: $V(t_{j-1}) = V_{j-1}$, $h(t_{j-1}) = h_{j-1}$, and $x(t_{j-1}) = x_{j-1}$, with $m(t_{j-1}) = m_{j-1}$ playing the role of a parameter during this phase ($m = const$). These initial values are known because the trajectory at the previous phase has already been obtained; note that, in practical cases, the first phase from the sequence σ is not a descent phase ($j \neq 1$). Let V_j and h_j be the values of the speed and the altitude, respectively, at the end of the descent (point j). The state equations (7.9) can be integrated until the singular arc (Eq. 6.15) is reached (point a_j). Then, using the first two Eqs. (7.25), λ_V and λ_h could be obtained at a_j, so that the adjoint equations (7.12) could be integrated backwards along the first bang. If V_j and h_j were known, the state equations could be integrated backwards along the second bang, that is, from j until the singular arc (Eq. 6.15) is reached (point b_j). Then, the state equations could be integrated along the singular arc (from point a_j to point b_j), and then, using the first two Eqs. (7.25), λ_V and λ_h could be obtained. Finally, the adjoint equations could be integrated along the second bang, starting at the singular arc (point b_j) and ending at j.

At the end (point j) one has the following final values: $V(t_j) = V_j$, $m(t_j) = m_j = m_{j-1}$, $h(t_j) = h_j$, $x(t_j) = x_j$, $\lambda_V(t_j^-)$ and $\lambda_h(t_j^-)$. At the beginning (point $j-1$) one has $\lambda_V(t_{j-1}^+)$ and $\lambda_h(t_{j-1}^+)$. Once the full state as well as the adjoints λ_V and λ_h are known, and in order to obtain the remaining adjoint variable λ_m, one has to integrate its dynamic equation along the entire descent phase (from $j-1$ to j), starting from $\lambda_m(t_{j-1}^+)$. Note that $\lambda_m(t_{j-1}^-)$ is known from the previous phase (again $j \neq 1$ in practical cases), and the necessary condition $\lambda_m(t_{j-1}^+) = \lambda_m(t_{j-1}^-)$ is imposed.

The initial (as $j \neq 1$ in practical cases) and final values of some of the adjoints are used to impose some necessary conditions for optimality and, hence, to define V_j and h_j. This task is performed by means of an iterative procedure, when all phases in σ are already computed (described in Section 7.3.4).

In all practical cases the descent phase is the last phase ($j = N$); in such a case, the second bang ends with the known final values $V(t_f) = V_f$ and $h(t_f) = h_f$, so that there is no unknown variable needed for the descent computation. However, the initial and final values of some of the adjoints, as well as the final value of the distance travelled $x(t_f)$, are used to impose some necessary conditions for optimality which are added (as closing equations) to the iterative procedure.

7.3.4 Closing Equations

As previously mentioned, given a phase sequence σ, the numerical procedure is built by sequentially piecing the corresponding phase algorithms together. Each phase algorithm may add some unknown parameters: three for climb phases and two for cruise and descent phases. However, those necessary conditions for optimality not explicitly taken into account in the phase algorithms allow for the definition of the unknown parameters by means of an iterative procedure.

Let n_{cl}, n_{cr} and n_d (with $n_{cl}+n_{cr}+n_d = N$) the number of climb phases, cruise phases and descent phases, respectively, considered in σ. Then, according to the explained algorithms, the number of total unknown parameters is $N_{un} = 1 + 3n_{cl} + 2n_{cr} + 2(n_d - 1)$ (taking into account that K is an unknown and that the final descent has zero unknowns). The number of closing equations can be obtained as follows.

A switching point j for $j = 1, ..., N-1$ is the beginning of the phase q_{j+1}. At the beginning of a phase q_{j+1}, one has three adjoint continuity equations, the first three Eqs. (7.13). If the phase q_{j+1} is a cruise or a descent, one of these adjoint continuity equations has already been used in the corresponding phase algorithm (the one involving the adjoint associated to the state that remains constant). This implies that at the beginning of a phase q_{j+1} for $j = 1, ..., N-1$ (that is, except for q_1) one has either two (if $q_{j+1} = cr$ or $q_{j+1} = d$) or three (if $q_{j+1} = cl$) adjoint continuity equations that have not been explicitly taken into account in the corresponding phase algorithm. Hence, because the first phase is a climb in all practical cases, one has $3(n_{cl} - 1) + 2n_{cr} + 2n_d$ closing equations stating adjoints continuity. Besides, one has two additional closing equations: $x(t_f) = x_f$ and $\lambda_m(t_f) = 0$. As a result, the number of total closing equations is $N_{ce} = 3(n_{cl} - 1) + 2n_{cr} + 2n_d + 2$, that is, $N_{ce} = N_{un}$. The resolution of this system of non-linear equations is performed using MATLAB's *fsolve*.

7.4 Application to a Climb-Cruise-Climb-Cruise-Descent Trajectory

As already seen, by conveniently piecing the phase algorithms together one can establish a numerical procedure to solve the problem given any possible solution structure. Typical solution structures include considering an initial climb from the given initial state, a final descent to the given final state and several cruise phases at different altitudes joined by climb phases (since experience shows that cruise altitudes should increase along the trajectory). Elements form this family of solution structures can be identified by the number of cruise phases considered n_{cr}. In this chapter, results are presented for a climb-cruise-climb-cruise-descent structure, $\sigma = (cl, cr, cl, cr, d)$, which is the element $n_{cr} = 2$ from the aforementioned family of solution structures.

In Fig. 7.1 a sketch of the expected optimal path is presented (the particular case of $\gamma_{min,cl} = \gamma_{max,d} = 0$ is depicted). For this particular case, and with additional assumptions, several simplifications can be made in the numerical procedure, as described next.

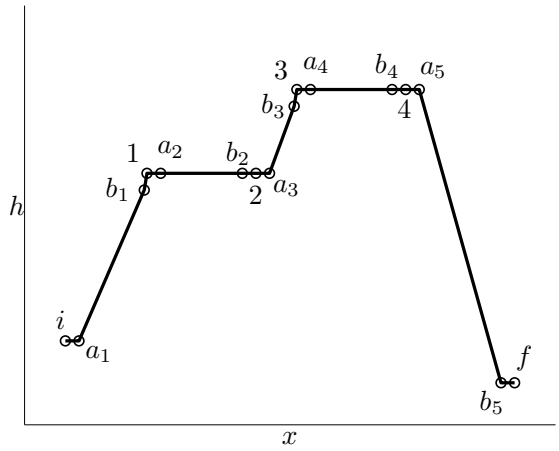

Figure 7.1: Sketch of the optimal global path.

First, at the switching point $j = 2$ (switching from the first cruise to the intermediate climb) $H_{cr} = H_{cl}$ holds, since the numerical method explicitly imposes $H_{cr} = 0$ and $H_{cl} = 0$ to compute the adjoints. Hence, from Eqs. (7.4), (7.7) and (7.17), at $t = t_2$ one has

$$-\frac{\lambda_V(t_2^-)D}{m} - K(V+w) + \left\{\frac{\lambda_V(t_2^-)}{m} + \left[1-\lambda_m(t_2^-)\right]c\right\} T_M \pi_{b_2} = -\frac{\lambda_V(t_2^+)D}{m} - K(V+w) + \left\{\frac{\lambda_V(t_2^+)}{m} + \left[1-\lambda_m(t_2^+)\right]c\right\} T_M \pi_{cl} + \left[\lambda_h(t_2^+)V - \lambda_V(t_2^+)\left(g + Vw'\right)\right]\gamma_{a_3} \tag{7.26}$$

were π_{b_2} is the value of the control variable at the final bang of the first cruise and γ_{a_3} is the value of the control variable at the initial bang of the intermediate climb. For simplicity, the dependence with respect to time of the state variables has not been included, since the numerical method explicitly imposes these to be continuous at the switching points.

Combining Eq. (7.26) with conditions $\lambda_V(t_2^-) = \lambda_V(t_2^+)$ and $\lambda_m(t_2^-) = \lambda_m(t_2^+)$, and assuming that the wind w is continuous at $j = 2$, one has

$$\left\{\frac{\lambda_V(t_2^-)}{m} + \left[1-\lambda_m(t_2^-)\right]c\right\} T_M \left(\pi_{b_2} - \pi_{cl}\right) = \left[\lambda_h(t_2^+)V - \lambda_V(t_2^+)\left(g + Vw'\right)\right]\gamma_{a_3} \tag{7.27}$$

The satisfaction of this equation along with the continuity condition for λ_m ensures satisfaction of the continuity condition for λ_V; hence, it is used as a closing equation instead of $\lambda_V(t_2^-) = \lambda_V(t_2^+)$.

Assuming $\gamma_{a_3} = \gamma_{min,cl}$ and considering $\gamma_{min,cl} = 0$, Eq. (7.27) becomes

$$\left\{\frac{\lambda_V(t_2^-)}{m} + \left[1-\lambda_m(t_2^-)\right]c\right\} T_M \left(\pi_{b_2} - \pi_{cl}\right) = 0 \tag{7.28}$$

Taking into account the Hamiltonian minimization condition, and the fact that $\pi_{min} \neq \pi_{cl} \neq \pi_{max}$, one has

$$\frac{\lambda_V(t_2^-)}{m} + \left[1-\lambda_m(t_2^-)\right]c = 0 \tag{7.29}$$

which implies that the switching point 2 belongs to the cruise singular arc (see Eq. 5.12), and then, $2 \equiv b_2$. As a consequence, the only value for the unknown V_2 satisfying the closing equation (7.29) is $V_2 = V_{b_2}$, and therefore, there is one decision variable less.

Second, at the switching point $j = 4$ (switching from the second cruise to the descent) $H_{cr} = H_d$ holds, since the numerical method explicitly imposes $H_{cr} = 0$ and $H_{cl} = 0$ to compute the adjoints. Hence, from Eqs. (7.7), (7.10) and (7.17), at $t = t_4$ one has

$$\begin{aligned} -\frac{\lambda_V(t_4^-)D}{m} - K(V+w) + \left\{ \frac{\lambda_V(t_4^-)}{m} + \left[1 - \lambda_m(t_4^-)\right] c \right\} T_M \pi_{b_4} = \\ -\frac{\lambda_V(t_4^+)D}{m} - K(V+w) + \left[\lambda_h(t_4^+)V - \lambda_V(t_4^+)\left(g + Vw'\right)\right] \gamma_{a_5} \end{aligned} \tag{7.30}$$

were π_{b_4} is the value of the control variable at the final bang of the second cruise and γ_{a_5} is the value of the control variable at the initial bang of the descent. Again, the dependence with respect to time of the state variables has not been included, since the numerical method explicitly imposes these to be continuous at the switching points.

Combining Eq. (7.30) with condition $\lambda_V(t_4^-) = \lambda_V(t_4^+)$, and assuming that the wind w is continuous at $j = 4$, one has

$$\left\{ \frac{\lambda_V(t_4^-)}{m} + \left[1 - \lambda_m(t_4^-)\right] c \right\} T_M \pi_{b_4} = \left[\lambda_h(t_4^+)V - \lambda_V(t_4^+)\left(g + Vw'\right)\right] \gamma_{a_5} \tag{7.31}$$

The satisfaction of this equation ensures satisfaction of the continuity condition for λ_V; hence, it is used as a closing equation instead of $\lambda_V(t_4^-) = \lambda_V(t_4^+)$.

Assuming $\gamma_{a_5} = \gamma_{max,d}$ and considering $\gamma_{max,d} = 0$, Eq. (7.31) becomes

$$\left\{ \frac{\lambda_V(t_4^-)}{m} + \left[1 - \lambda_m(t_4^-)\right] c \right\} T_M \pi_{b_4} = 0 \tag{7.32}$$

Taking into account the Hamiltonian minimization condition, and the fact that in cruise $\pi_{min} \neq 0$, one has

$$\frac{\lambda_V(t_4^-)}{m} + \left[1 - \lambda_m(t_4^-)\right] c = 0 \tag{7.33}$$

which implies that the switching point 4 belongs to the cruise singular arc (see Eq. 5.12), and then, $4 \equiv b_4$. As a consequence, the only value for the unknown V_4 satisfying the closing equation (7.33) is $V_4 = V_{b_4}$, and therefore, there is one decision variable less.

According to the two previous developments, the optimal cruise phase considered in this chapter has a bang-singular structure instead of a bang-singular-bang structure. As a consequence, when setting up the global numerical procedure, the algorithm for optimal cruise phase (from $j-1$ to j) has one decision variable less (V_{b_j}) and one closing equation less (continuity of λ_V at j) than the algorithm described in Section 7.3.2.

7.5 Results

The aircraft model considered in this thesis for the numerical applications (corresponding to a Boeing 767-300ER) is described in Appendix B, and the atmosphere model is the International Standard Atmosphere (ISA).

For the wind model, linear profiles are considered, with the absolute value of the wind speed increasing with altitude (see Ref. [50]). The profiles are defined as follows

$$w(h) = \bar{w} + \Delta w \frac{h - \bar{h}}{h_{high} - \bar{h}} \tag{7.34}$$

where $\bar{w}$ is the average wind; Δw is the wind-shear parameter; $h_{high} = 33000$ ft and $h_{low} = 10000$ ft are reference altitudes; and $\bar{h} = (h_{low} + h_{high})/2 = 21500$ ft is the average altitude. Note that, on one hand, the average wind speed $\bar{w}$ is the wind speed at the average altitude, that is, $\bar{w} = w(\bar{h})$; on the other hand, Δw defines the wind shear $\dfrac{\mathrm{d}w}{\mathrm{d}h}$, and, in particular, $\Delta w = 0$ defines a uniform wind profile. In the following, both tailwinds (TW) and headwinds (HW) are considered, with the linear profiles defined as follows: for TW one has $\bar{w} > 0$ and $\Delta w \geq 0$, and for HW $\bar{w} < 0$ and $\Delta w \leq 0$.

The initial conditions (corresponding to a hypothetical SID final fix) are $CAS_i = 250$ kt, $h_i = 10000$ ft, and the final conditions (corresponding to a hypothetical approach fix within the TMA) are $CAS_f = 210$ kt, $h_f = 9000$ ft. The final value of the horizontal distance travelled is $x_f = 6000$ km. The throttle setting during climb is π_{cl} =0.75, so that typical performance is obtained for the range of parameters considered in the chapter. Moreover, the bounds on the control are $\pi_{min} = 0.015$, $\pi_{max} = 1$, $\gamma_{min,cl} = 0$, $\gamma_{max,cl} = 10$ deg, $\gamma_{min,de} = -10$ deg, and $\gamma_{max,de} = 0$.

To analyze the wind effects on the optimal trajectories, the initial aircraft weight is $W_i = 1500$ kN, the average wind ranges from -30 kt to 30 kt, and the absolute value of the wind-shear parameter ranges from 0 to 20 kt. In the analysis of the effect of the initial aircraft weight on the results, no wind is considered, and W_i ranges from 1450 kN to 1550 kN.

The outline of this section is as follows: the effects of the average wind speed (Section 7.5.1), the wind-shear parameter (Section 7.5.2), and the aircraft weight (Section 7.5.3) on the optimal trajectories as well as on the optimal control are analyzed, and then, the global variables such as minimum fuel consumption, flight time and cruise altitudes are analyzed in Section 7.5.4.

7.5.1 Effect of the Average Wind Speed

The optimal trajectory $V(h)$, the speed profile $V(x)$, and the flight path $h(x)$ are represented in Figs. 7.2, 7.3a, and 7.3b, respectively, for different values of the average wind speed ($\bar{w}$ ranging from -30 kt to 30 kt) and for a wind shear parameter $\Delta w = 0$. In the optimal trajectories, the climb phases start with a horizontal acceleration and end with a steep climb out; the cruise phases start with an initial deceleration; and the descent phase starts and ends with horizontal decelerations. During the initial climb, the speed continuously increases, reaches a maximum and then slowly decreases. Along the cruise phases, the speed slowly decreases. The intermediate climb takes place with slightly higher speeds than those of cruise phases. During the descent phase the speed continuously decreases. The influence of $\bar{w}$ on the optimal profiles is clear: As $\bar{w}$ increases, the speed decreases at all phases, so that for TW one has slower speeds than for HW.

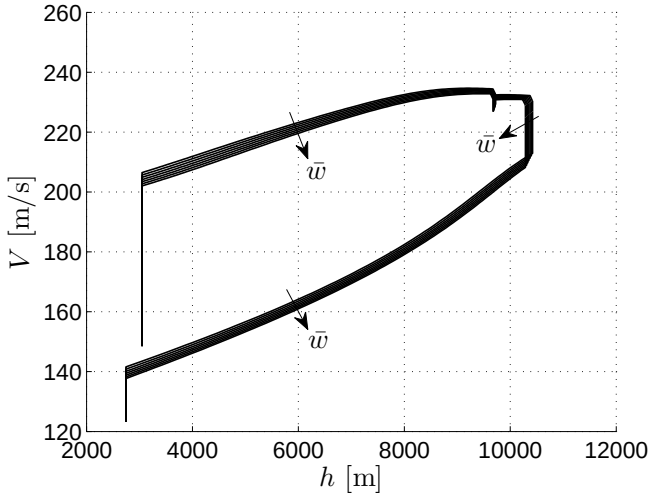

Figure 7.2: Optimal trajectory $V(h)$ for $\bar{w} = -30, -20, -10, 0, 10, 20, 30$ kt and $\Delta w = 0$.

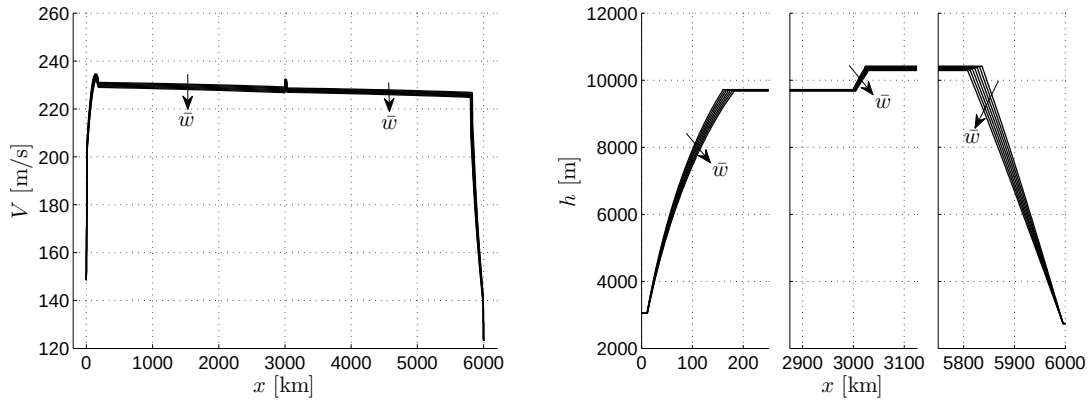

(a) (b)

Figure 7.3: Optimal speed profile and flight path for $\bar{w} = -30, -20, -10, 0, 10, 20, 30$ kt, and $\Delta w = 0$. (a) $V(x)$, (b) $h(x)$.

The optimal controls $\gamma(h)$ and $\pi(x)$ are represented in Fig. 7.4 for the same values of $\bar{w}$ as before and $\Delta w = 0$. They are discontinuous, not only at the switchings, but also within a phase. For the optimal climbs, one has three segments, all of them with $\pi = \pi_{cl}$: the initial arc with $\gamma_{min,cl} = 0$, the singular arc, in which γ decreases as the altitude increases, and the arc with $\gamma_{max,cl}$. For the optimal cruise, one has two segments, all of them with $\gamma = 0$: the initial arc with π_{min} and the singular arc, in which π decreases along the flight. For the optimal descent, one has three segments, all of them with $\pi = 0$: the initial and final arcs with $\gamma_{max,d} = 0$, along with the singular arc, in which γ remains roughly constant as the altitude decreases. The structure of the optimal control has been confirmed by the numerical results of the switching function at each phase. The average wind speed has very little influence on the singular optimal controls and on the bang-singular and singular-bang switching points.

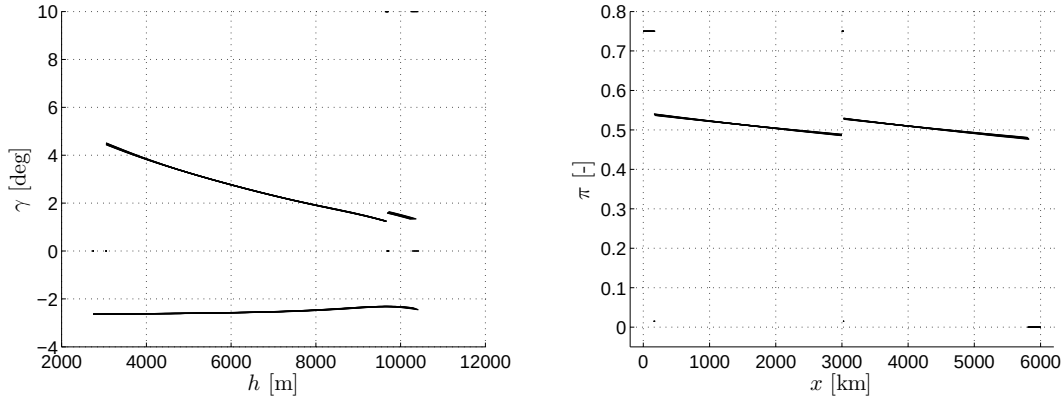

(a) (b)

Figure 7.4: Optimal controls $\gamma(h)$ and $\pi(x)$ for $\bar{w} = -30$, -20, -10, 0, 10, 20, 30 kt, and $\Delta w = 0$. (a) $\gamma(h)$, (b) $\pi(x)$.

7.5.2 Effect of the Wind Shear

The optimal trajectory $V(h)$, speed profile $V(x)$, and flight path $h(x)$ are represented in Figs. 7.5, 7.6, and 7.7, respectively, for different values of the wind-shear parameter ($|\Delta w|$ ranging from 0 kt to 20 kt), and for two values of the average wind ($\bar{w} = 30$ kt, TW, and $\bar{w} = -30$ kt, HW). The optimal trajectories have the same structure as mentioned before. The influence of Δw on the optimal speed profiles and on the optimal flight path corresponding to the initial climb and to the descent is very small; on the contrary, the influence on the cruise altitudes is much larger.

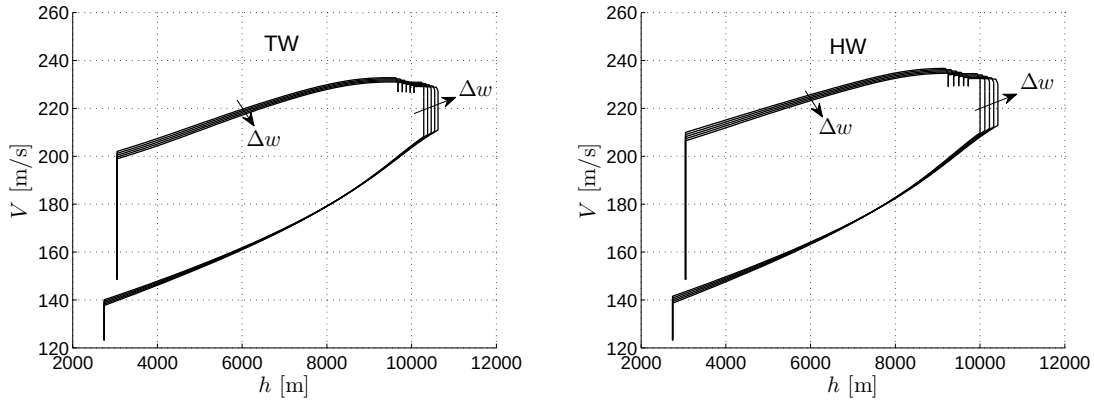

(a) (b)

Figure 7.5: Optimal trajectory $V(h)$. (a) TW ($\bar{w} = 30$ kt, $\Delta w = 0$, 5, 10, 15, 20 kt), (b) HW ($\bar{w} = -30$ kt, $\Delta w = 0$, -5, -10, -15, -20 kt).

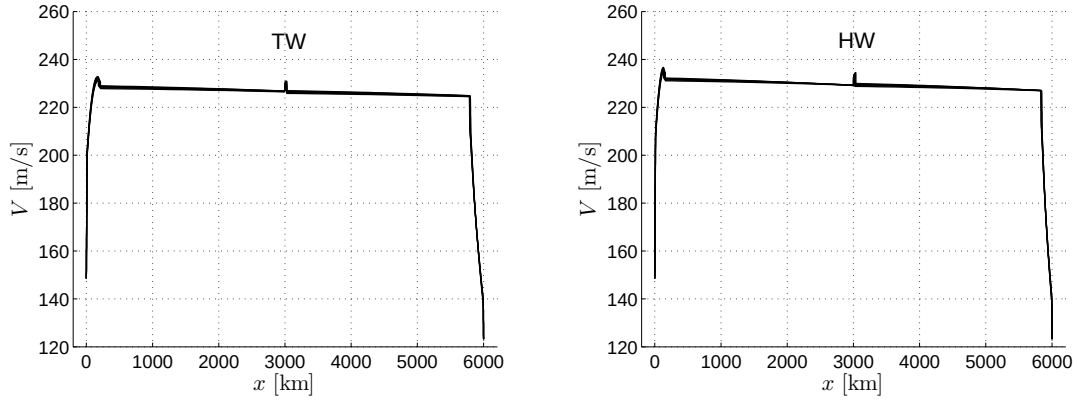

(a) (b)

Figure 7.6: Optimal speed profile $V(x)$. (a) TW ($\bar{w} = 30$ kt, $\Delta w = 0$, 5, 10, 15, 20 kt), (b) HW ($\bar{w} = -30$ kt, $\Delta w = 0$, -5, -10, -15, -20 kt).

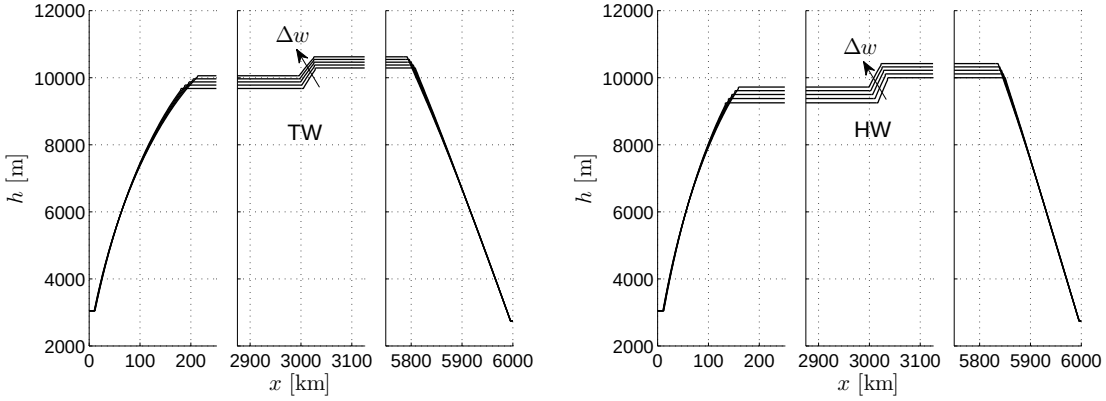

(a) (b)

Figure 7.7: Optimal flight path $h(x)$. (a) TW ($\bar{w} = 30$ kt, $\Delta w = 0$, 5, 10, 15, 20 kt), (b) HW ($\bar{w} = -30$ kt, $\Delta w = 0$, -5, -10, -15, -20 kt).

The optimal controls $\gamma(h)$ and $\pi(x)$ are represented in Figs. 7.8 and 7.9, respectively, for the same values of Δw and $\bar{w}$ (TW and HW) as before. They present the same discontinuous structure as mentioned before, which has been again confirmed by the numerical results of the switching function at each phase. During climb and descent, the wind-shear factor has little influence on the singular optimal control γ, although somewhat larger than the influence of the average wind speed; however, it importantly affects the bang-singular and singular-bang switching times. During cruise, the wind-shear factor has an important influence on the singular optimal control π, since it affects the cruise altitudes: As Δw increases, π increases (note that, for HW, when Δw increases $|\Delta w|$ decreases).

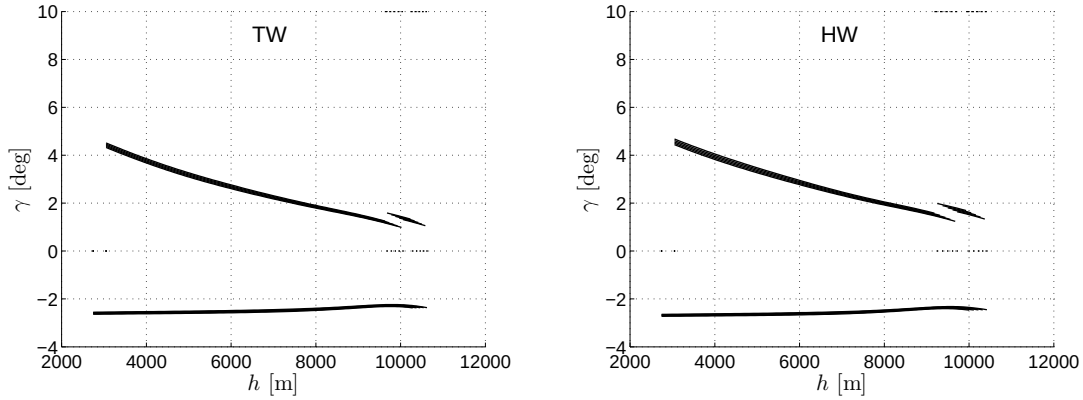

(a) (b)

Figure 7.8: Optimal control $\gamma(h)$. (a) TW ($\bar{w} = 30$ kt, $\Delta w = 0$, 5, 10, 15, 20 kt), (b) HW ($\bar{w} = -30$ kt, $\Delta w = 0$, -5, -10, -15, -20 kt).

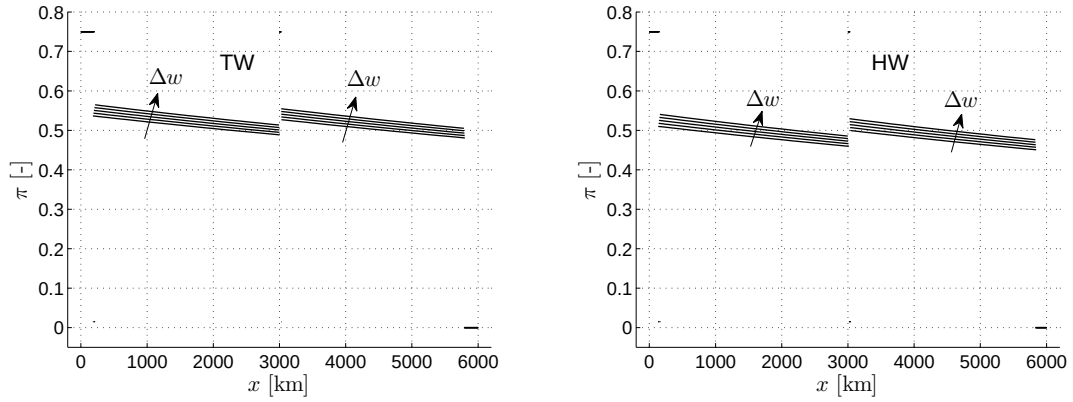

(a) (b)

Figure 7.9: Optimal control $\pi(x)$. (a) TW ($\bar{w} = 30$ kt, $\Delta w = 0$, 5, 10, 15, 20 kt), (b) HW ($\bar{w} = -30$ kt, $\Delta w = 0$, -5, -10, -15, -20 kt).

7.5.3 Effect of the Initial Aircraft Weight

The optimal trajectory $V(h)$, speed profile $V(x)$, and flight path $h(x)$ are represented in Figs. 7.10, 7.11a, and 7.11b, respectively, for different values of the initial aircraft weight (W_i ranging from 1450 kN to 1550 kN) and for no wind ($\bar{w} = 0$ and $\Delta w = 0$). The optimal trajectories have the same structure as mentioned before. The influence of W_i on the optimal profiles is clear: As W_i increases, the speed increases at all phases.

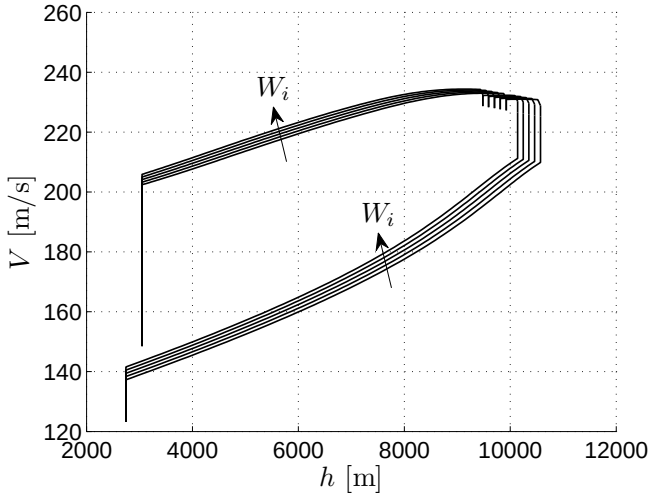

Figure 7.10: Optimal trajectory $V(h)$ for W_i = 1450, 1475, 1500, 1525 and 1550 kN ($\bar{w} = \Delta w = 0$).

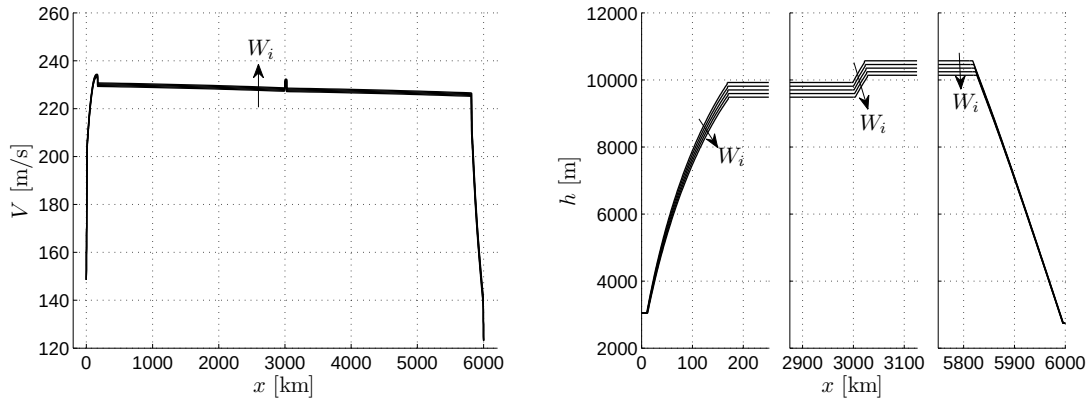

(a) (b)

Figure 7.11: Optimal speed profile and flight path for W_i = 1450, 1475, 1500, 1525 and 1550 kN ($\bar{w} = \Delta w = 0$).

The optimal controls $\gamma(h)$ and $\pi(x)$ are represented in Fig. 7.12 for the same values of the initial aircraft weight and no wind. They present the same discontinuous structure as mentioned before, which has been again confirmed by the computation results of the switching function at each phase. The initial aircraft weight has a clear influence on the singular optimal controls during climb and cruise: As the initial aircraft weight increases, γ decreases, whereas π slightly increases. During the descent phase, the initial aircraft weight has very little influence on the singular optimal control.

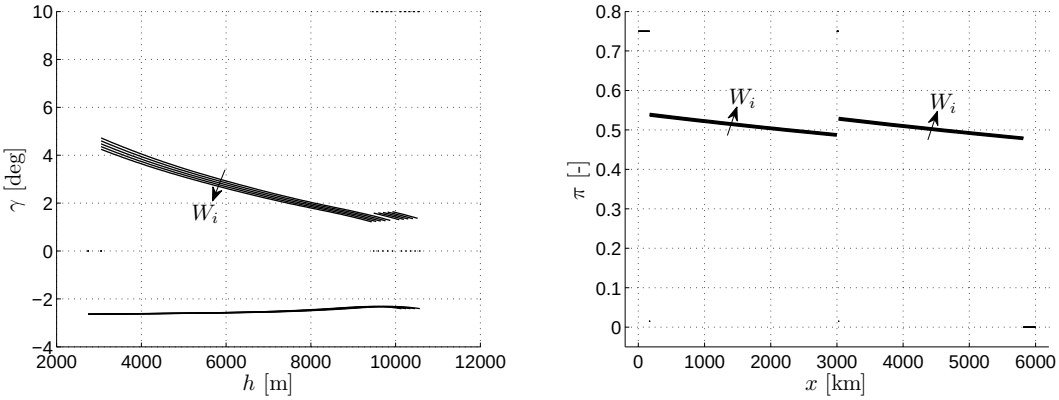

(a) (b)

Figure 7.12: Optimal controls $\gamma(h)$ and $\pi(x)$ for $W_i = 1450$, 1475, 1500, 1525 and 1550 kN ($\bar{w} = \Delta w = 0$). (a) $\gamma(h)$, (b) $\pi(x)$.

7.5.4 Analysis of Global Variables

In this section, global variables are analyzed along with the minimum fuel consumption. In Figs. 7.13, 7.14, 7.15, 7.16, 7.17, and 7.18 the following variables are represented: the minimum fuel consumption (m_F), the flight time (t_f), the climb range (x_c), the final distance of the first cruise (or transition distance, x_2), the descent range (x_d), and the cruise altitudes (h_1 and h_3). They are depicted, first, as functions of the wind-shear parameter for two values of the average wind ($\bar{w} = 30$ kt TW and $\bar{w} = -30$ kt HW) and $W_i = 1500$ kN, and second, as functions of the average wind for different values of the initial aircraft weight (W_i ranging from 1450 to 1550 kN) and $\Delta w = 0$. It is interesting to note that, in this chapter, the cruise altitudes are free variables which are obtained as results of the trajectory optimization problem.

Some numerical values are given in Table 7.1. The results show the following: 1) the stronger the wind shear for TW, the smaller the fuel consumption, the flight time, and the transition distance, but the larger the climb range, the descent range and the cruise altitudes; 2) the stronger the wind shear for HW (in absolute value), the larger the fuel consumption, the flight time, and the transition distance, but the smaller the climb range, the descent range and the cruise altitudes; 3) the higher the average wind speed, the lower the fuel consumption, the flight time, and the cruise altitudes, but the higher the climb range, the transition distance, and the descent range; and 4) the heavier the aircraft, the larger the fuel consumption, the climb range, and the transition distance, but the smaller the flight time, the descent range and the cruise altitudes. These trends are now quantified (using the values given in Table 7.1).

Table 7.1: Flight variables for different winds and initial aircraft weights (optimum values)

$W_i = 1500\,\mathrm{kN}$				
	$\bar{w} = -30\,\mathrm{kt}$ (HW)		$\bar{w} = 30\,\mathrm{kt}$ (TW)	
	$\Delta w = -20\,\mathrm{kt}$	$\Delta w = 0\,\mathrm{kt}$	$\Delta w = 0\,\mathrm{kt}$	$\Delta w = 20\,\mathrm{kt}$
m_F [kg]	31926.4	30710.0	27149.0	26198.6
t_f [min]	491.16	473.36	417.32	401.90
x_c [km]	133.43	159.19	180.47	213.30
x_2 [km]	3013.59	2996.99	3001.28	2993.65
x_d [km]	156.13	169.17	199.37	214.22
h_1 [m]	9250	9721	9680	10056
h_3 [m]	10000	10420	10288	10623
$\Delta w = 0\,\mathrm{kt}$				
	$\bar{w} = -30\,\mathrm{kt}$ (HW)		$\bar{w} = 30\,\mathrm{kt}$ (TW)	
	$W_i = 1450\,\mathrm{kN}$	$W_i = 1550\,\mathrm{kN}$	$W_i = 1450\,\mathrm{kN}$	$W_i = 1550\,\mathrm{kN}$
m_F [kg]	29696.8	31723.1	26241.7	28056.6
t_f [min]	475.22	471.58	418.80	415.90
x_c [km]	158.01	160.30	179.26	181.59
x_2 [km]	2994.95	2998.96	2998.71	3003.75
x_d [km]	172.69	165.72	203.96	194.90
h_1 [m]	9945	9541	9903	9462
h_3 [m]	10639	10207	10507	10075

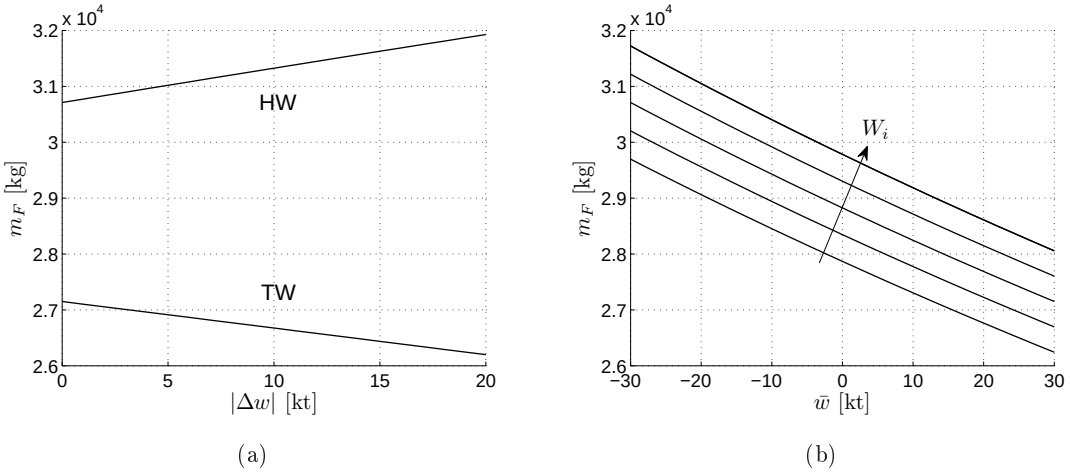

Figure 7.13: Minimum fuel consumption: (a) vs. wind-shear parameter for TW ($\bar{w} = 30$ kt) and HW ($\bar{w} = -30$ kt), for $W_i = 1700$ kN; (b) vs. average wind speed for $W_i = 1450$, 1475, 1500, 1525 and 1550 kN, for $\Delta w = 0$.

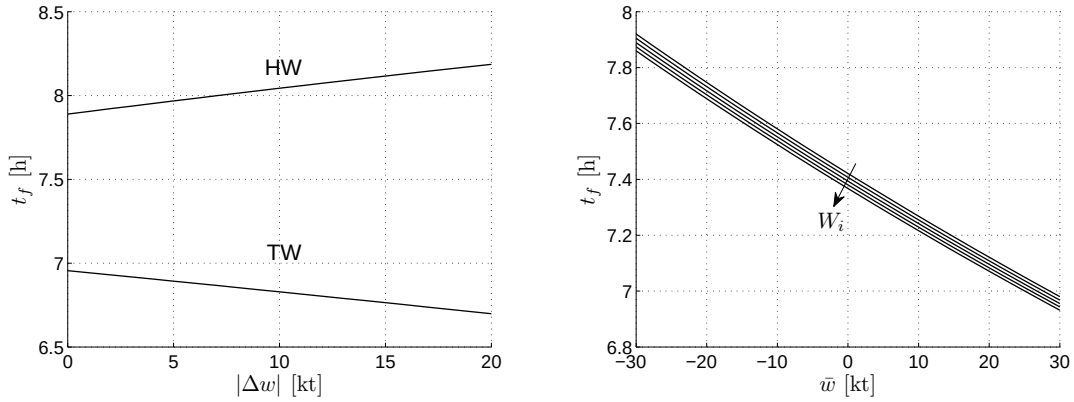

(a) (b)

Figure 7.14: Flight time: (a) vs. wind-shear parameter for TW ($\bar{w} = 30$ kt) and HW ($\bar{w} = -30$ kt), for $W_i = 1700$ kN; (b) vs. average wind speed for $W_i = 1450$, 1475, 1500, 1525 and 1550 kN, for $\Delta w = 0$.

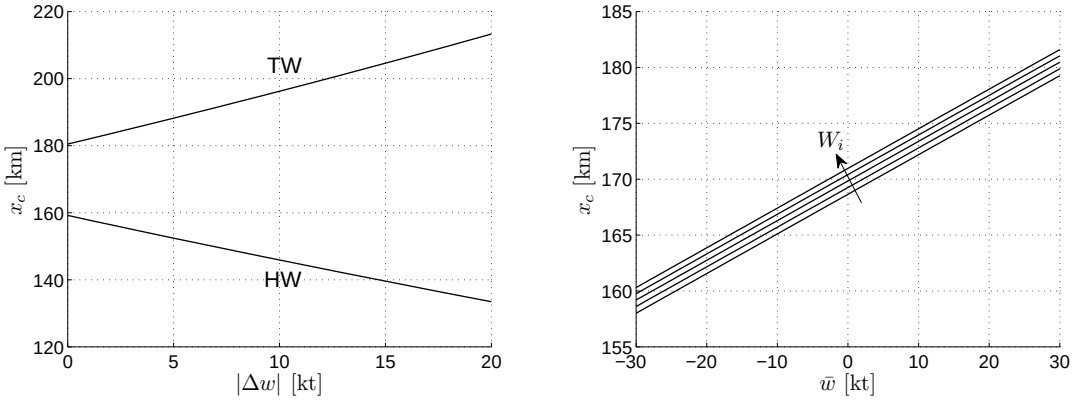

(a) (b)

Figure 7.15: Climb distance: (a) vs. wind-shear parameter for TW ($\bar{w} = 30$ kt) and HW ($\bar{w} = -30$ kt), for $W_i = 1700$ kN; (b) vs. average wind speed for $W_i = 1450$, 1475, 1500, 1525 and 1550 kN, for $\Delta w = 0$.

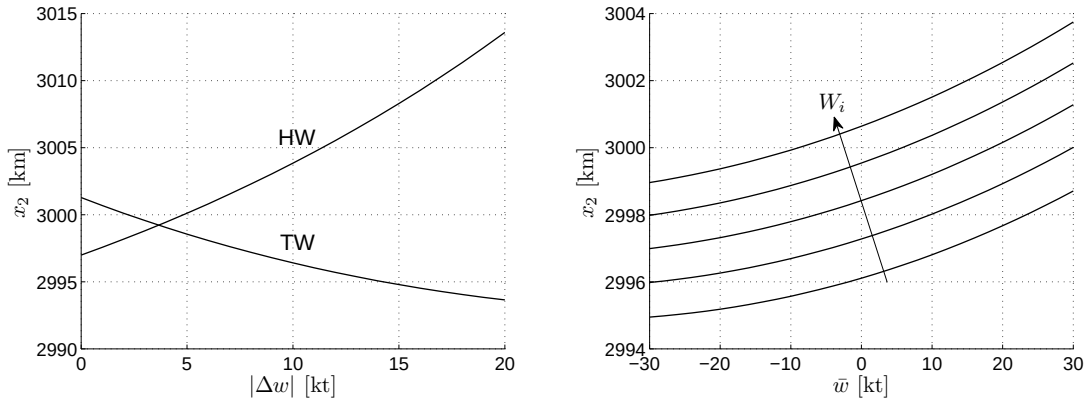

(a) (b)

Figure 7.16: Transition distance: (a) vs. wind-shear parameter for TW ($\bar{w} = 30$ kt) and HW ($\bar{w} = -30$ kt), for $W_i = 1700$ kN; (b) vs. average wind speed for $W_i = 1450$, 1475, 1500, 1525 and 1550 kN, for $\Delta w = 0$.

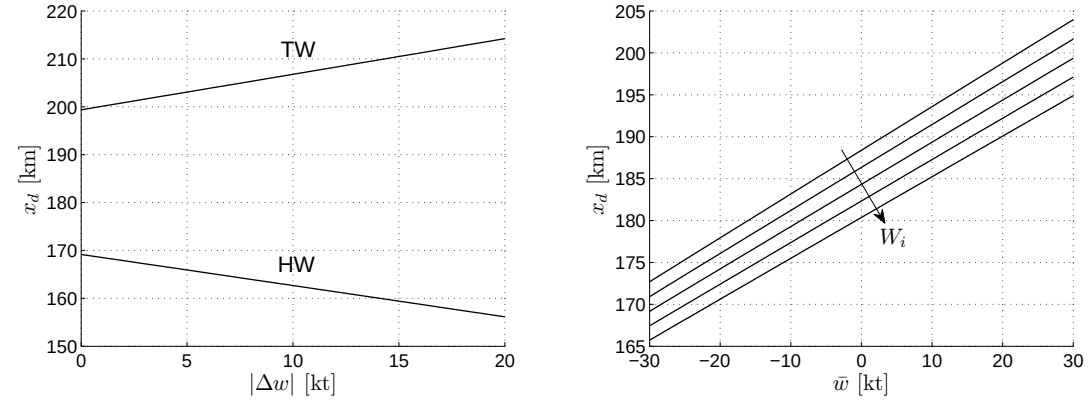

(a) (b)

Figure 7.17: Descent distance: (a) vs. wind-shear parameter for TW ($\bar{w} = 30$ kt) and HW ($\bar{w} = -30$ kt), for $W_i = 1700$ kN; (b) vs. average wind speed for $W_i = 1450$, 1475, 1500, 1525 and 1550 kN, for $\Delta w = 0$.

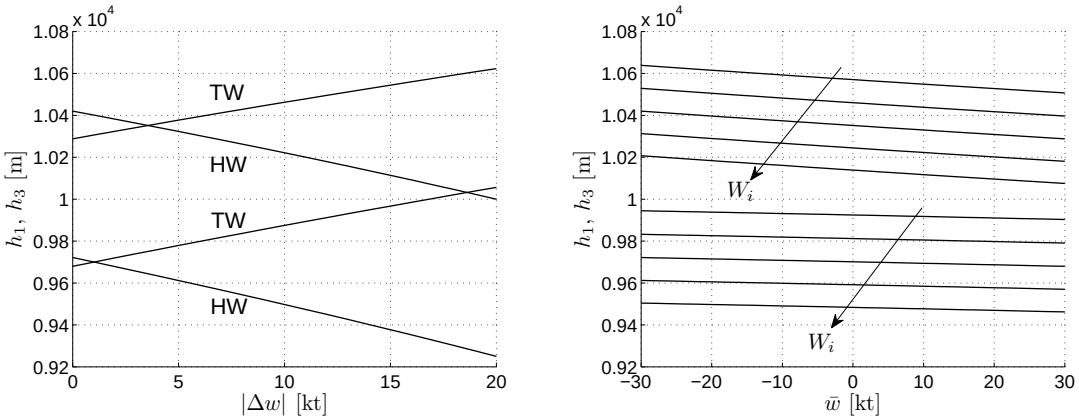

(a) (b)

Figure 7.18: Cruise altitudes: (a) vs. wind-shear parameter for TW ($\bar{w} = 30$ kt) and HW ($\bar{w} = -30$ kt), for $W_i = 1700$ kN; (b) vs. average wind speed for $W_i = 1450$, 1475, 1500, 1525 and 1550 kN, for $\Delta w = 0$.

The effect of the average wind speed on the minimum fuel consumption, the flight time, the climb range, the descent range, and the altitude of the second cruise is quite large, whereas its effect on the transition distance and the altitude of the first cruise is quite small. When $\bar{w}$ increases from -30 kt to 30 kt (for $\Delta w = 0$ and $W_i = 1500$ kN), the increases in x_c and x_d are 21.28 km and 30.20 km, respectively, that is 12.5%, and 16.4%, and the decreases in m_F, t_f, and h_3 are 3561.0 kg, 56.04 min, and 132.1 m, respectively, that is 12.4%, 12.6%, and 1.28%, whereas the increases in x_2 is 4.29 km, that is 0.143%, and the decrease in h_1 is 42.0 m, that is 0.433%.

The effect of the wind shear on m_F, t_f, x_c, x_d, h_1, and h_3 in the case of TW ($\bar{w} = 30$ kt) is quite large, especially its effect on x_c, whereas its effect on x_2 is quite small; when Δw increases from 0 to 20 kt, the decreases in m_F and t_f are 950.4 kg and 15.42 min, respectively, that is 3.50% and 3.70%, and the increases in x_c, x_d, h_1, and h_3 are 32.83 km, 14.86 km, 376.8 m, and 335.2 m, respectively, that is, 18.2%, 7.45%, 3.89%, and 3.26%, whereas the increase in x_2 is of just 7.63 km, that is 0.254%. In the case of HW ($\bar{w} = -30$ kt) similar trends are obtained; when Δw increases from -20 kt to 0, the decreases in m_F and t_f are 1216.4 kg and 17.80 min, respectively, that is 3.96% and 3.76%, and the increases in x_c, x_d, h_1, and h_3 are 25.75 km, 13.03 km, 471.4 m, and 420.5 m, respectively, that is, 16.2%, 7.70%, 4.85%, and 4.04%, whereas the increase in x_2 is of just 16.60 km, that is 0.551%.

The effect of the initial aircraft weight, can be quantified as follows. For $\bar{w} = -30$ kt HW, when W_i increases from 1450 kN to 1550 kN, the increases in m_F, x_c, and x_2 are 2026.3 kg, 2.30 km, and 4.01 km, respectively, that is 6.60%, 1.44%, and 0.134%, and the decreases in t_f, x_d, h_1, and h_3 are 3.64 min, 6.97 km, 404.1 m, and 431.3 m, respectively, that is 0.769%, 4.12%, 4.16%, and 4.14%. For $\bar{w} = 30$ kt TW, the increases in m_F, x_c, and x_2 are 1814.87 kg, 2.33 km, and 5.04 km, respectively, that is 6.68%, 1.29%, and 0.168%, and the decreases in t_f, x_d, h_1, and h_3 are 2.90 min, 9.07 km, 440.9 m, and 432.1 m, respectively, that is 0.695%, 4.55%, 4.55%, and 4.20%.

7.6 Summary

An analysis of minimum-fuel global trajectories in the presence of altitude-dependent winds has been made, using the theory of singular optimal control and switched control systems. The optimal trajectory are composed of several phases, in which optimal control is of the bang-singular-bang type, with optimal paths formed by a singular arc and two minimum/maximum-control arcs joining the singular arc with the initial and final switching points.

Results have been presented for the particular case of a climb-cruise-climb-cruise-descent trajectory with $\gamma_{min,cl} = \gamma_{max,d} = 0$, $\pi_{min} \neq \pi_{cl} \neq \pi_{max}$, and initial $\gamma_{min,cl}$-arc and $\gamma_{max,d}$-arc in the intermediate climb phase and in the descent phase, respectively. In cruise phases, these assumptions lead to the optimal control being of the bang-singular type instead, with optimal paths formed by a singular arc and a minimum-π arc joining the singular arc with the initial switching point, since the final switching point belongs to the singular arc. In climb and descent phases, these assumptions lead to a short horizontal acceleration segment and a steep climb out segment at the beginning and at the end, respectively, of both climb phases, and two short horizontal deceleration segments at the beginning and end of the descent phase.

This study has been quite general, in the sense that it has been made for a general aircraft model and a general horizontal wind profile, although results have been presented for linear profiles. In the numerical applications, the linear wind profiles have been defined by two parameters: the average wind and the wind shear. The influence of these two parameters on the results and the influence of the initial aircraft weight have been analyzed.

The results have shown that as the average wind increases, the fuel consumption and the flight time decrease (as expected). Of particular importance in this chapter has been the analysis of the influence of the wind shear on the global-trajectory performance. The influence of the wind shear on fuel consumption and flight time is comparable to that of the average wind, however not so large; in these variables the wind shear reinforces the effects of the average wind. With respect to the initial aircraft weight, as it increases the fuel consumption importantly increases whereas the final time is barely unaffected.

An interesting remark is that the approach considered has the advantage of providing the altitudes at which cruise phases should take place in order to minimize the fuel consumption of the global trajectory. Therefore, the influence of the average wind, the wind shear, and the initial aircraft weight on the cruise altitudes have been also analyzed. The average wind has very little influence on the optimal values of the cruise altitudes, whereas the wind shear and the aircraft weight importantly affect them. With tailwinds, the stronger the wind shear, the higher the cruise altitudes, whereas with headwinds, the stronger the wind shear (in absolute value), the lower the cruise altitudes. As the initial aircraft weight increases, the cruise altitudes decrease.

8 Conclusions

In this thesis, an analysis of optimal aircraft trajectories has been made, using the theory of singular optimal control. An indirect method is proposed, in which necessary conditions for optimality are explicitly involved to obtain the optimal trajectory, i.e., the optimal control law and the associate evolution of the states that optimize some property derived from the trajectory.

As previously mentioned, the employed optimization approach features the following advantages:

1. It provides analytical state-feedback control laws that can be directly used to guide the aircraft along the optimal path, allowing for an easy implementation.
2. It leads to more accurate results than those obtained by direct trajectory optimization methods.
3. It allows for generating trajectories with the best performance which, although these may not be flyable according to present-day air-traffic-control procedures and regulations, they can be used either as references to the design of improved flight procedures, or to assess the optimality of standard flight procedures commonly used in practice, such as CAS/Mach climbs, constant-Mach cruises and Mach/CAS descents.

The proposed approach has been applied to optimize multiphase aircraft trajectories with a prescribed phase sequence in the presence of altitude-dependent winds. It has successfully provided results for a broad range of cases considered, with computation times for an optimal multiphase aircraft trajectory less than 1.5 min, for a relative tolerance in the unknown variables of 10^{-9}. This figures are obtained when MATLAB 7.8.0 (R2009a) is running in a PC with an Intel DH67VR motherboard, an Intel Core i7-2600 microprocessor (4 cores, 8 MB cache, 3.4 GHz), and a Windows 7 (64 bits) Operating System.

In order to simplify as much as possible the formulation considered, state constraints have not been explicitly taken into account. However, all the computed optimal trajectory presented in this thesis have been checked to provide suitable state laws in which states do not saturate.

The atmosphere model considered in this thesis do not meet the regularity requirements assumed in Chapter 3 at the tropopause. However, in all the results presented in this thesis, optimal trajectories take place within the troposphere, and therefore, it is not necessary for this lack of regularity to be explicitly taken into account.

Optimizing global trajectories implies not only addressing each flight phase, but also taking into account the interactions among them as well as looking for a global objective. The

aim for a global objective has been achieved by considering a global performance index, which is split into the contributions of each phase and particularized to the additional constraint imposed at each phase. The interactions have been taken into account by appropriately imposing the transversality conditions and by enforcing state and adjoint continuity at the switching points.

As a conclusion, an optimal global trajectory cannot be obtained by simply piecing individually optimized phases together, not even when each phase is optimized with a performance index suitable for a global objective, because the transversality conditions do not provide the same results for the evolution of the adjoints. However, conclusions regarding the optimal control and optimal path structure for a single-phase optimal trajectory also apply at each phase of an optimal multiphase trajectory. This justifies that, prior to optimizing multiphase aircraft trajectories, the proposed approach has been applied to some auxiliary problems in which a single-phase aircraft trajectory is optimized.

9 Future Work

In this thesis, several future research lines can be identified. First of all, the results presented can be extended.

On one hand, in this thesis results are presented for linear wind profiles in climb, descent and global trajectories, whereas a uniform wind is considered for cruise trajectories. A straightforward extension can be presenting results for optimal cruise in the presence of linear wind profiles. Moreover, for any of the applications considered, results can be presented for other types of wind profiles. This would allow, for example, to compute cruise altitudes for a global trajectory in the presence of a jet stream.

On the other hand, in the optimal global trajectory problem, results are presented for one phase sequence, climb-cruise-climb-cruise-descent. An extension can be presenting results for some other phase sequences, such as those with only one cruise phase and no intermediate climb, or with three cruise phases and two intermediate climbs. With these extensions, a comparison among the different proposed trajectories could be performed, which would allow, for instance, to analyze the effect of the flight range on the selection of the phase sequence.

Second, as in the applications involving only one flight phase, results from optimal global multiphase trajectories could be used to assess the optimality of global trajectories composed of segments performing standard procedures. As an example, a standard global trajectory could be composed by piecing a CAS/Mach climb, a constant-Mach cruise, another CAS/Mach climb, another constant-Mach cruise and a constant-CAS descent together. Therefore, the optimized standard global trajectory could be compared with the optimal climb-cruise-climb-cruise-descent trajectory, which would provide an optimality assessment of such a standard global trajectory.

Third, the optimization approach presented in this thesis can be extended to analyze problems with other cost functions, such as global trajectories minimizing the direct operating cost. To analyze minimum-DOC global trajectory composed of climb, cruise and descent phases, it is convenient to perform a previous analysis considering only one phase, because conclusions regarding the optimal control and optimal path structure for a single-phase optimal trajectory also apply at each phase of an optimal multiphase trajectory, as it has been already shown. In this context, the problem of minimum-cost cruise, considering not only the DOC but also the arrival-error cost, has already been analyzed by Franco and Rivas [31]. Therefore, prior to studying minimum-DOC global trajectories, it just remains to analyze minimum-DOC climbs penalizing small distance travelled, as well as maximum-range unpowered descents penalizing large flight time.

Fourth, the optimization approach presented in this thesis can also be extended to account for tropopause crossings during climb and descent phases. One possible approach is based on regularizing the atmosphere model, that is, adopting an alternative atmosphere model which coincides with the ISA model except at altitudes in a neighborhood of the tropopause, for which a sufficiently regular model is considered. Another possible approach is based on explicitly taking into account the lack of regularity of the atmosphere model, which may force to change the considered structure of the solution (for instance, by introducing an additional horizontal segment at the tropopause altitude).

Bibliography

[1] Asselin, M., *An Introduction to Aircraft Performance*, AIAA Education Series, Reston, VA, 1997, p. 323.

[2] Athans, M., and Falb, P.L., *Optimal control. An Introduction to the Theory and its Applications*, McGraw-Hill, 1966.

[3] Barman, J.F., and Erzberger, H., "Fixed-Range Optimum Trajectories for Short-Haul Aircraft", *Journal of Aircraft*, Vol. 13, No.10, 1976, pp. 748-754.

[4] Bell, D.J., and Jacobson, D.H., *Singular Optimal Control Problems*, Academic Press, New York, 1975.

[5] Bellman, R., *Dynamic Programming*, Princeton University Press, Princeton, NJ, 1957.

[6] Ben-Asher, J. Z., *Optimal Control Theory with Aerospace Applications*, AIAA Education Series, AIAA, Reston, VA, 2010.

[7] Betts, J.T., "Survey of Numerical Methods for Aircraft Trajectory Optimization", *Journal of Guidance, Control, and Dynamics*, Vol. 21, No. 2, 1998, pp. 193-207.

[8] Biegler, L.T., and Grossmann, I.E., "Retrospective on Optimization", *Computers and Chemical Engineering*, Vol. 28, No. 8, 2004, pp. 1169-1192.

[9] Bilimoria, K.D., Cliff, E.M., and Kelley, H.J., "Classical and Neo-Classical Cruise-Dash Optimization", *Journal of Aircraft*, Vol. 22, No. 7, 1985, pp. 555-560.

[10] Bilimoria, K.D., and Cliff, E.M., *Singular Trajectories in Airplane Cruise-Dash Optimization*, NASA-CR-180636, 1987.

[11] Bilimoria, K.D., and Lee, H.Q., *Aircraft Conflict Resolution with an Arrival Time Constraint*, AIAA paper 2002-4444, 2002.

[12] Branicky, M.S., Borkar, V.S., and Mitter, S.K., "A Unified Framework for Hybrid Control: Model and Optimal Control Theory", *IEEE Transactions on Automatic Control*, Vol. 43, No. 1, 1998, pp. 31-45.

[13] Bryson, A.E., and Denham, W.F., "A Steepest-Ascent Method for Solving optimum Programming problems", *Journal of Applied Mechanics*, Vol. 29, No. 2, 1962, pp. 247-257.

[14] Bryson, A.E., Desai, M.N., and Hoffman, W.C., "Energy-State Approximation in Performance Optimization of Supersonic Aircraft", *Journal of Aircraft*, Vol. 6, No. 6, 1969, pp. 481-488.

[15] Bryson, A.E., and Ho, Yu-Chi, *Applied Optimal Control*, Hemisphere Publishing Corporation, Washington, DC, 1975.

[16] Bryson, A.E., "Optimal Control-1950 to 1985", *IEEE Control Systems*, Vol. 16, No. 3, 1996, pp. 26-33.

[17] Burrows, J.W., "Fuel Optimal Trajectory Computation", *Journal of Aircraft*, Vol. 19, No. 4, 1982, pp. 324-329.

[18] Burrows, J.W., "Fuel-Optimal Aircraft Trajectories with Fixed Arrival Times", *Journal of Guidance, Control, and Dynamics*, Vol. 6, No. 1, 1983, pp. 14-19.

[19] Caines, P.E., Clarke, F.H., Liu, X., and Vinter, R.B., *A Maximum Principle for Hybrid Optimal Control Problems with Pathwise State Constraints*, Proceedings of the 45th IEEE Conference on Decision and Control, San Diego, California, December 2006, pp. 4821-4825.

[20] Cavcar, A., and Cavcar, M., "Approximate Solutions of Range for Constant Altitude-Constant High Subsonic Speed Flight of Transport Aircraft", *Aerospace Science and Technology*, Vol. 8, 2004, pp. 557-567.

[21] Chakravarty, A., "Four-Dimensional Fuel-Optimal Guidance in the Presence of Winds", *Journal of Guidance, Control, and Dynamics*, Vol. 8, No. 1, 1985, pp. 16-22.

[22] Chakravarty, A., "Selection of an Optimal Cost Index for Airline Hub Operation", *Journal of Guidance, Control, and Dynamics*, Vol. 8, No. 6, 1985, pp. 777-781.

[23] Clarke, F.H., and Vinter, R.B., "Optimal Multiprocesses", *SIAM Journal on Control and Optimization*, Vol. 27, No. 5, 1989, pp. 1072-1091.

[24] Clarke, F.H., *Functional Analysis, Calculus of Variations and Optimal Control*, Springer-Verlag, London, 2013.

[25] Clarke, J.P.B., Ho, N.T., Ren, L., et al., "Continuous Descent Approach: Design and Flight Test for Louisville International Airport", *Journal of Aircraft*, Vol. 41, No. 5, 2004, pp. 1054-1066.

[26] Coppenbarger, R.A., *Climb Trajectory Prediction Enhancement Using Airline Flight-Planning Information*, AIAA paper 99-4147, AIAA, 1999, pp. 1-11.

[27] Dimitruk, A.V., Kaganovich, A.M., "The Hybrid Maximum Principle is a Consequence of Pontryagin Maximum Principle", *Systems & Control Letters*, Vol. 57, No. 11, 2008, pp. 964-970.

[28] Erzberger, H., and Lee, H., "Constrained Optimum Trajectories with Specified Range", *Journal of Guidance, Control, and Dynamics*, Vol. 3, No. 1, 1980, pp. 78-85.

[29] Fletcher, R., *Practical Methods of Optimization*, John Wiley & Sons, Ltd., Chichester, England, 1987, p. 304.

[30] Franco, A., Rivas, D., and Valenzuela, A., "Minimum-Fuel Cruise at Constant Altitude with Fixed Arrival Time", *Journal of Guidance, Control, and Dynamics*, Vol. 33, No. 1, 2010, pp. 280-285.

[31] Franco, A., and Rivas, D., "Minimum-Cost Cruise at Constant Altitude of Commercial Aircraft Including Wind Effects", *Journal of Guidance, Control, and Dynamics*, Vol. 34, No. 4, 2011, pp. 1253-1260.

[32] Franco, A., Rivas, D., and Valenzuela, A., "Optimization of Unpowered Descents of Commercial Aircraft in Altitude-Dependent Winds", *Journal of Aircraft*, Vol. 49, No. 5, 2012, pp. 1460-1470.

[33] Franco, A., and Rivas, D., "Analysis of Optimal Aircraft Cruise with Fixed Arrival Time Including Wind Effects", accepted for publication in *Aerospace Science and Technology*, 2013.

[34] Franco, A., Rivas, D., and Valenzuela, A., "Analysis of Fuel-Optimal Fixed-Rating Aircraft Climbs in Altitude-Dependent Winds", submitted to *Journal of Aircraft*, 2013.

[35] Goldstine, H.H., "A History of the Calculus of Variations from the 17th through the 19th Century", *Studies in the History of Mathematics and Physical Sciences*, Vol. 5, 1980.

[36] Hestenes, M.R., *Calculus of Variations and Optimal Control*, John Wiley and Sons, New York, NY, 1966.

[37] Ho, N.T., and Clarke, J.P., "Methodology for Optimizing Parameters of Noise-Abatement Approach Procedures", *Journal of Aircraft*, Vol. 44, No. 4, 2007, pp. 1168-1176.

[38] Houlihan, S.C., Cliff, E.M., and Kelley, H.J., "Study of Chattering Cruise", *Journal of Aircraft*, Vol. 19, No. 2, 1982, pp. 119-124.

[39] Jackson, M.R., Zhao, Y., and Slattery, R.A., "Sensitivity of Trajectory Prediction in Air Traffic Management", *Journal of Guidance, Control, and Dynamics*, Vol. 22, No. 2, 1999, pp. 219-228.

[40] Kelley, H.J., Kopp, R.E., and Moyer, H.G., "Singular Extremals", *Topics in Optimization*, edited by G. Leitmann, Academic Press, New York, 1967, p. 75.

[41] Leitmann, G., *The Calculus of Variations and Optimal Control*, Plenum Publishing Corporation, New York, NY, 1983.

[42] Liden, S., "Practical Considerations in Optimal Flight Management Computations", *Journal of Guidance, Control, and Dynamics*, Vol. 9, No. 4, 1986, pp. 427-432.

[43] Mattingly, J.D., Heiser, W.H., and Pratt, D.T., *Aircraft Engine Design*, 2nd edition, AIAA Education Series, AIAA, Reston, VA, 2002, pp. 38,71.

[44] Maurer, H., "Numerical Solution of Singular Control Problems Using Multiple Shooting Techniques", *Journal of Optimization Theory and Applications*, Vol. 18, No. 2, 1976, pp. 235-257.

[45] McDanell, J.P., and Powers, W.F., "Necessary Conditions for Joining Optimal Singular and Nonsingular Subarcs", *SIAM Journal on Control*, Vol. 9, No. 2, 1971, pp. 161-173.

[46] Menon, P.K.A., "Study of Aircraft Cruise", *Journal of Guidance, Control, and Dynamics*, Vol. 12, No. 5, 1989, pp. 631-639.

[47] Miele, A., *General Solutions of Optimum Problems in Nonstationary Flight*, NACA TM 1388, 1955.

[48] Miele, A., Wang, T., and Melvin, W.W., "Optimization and Acceleration Guidance of Flight Trajectories in a Windshear", *Journal of Guidance, Control, and Dynamics*, Vol. 10, No. 4, 1987, pp. 368-377.

[49] Neuman, F., and Kreindler, E., "Minimum-Fuel, Three-Dimensional Flight Paths for Jet Transports", *Journal of Guidance, Control, and Dynamics*, Vol. 8, No. 5, 1985, pp. 650-657.

[50] Oseguera, R.M., and Williams, D.H., *Flight Evaluation of the CTAS Descent Advisor Trajectory Prediction*, Proceedings of the American Control Conference, Seattle, Washington, June 1995, pp. 3435-3439.

[51] Pargett, D.M., and Ardema, M.D., "Flight Path Optimization at Constant Altitude", *Journal of Guidance, Control, and Dynamics*, Vol. 30, No. 4, 2007, pp. 1197-1201, 2007.

[52] Powell, M. J. D., "A Fortran Subroutine for Solving Systems of Nonlinear Algebraic Equation", *Numerical Methods for Nonlinear Algebraic Equations*, edited by P. Rabinowitz, Gordon and Breach, London, 1970.

[53] Rao, A.V., "A Survey of Numerical Methods for Optimal Control", *Adavnces in the Astronautical Sciences*, Vol. 135, No. 1, 2009, pp. 497-528.

[54] Riedinger, P., Kratz, F., Iung, C., and Zanne, C., *Linear Quadratic Optimization for Hybrid Systems*, Proceedings of the 38th IEEE Conference on Decision and Control, Phoenix, Arizona, December 1999, pp. 3059-3064.

[55] Rivas, D., and Valenzuela, A., "Compressibility Effects on Maximum Range Cruise at Constant Altitude", *Journal of Guidance, Control, and Dynamics*, Vol. 32, No. 5, 2009, pp. 1654-1658, 2009.

[56] Rivas, D., Lopez-Garcia, O., Esteban, S., and Gallo, E., "An Analysis of Maximum Range Cruise Including Wind Effects", *Aerospace Science and Technology*, Vol. 14, 2010, pp. 38-48.

[57] Rivas, D., Franco, A., and Valenzuela, A., *Optimization of Unpowered Descents for Commercial Aircraft*, AIAA paper 2011-7019, 2011, pp. 1-12.

[58] Ross, I.M., *A Primer on Pontryagin's Principle in Optimal Control*, Collegiate Publishers, Carmel, CA, 2009.

[59] Sachs, G., and Christodoulou, T., "Reducing Fuel Consumption of Subsonic Aircraft by Optimal Cyclic Cruise", *Journal of Aircraft*, Vol. 24, No. 9, 1987, pp. 616-622.

[60] Schultz, R.L. and Zagalsky, N.R., "Aircraft Performance Optimization", *Journal of Aircraft*, Vol. 9, No. 2, 1972, pp. 108-114.

[61] Schultz, R.L., "Fuel Optimality of Cruise", *Journal of Aircraft*, Vol. 11, No. 9, 1974, pp. 586-587.

[62] Shaikh, M.S., and Caines, P.E., "On the Hybrid Optimal Control Problem: Theory and Algorithms", *IEEE Transactions on Automatic Control*, Vol. 52, No. 9, 2007, pp. 1587-1603.

[63] Shampine, L.F., and Reichelt, M. W., "The MATLAB ODE Suite", *SIAM Journal on Scientific Computing*, Vol. 18, No. 1, 1997, pp. 1-22.

[64] Shapira, I., and Ben-Asher, J.Z., "Singular Perturbation Analysis of Optimal glide", *Journal of Guidance, Control, and Dynamics*, Vol. 27, No. 5, 2004, pp. 915-918.

[65] Shapira, I., and Ben-Asher, J.Z., "Range Maximization for Emergency Landing After Engine Cutoff", *Journal of Aircraft*, Vol. 42, No. 5, 2005, pp. 1296-1306.

[66] Slattery, R., and Zhao, Y., "Trajectory Synthesis for Air Traffic Automation", *Journal of Guidance, Control, and Dynamics*, Vol. 20, No. 2, 1997, pp. 232-238.

[67] Soler, M., Olivares, A., and Staffetti, E., "Hybrid Optimal Control Approach to Commercial Aircraft Trajectory Planning", *Journal of Guidance, Control, and Dynamics*, Vol. 33, No. 3, 2010, pp. 985-991.

[68] Sorensen, J.A., and Waters, M.H., "Airborne Method to Minimize Fuel with Fixed Time-of-Arrival Constraints", *Journal of Guidance, Control, and Dynamics*, Vol. 4, No. 3, 1981, pp. 348-349.

[69] Speyer, J.L., "On the Fuel Optimality of Cruise", *Journal of Aircraft*, Vol. 10, No. 12, 1973, pp. 763-765.

[70] Speyer, J.L., "Nonoptimality of the Steady-State Cruise for Aircraft", *AIAA Journal*, Vol. 14, No. 11, 1976, pp. 1604-1610.

[71] Speyer, J. L., and Jacobson, D. H. *Primer on Optimal Control Theory*, SIAM, 2010.

[72] Sussmann, H.J., and Willems, J.C., "300 Years of Optimal Control: From The Brachystochrone Problem to the Maximum Principle", *IEEE Control Systems*, Vol. 17, No. 3, 1997, pp. 32-44.

[73] Sussmann, H.J., *A Maximum Principle for Hybrid Optimal Control Problems*, Proceedings of the 38th IEEE Conference on Decision and Control, Phoenix, Arizona, December 1999, pp. 425-430.

[74] Torenbeek, E., "Cruise Performance and Range Prediction Reconsidered", *Progress in Aerospace Sciences*, Vol. 33, 1997, pp. 285-321.

[75] Torenbeek, E., *Flight Physics*, Springer, 2009.

[76] Torres, R., Chaptal, J., Bès, C. and Hiriart-Urruty, B., "Optimal, Environmental Friendly Departure Procedures for Civil Aircraft", *Journal of Aircraft*, Vol. 48, No. 1, 2011, pp. 11-22.

[77] Vincent, T.L., and Brusch, R.G., *Applications of the Calculus of Variations to Aircraft Performance*, NACA CR-499, May 1966.

[78] Vincent, T.L., and Brusch, R.G., *Minimum Time Aircraft Trajectories between Two Points in Range Altitude Space*, NACA CR-631, October 1966.

[79] Visser, H.G. and Wijnen, R.A.A., "Optimization of Noise Abatement Departure Trajectories", *Journal of Aircraft*, Vol. 38, No. 4, 2001, pp. 620-627.

[80] Von Stryk, O., and Bulirsch, R., "Direct and Indirect Methods for Trajectory Optimization", *Annals of Operations Research*, Vol. 37, 1992, pp. 357-373.

[81] Williams, D.H., *Fuel Penalties and Time Flexibility of 4D Flight Profiles under Mismodeled Wind Conditions*, NASA-TM-89128, 1987.

[82] Wu, D. and Zhao, Y.J., *Optimization and Sensitivity Analysis of Climb and Descent Trajectories for Reducing Fuel Burn and Emissions*, AIAA paper 2011-6879, AIAA, 2011, pp. 1-23.

[83] Xu, X., Antsaklis, P.J., "Optimal Control of Switched Systems Based on Parameterization of the Switching Instants", *IEEE Transactions on Automatic Control*, Vol. 49, No. 1, 2004, pp. 2-16.

[84] Zagalsky, N.R., Irons, R.P., and Schultz, R.L., "Energy State Approximation and Minimum-Fuel Fixed-Range Trajectories", *Journal of Aircraft*, Vol. 8, No. 6, 1971, pp. 488-490.

A Nomenclature

a	speed of sound
c	specific fuel consumption
CAS	calibrated airspeed
CAS_d^*	optimum descent calibrated airspeed
C_C	specific fuel consumption coefficient
C_D	drag coefficient
C_L	lift coefficient
C_T	thrust coefficient
CI	cost index
D	aerodynamic drag
DOC	direct operating cost
g	gravity acceleration
$h, h_t, \bar{h}$	altitude, CAS/Mach transition altitude, average altitude
H	Hamiltonian
$\overline{\mathcal{H}}$	constant value of the Hamiltonian
J	objective function
K	cost factor
l	running cost
L	aerodynamic lift
m, m_F	aircraft mass, fuel consumption
M	Mach number
p	pressure
R_a	air gas constant
S	switching function
S_W	reference wing surface
$t, t_f, \Delta t_f$	time, flight time, flight delay
T, T_M	thrust, maximum thrust
$\mathbf{u}, u$	control vector, control variable
V	aerodynamic speed
$w, \bar{w}, \Delta w, \delta w$	wind speed, average wind speed, wind-shear parameter, mismodeled wind
W	aircraft weight
x, x_f, x_{max}	horizontal distance, range, maximum range
$\mathbf{y}$	state vector
γ, γ_g	aerodynamic flight-path angle, ground path angle
δ	pressure ratio

θ	temperature ratio
Θ	temperature
κ	ratio of specific heats
λ	adjoint variable
π	throttle setting
ρ	density
σ	phase sequence
τ	sequence of switching times
Ω	cruise singular-arc parameter

Subindices

cl	climb
cr	cruise
d	descent
f	final
i	initial or counter
j	counter
q	flight segment
SL	sea level (ISA model)

B Supplementary Models

B.1 Earth Model

The Earth model adopted has the following characteristics:

- flat Earth,
- constant gravity g=9.80665 m/s^2,
- air, a perfect gas defined by a gas constant R_a =287.053 J/(kgK) and a ratio of specific heats κ=1.4, and
- standard atmosphere ISA (it defines temperature, Θ, pressure, p, and density, ρ, as functions of altitude h, with Θ_{SL}, p_{SL} and ρ_{SL} as the reference sea-level values).

B.2 Aircraft Model for Boeing 767-300ER

The aircraft model of the Boeing 767-300ER considered in this thesis for the numerical applications has a wing surface area S_W =283.3 m^2, a maximum take-off mass of 186880 kg and a maximum fuel mass of 73635 kg.

The aerodynamic model defines the drag polar $C_D = C_D(M, C_L)$, that gives the drag coefficient as a function of Mach number, M, and lift coefficient, C_L. The lift and drag coefficients are defined by $L = \frac{1}{2}\rho V^2 S C_L$ and $D = \frac{1}{2}\rho V^2 S C_D$, respectively. The drag polar defined by Cavcar and Cavcar [20] is considered; it is given by

$$\begin{aligned} C_D = &\left(C_{D_{0,i}} + \sum_{j=1}^{5} k_{0j} \overline{K}^j (M) \right) + \left(C_{D_{1,i}} + \sum_{j=1}^{5} k_{1j} \overline{K}^j (M) \right) C_L \\ &+ \left(C_{D_{2,i}} + \sum_{j=1}^{5} k_{2j} \overline{K}^j (M) \right) C_L^2 \end{aligned} \tag{B.1}$$

where

$$\overline{K}(M) = \frac{(M - 0.4)^2}{\sqrt{1 - M^2}} \tag{B.2}$$

The incompressible drag polar coefficients are $C_{D_{0,i}} = 0.01322$, $C_{D_{1,i}} = -0.00610$, $C_{D_{2,i}} = 0.06000$, and the compressible coefficients are given in table B.1. This polar is valid for $M \geq 0.4$; for $M \leq 0.4$, the incompressible drag polar applies (obtained by setting $\bar{K} = 0$ in equation B.1).

j	1	2	3	4	5
k_{0j}	0.0067	−0.1861	2.2420	−6.4350	6.3428
k_{1j}	0.0962	−0.7602	−1.2870	3.7925	−2.7672
k_{2j}	−0.1317	1.3427	−1.2839	5.0164	0.0000

Table B.1: Compressible drag-polar coefficients for the Boeing 767-300ER

The propulsion model defines the thrust available and the specific fuel consumption. For the available thrust the following general model is considered (see Torenbeek [74])

$$T = W_{TO}\delta C_T(M, N_c) \tag{B.3}$$

where W_{TO} is the reference take-off weight, $\delta = p/p_{SL}$ is the pressure ratio (p_{SL} being the reference sea-level pressure), and C_T is the thrust coefficient, which in general is a function of the Mach number and the engine control parameter N_c. The control parameter is a function of Mach number, altitude and the throttle-setting parameter π ($N_c(M, h, \pi)$), therefore one can also write the model as $T = T(M, h, \pi)$, that is, thrust dependent on Mach number, altitude and throttle-setting parameter.

Although different functional dependencies should be used for the different values of the throttle-setting parameter, in this thesis, for simplicity, the following single model is considered $C_T = \pi C_{T,max}$ and the maximum thrust coefficient $C_{T,max}$ is given by (see Mattingly [43] and Barman and Erzberger [3])

$$C_{T,max} = \frac{T_{M,SL}}{W_{TO}}\left(1 + \frac{\kappa - 1}{2}M^2\right)^{\frac{\kappa}{\kappa-1}}\left(1 - 0.49\sqrt{M}\right)\frac{1}{\theta} \tag{B.4}$$

where $\theta = \Theta/\Theta_{SL}$ is the temperature ratio (Θ_{SL} being the reference sea-level temperature), and $T_{M,SL}$ is the maximum thrust at sea level and for $M = 0$.

As a consequence, the model can be rewritten as $T = \pi T_M(M, h)$ where T_M satisfies $T_M = W_{TO}\delta C_{T,max}(M, h)$ with $C_{T,max}$ given by equation (B.4). The values used for this aircraft are $T_{M,SL}$ =5.00×10^5 N.

For the specific fuel consumption the following general model is considered (see Torenbeek [74])

$$c = \frac{a_{SL}\sqrt{\theta}}{L_H}C_C(M) \tag{B.5}$$

where $a_{SL} = \sqrt{\kappa R_a \Theta_{SL}}$ is the speed of sound at sea level, L_H is the fuel latent heat, and C_C is the specific fuel consumption coefficient (in general C_C depends on C_T, but this dependence is neglected, since it is very weak in practice [74]). For the fuel latent heat, one can take $L_H = 43 \times 10^6$ J/kg. For the specific fuel consumption coefficient, the linear model defined by Mattingly [43] is considered; it is given by

$$C_C = c_{SL}\frac{L_H}{a_{SL}}(1.0 + 1.2M) \tag{B.6}$$

where c_{SL} is the specific fuel consumption at sea level and for $M = 0$. For this aircraft, c_{SL} =9.0×10^{-6} kg/(s N) is used.

C Singular control functions at climb

In the following, the functions A_1, A_2, A_3, A_4, B_1, B_2, and B_3, which define the optimal singular control during climb (see Chapter 4, Section 4.2.4.2) are given.

$$\begin{aligned}
A_1 =& V^2\left(cT+\frac{\partial D}{\partial V}-\frac{\partial T}{\partial V}\right)\left[\left(1+\frac{Vw'}{g}\right)\left(\frac{\partial T}{\partial V}-\frac{\partial D}{\partial V}\right)-\frac{V}{g}\left(\frac{\partial T}{\partial h}-\frac{\partial D}{\partial h}\right)-\frac{w'}{g}\left(T-D\right)\right]\\
&+\left(T-D\right)V^2\frac{\partial}{\partial V}\left[\left(1+\frac{Vw'}{g}\right)\left(\frac{\partial T}{\partial V}-\frac{\partial D}{\partial V}\right)-\frac{V}{g}\left(\frac{\partial T}{\partial h}-\frac{\partial D}{\partial h}\right)-\frac{w'}{g}\left(T-D\right)\right]\\
&+V^2mcT\left[\left(1+\frac{Vw'}{g}\right)\frac{\partial^2 D}{\partial V\partial m}-\frac{V}{g}\frac{\partial^2 D}{\partial h\partial m}-\frac{w'}{g}\frac{\partial D}{\partial m}\right]\\
&-\frac{V^2}{g}\left(\frac{\partial T}{\partial h}-\frac{\partial D}{\partial h}\right)\left(T-D\right)\\
&-V^2cT\left(T-D+m\frac{\partial D}{\partial m}\right)\left[\left(1+\frac{Vw'}{g}\right)\left(\frac{1}{T}\frac{\partial T}{\partial V}+\frac{1}{c}\frac{\partial c}{\partial V}\right)-\frac{V}{g}\left(\frac{1}{T}\frac{\partial T}{\partial h}+\frac{1}{c}\frac{\partial c}{\partial h}\right)\right]
\end{aligned} \tag{C.1}$$

$$A_2 = VcT\left(T-D+m\frac{\partial D}{\partial m}\right)+V\left(\frac{\partial T}{\partial V}-\frac{\partial D}{\partial V}\right)\left(T-D\right) \tag{C.2}$$

$$\begin{aligned}
A_3 =& -V^2T\left(\frac{1}{T}\frac{\partial T}{\partial V}+\frac{1}{c}\frac{\partial c}{\partial V}\right)\left[\left(1+\frac{Vw'}{g}\right)\left(\frac{\partial T}{\partial V}-\frac{\partial D}{\partial V}\right)-\frac{V}{g}\left(\frac{\partial T}{\partial h}-\frac{\partial D}{\partial h}\right)-\frac{w'}{g}\left(T-D\right)\right]\\
&-T\left(T-D\right)\frac{V^2}{g}\left(\frac{1}{T}\frac{\partial T}{\partial h}+\frac{1}{c}\frac{\partial c}{\partial h}\right)\\
&+\left(T-D\right)\frac{V^2}{c}\frac{\partial}{\partial V}\left[\left(1+\frac{Vw'}{g}\right)\left(c\frac{\partial T}{\partial V}+T\frac{\partial c}{\partial V}\right)-\frac{V}{g}\left(c\frac{\partial T}{\partial h}+T\frac{\partial c}{\partial h}\right)\right]
\end{aligned} \tag{C.3}$$

$$A_4 = V\left(1+\frac{Vw'}{g}\right)\left(\frac{\partial T}{\partial V}-\frac{\partial D}{\partial V}\right)-\frac{V^2}{g}\left(\frac{\partial T}{\partial h}-\frac{\partial D}{\partial h}\right) \tag{C.4}$$

$$
\begin{aligned}
B_1 =& \frac{V^2 w'}{g}\left[\left(1+\frac{Vw'}{g}\right)\left(\frac{\partial T}{\partial V}-\frac{\partial D}{\partial V}\right)-\frac{V}{g}\left(\frac{\partial T}{\partial h}-\frac{\partial D}{\partial h}\right)-\frac{w'}{g}(T-D)\right] \\
&-\left(1+\frac{Vw'}{g}\right)V^2\frac{\partial}{\partial V}\left[\left(1+\frac{Vw'}{g}\right)\left(\frac{\partial T}{\partial V}-\frac{\partial D}{\partial V}\right)-\frac{V}{g}\left(\frac{\partial T}{\partial h}-\frac{\partial D}{\partial h}\right)-\frac{w'}{g}(T-D)\right] \\
&+\frac{V^3}{g}\frac{\partial}{\partial h}\left[\left(1+\frac{Vw'}{g}\right)\left(\frac{\partial T}{\partial V}-\frac{\partial D}{\partial V}\right)-\frac{V}{g}\left(\frac{\partial T}{\partial h}-\frac{\partial D}{\partial h}\right)-\frac{w'}{g}(T-D)\right]+\frac{V^3}{g^2}w''
\end{aligned}
\tag{C.5}
$$

$$
B_2 = -2V\left[\left(1+\frac{Vw'}{g}\right)\left(\frac{\partial T}{\partial V}-\frac{\partial D}{\partial V}\right)-\frac{V}{g}\left(\frac{\partial T}{\partial h}-\frac{\partial D}{\partial h}\right)\right]-\frac{Vw'}{g}(T-D) \tag{C.6}
$$

$$
\begin{aligned}
B_3 =& -\left(1+\frac{Vw'}{g}\right)\frac{V^2}{c}\frac{\partial}{\partial V}\left[\left(1+\frac{Vw'}{g}\right)\left(c\frac{\partial T}{\partial V}+T\frac{\partial c}{\partial V}\right)-\frac{V}{g}\left(c\frac{\partial T}{\partial h}+T\frac{\partial c}{\partial h}\right)\right] \\
&+\frac{V^3}{gc}\frac{\partial}{\partial h}\left[\left(1+\frac{Vw'}{g}\right)\left(c\frac{\partial T}{\partial V}+T\frac{\partial c}{\partial V}\right)-\frac{V}{g}\left(c\frac{\partial T}{\partial h}+T\frac{\partial c}{\partial h}\right)\right]
\end{aligned}
\tag{C.7}
$$

D Optimized Standard Procedures

In this appendix, the optimized CAS/Mach climb analyzed by Franco et al. [34] as well as the optimized constant-CAS descent analyzed by Franco et al. [32] are reproduced for the sake of completeness.

D.1 Optimized CAS/Mach Climb

The CAS/Mach procedure considered in Ref. [34] is formed by four segments, all of them with fixed engine rating, that is, with given thrust $T(V,h)$: 1) an initial acceleration segment at constant altitude h_i from the initial speed V_i to the climb CAS (CAS_c), 2) a climb segment with constant CAS (CAS_c) from h_i to the transition altitude h_t at which climb Mach M_c is reached, 3) a climb segment with constant Mach (M_c) from h_t to the final altitude h_f, and 4) a final acceleration at constant altitude h_f from M_c to the final speed V_f. This procedure is similar to the one used by Coppenbarger [26] in his analysis of climb trajectory prediction enhancement using airline flight-planning information.

To solve the equations of motion (4.1) for each flight segment, a flight constraint must be given (besides the engine rating) so that the control parameter γ can be determined. For the initial and final flight segments the flight constraint is $h = const$, and therefore $\gamma = 0$. For the constant-CAS segment, it is $CAS = const = CAS_c$, which is in fact a speed law $V = V_C(h)$ (see Asselin [1]) given by

$$V_C = \sqrt{\frac{2}{k} R_a \Theta(h) \left[\left(1 + \frac{p_{SL}}{p(h)} \left[\left(1 + \frac{k}{2} \frac{\rho_{SL}}{p_{SL}} CAS_c^2 \right)^{1/k} - 1 \right] \right)^{k} - 1 \right]}, \tag{D.1}$$

where $k = (\kappa - 1)/\kappa$. For the constant-Mach segment, the flight constraint is $M = const = M_c$, which is in fact a speed law $V = V_M(h)$ given by

$$V_M = M_c \sqrt{\kappa R_a \Theta(h)}, \tag{D.2}$$

Note that the transition altitude h_t is defined by the relation

$$V_C(h_t) = V_M(h_t) \tag{D.3}$$

For the initial and final horizontal segments the equations of motion (4.1) reduce to

$$\begin{aligned} \dot{V} &= \frac{T(V,h_A) - D(V,m,h_A)}{m} \\ \dot{m} &= -c(V,h_A) T(V,h_A) \\ \dot{x} &= V + w(h_A) \end{aligned} \tag{D.4}$$

where h_A stands for the initial and final altitudes, h_i and h_f, respectively.

For the constant-CAS and constant-Mach segments, let $V = V_A(h)$ stand for the known speed laws $V = V_C(h)$ and $V = V_M(h)$, respectively. Then one has

$$\frac{\mathrm{d}V}{\mathrm{d}t} = V_A' \frac{\mathrm{d}h}{\mathrm{d}t} = V_A'(h) V_A(h) \gamma \tag{D.5}$$

therefore, the first equation of motion (4.1) defines the control variable γ as a function of m and h, say $\gamma = \gamma_A(m, h)$, as follows

$$\gamma_A = \frac{T(V_A(h), h) - D(V_A(h), m, h)}{m \left[g + V_A(h) \left(w'(h) + V_A'(h) \right) \right]} \tag{D.6}$$

Once γ is known, one must integrate the following equations

$$\begin{aligned} \dot{m} &= -c(V_A(h), h) T(V_A(h), h) \\ \dot{h} &= V_A(h) \gamma_A(m, h) \\ \dot{x} &= V_A(h) + w(h) \end{aligned} \tag{D.7}$$

The computation of the CAS/Mach climb is performed as follows: For the initial segment, Eqs. (D.4) are integrated from $V = V_i$, $m = m_i$ and $x = 0$ until $V = V_C(h_i)$; at the end of the segment one has m_1 and x_1. For the constant-CAS segment, Eqs. (D.7) are integrated starting at $m = m_1$, $h = h_i$ and $x = x_1$ until $h = h_t$; at the end of the segment one has m_2 and x_2. For the constant-Mach segment, Eqs. (D.7) are integrated starting at $m = m_2$, $h = h_t$ and $x = x_2$ and stopping at $h = h_f$; at the end of the segment one has m_3 and x_3. Finally, for the last segment, Eqs. (D.4) are integrated from $V = V_M(h_f)$, $m = m_3$, and $x = x_3$ until $V = V_f$; at the end of the segment one has the final mass m_f and the final distance x_f. The fuel consumption is therefore $m_F = m_i - m_f$.

This procedure to obtain the final distance and the fuel consumption for given values of CAS and Mach can be written in symbolic form as

$$\begin{aligned} x_f &= x_f(CAS_c, M_c) \\ m_F &= m_F(CAS_c, M_c) \end{aligned} \tag{D.8}$$

The CAS/Mach procedure is now optimized to give minimum performance index, taking CAS_c and M_c as the optimization parameters. The optimum values of CAS_c and M_c are obtained solving the following parametric optimization problem

$$\begin{aligned} \text{minimize} \quad & m_F(CAS_c, M_c) - K x_f(CAS_c, M_c) \\ \text{subject to} \quad & CAS_c \geq CAS_i \\ & M_c \leq M_f \\ & h_i \leq h_t(CAS_c, M_c) \leq h_f \end{aligned} \tag{D.9}$$

where CAS_i and M_f are the values of CAS and Mach that correspond to V_i, h_i and V_f, h_f respectively. The constraints guarantee that the climb procedure has the segments considered in its definition. In this application, the optimization solver used is MATLAB's *fmincon*, a sequential quadratic programming (SQP) method (see Ref. [29]).

D.2 Optimized Constant-Calibrated-Airspeed Descent

The constant-CAS procedure considered in Ref. [32] is formed by three segments, all of them with zero thrust: 1) an initial deceleration segment at constant altitude h_i from the initial speed V_i to the descent CAS (CAS_d), 2) a descent segment with constant CAS (CAS_d) from h_i to the final altitude h_f, and 3) a deceleration segment at constant altitude h_f from CAS_d to the final speed V_f.

To solve the equations of motion (6.1) for each flight segment, a flight constraint must be given (besides flying unpowered) so that the control parameter γ can be determined. For the initial and final flight segments, the flight constraint is $h = const$, and therefore $\gamma = 0$; for the constant-CAS segment, it is $CAS = const = CAS_d$, which is in fact the same speed law $V = V_C(h)$ as in (D.1) but with CAS_d, instead of CAS_c, that is

$$V_C = \sqrt{\frac{2}{k} R_a \Theta(h) \left[\left(1 + \frac{p_{SL}}{p(h)} \left[\left(1 + \frac{k}{2} \frac{\rho_{SL}}{p_{SL}} CAS_d^2 \right)^{1/k} - 1 \right] \right)^k - 1 \right]}, \tag{D.10}$$

For the initial and final horizontal segments the equations of motion (6.1) reduce to

$$\begin{aligned} \dot{V} &= -\frac{D(V, h_A)}{m} \\ \dot{x} &= V + w(h_A) \end{aligned} \tag{D.11}$$

where h_A stands for the initial and final altitudes, h_i and h_f, respectively.

For the constant-CAS segment, because $V = V_C(h)$ is given, one has

$$\frac{\mathrm{d}V}{\mathrm{d}t} = \frac{\mathrm{d}V_C}{\mathrm{d}h} \frac{\mathrm{d}h}{\mathrm{d}t} = \frac{\mathrm{d}V_C}{\mathrm{d}h} V_C(h) \gamma \tag{D.12}$$

therefore, the first equation of motion (6.1) defines the control variable γ as a function of h, say $\gamma = \gamma_C(h)$, as follows

$$\gamma_C = -\frac{D(V_C(h), h)}{m} \left[g + V_C(h) \frac{\mathrm{d}w}{\mathrm{d}h} + V_C(h) \frac{\mathrm{d}V_C}{\mathrm{d}h} \right]^{-1} \tag{D.13}$$

Once γ is known, one must integrate the following equations

$$\begin{aligned} \dot{h} &= V_C(h) \gamma_C(h) \\ \dot{x} &= V_C(h) + w(h) \end{aligned} \tag{D.14}$$

The computation of the constant-CAS descent is performed as follows: For the initial segment, Eqs. (D.11) are integrated from $V = V_i$ and $x = 0$ until $V = V_C(h_i)$; at the end of the segment, one has $x_1 = \Delta x_1$. For the constant-CAS segment, Eqs. (D.14) are integrated starting at $h = h_i$ and $x = x_1$, and stopping at $h = h_f$; at the end of the segment one has $x_2 = x_1 + \Delta x_2$. Finally, for the last segment, Eqs. (D.11) are integrated from from $V = V_C(h_f)$ and $x = x_2$ until $V = V_f$; at the end of the segment one has the final distance $x_f = x_2 + \Delta x_3$. The range is therefore $x_f = \Delta x_1 + \Delta x_2 + \Delta x_3$.

This procedure to obtain the range for a given value of CAS can be written in symbolic form as

$$x_f = x_f(CAS_d) \tag{D.15}$$

The constant-CAS procedure is now optimized to give maximum range, taking CAS_d as the optimization parameter. The optimum value of CAS_d, say CAS_d^*, is obtained solving the following parametric optimization problem

$$\begin{aligned} \text{minimize} \quad & -x_f(CAS_d) \\ \text{subject to} \quad & CAS_f \leq CAS_d \leq CAS_i \end{aligned} \tag{D.16}$$

where CAS_i and CAS_f are the values of CAS that correspond to V_i, h_i and V_f, h_f, respectively. In this chapter, the optimization solver used is MATLAB's *fmincon*, a sequential quadratic programming (SQP) method (see Fletcher [29], for example).